Victor Hugo Acevedo Donato

Cardiomyocyte-driven Intra-body Communication System

Master's thesis in Embedded Computing Systems
Supervisor: Ilangko Balasingham
July 2019

Master's thesis

NTNU
Norwegian University of Science and Technology
Faculty of Information Technology and Electrical Engineering
Department of Electronic Systems

NTNU
Norwegian University of
Science and Technology

Victor Hugo Acevedo Donato

Cardiomyocyte-driven Intra-body Communication System

Master's thesis in Embedded Computing Systems
Supervisor: Ilangko Balasingham
July 2019

Norwegian University of Science and Technology
Faculty of Information Technology and Electrical Engineering
Department of Electronic Systems

NTNU
Norwegian University of
Science and Technology

Abstract

Molecular communications allows the transmission of information using particles, molecules or biological structures at a cellular scale. The importance of its study lies in the need to find more feasible alternatives to establish communication links between implantable sensors and medical devices.

The heart is a vital organ for the functioning of the body, and the cells that compose it use electrical pulses in their natural operation of systole and diastole, their inherent characteristics can be used for the modeling of a communication system.

The Action Potential is the signal that is propagated through the myocardial tissue, the subthreshold region behavior, if correctly modeled, can be used to propagate digital signals without disturbing the tissue or its normal function. In this thesis the electrical functions taking part on the generation of the Action Potential, are modeled using mathematical functions, as well as the characteristics of the tissue through which the signals are being propagated, proposing a new model of operation of Action Potential in which 14 currents are used to describe it, and will make more viable to use the subthreshold region, adding hyperpolarization and potassium handling. Dirac delta functions and square wave signals were used in simulations of one cell, arrangement of cells in one dimension, and a sheet of tissue in two dimensions.

It was found that each of these signals will have a different utility. The Dirac delta function, being of a very short duration, does not propagate satisfactorily by a large amount of tissue, however, by using a very short time fragment for transmission, it is possible to transmit a large amount of information. On the other hand, the square wave signal needs a greater amount of time to be transmitted, however, this signal has a great propagation along the tissue. The results were obtained in a limited simulation environment, in order to increase the confidence level of these results, laboratory experiments may be required.

Acknowledgements

I would like first to thank to my thesis supervisor Ilangko Balasingham the person who welcomed me to work with his team, his office was always open whenever I ran into trouble and despite some troubles found along the way he always supported me. To my supervisors Mladen Veletic and Farrokh Hejri, members of professor Ilangko team they were always open to help and support this project with their knowledge.

To my parents Victor, Carmen and my sister Valeria for their love and support throughout my life. Thank you for giving me the strength to reach for the stars and chase my dreams I wouldnt be where I am, nor would I be the man that I am now if it werent for you.

To you Lucero, thank you for your love and support and walking with me this path, we went through a lot and continue to do it, you are also part of this achievement.

To the 3, yes, you are always there.

To M L you are the brothers that I a chose.

To my whole family Acevedo, Donato, I couldnt have had a better family.

To all the admirable and amazing friends i did during my adventure overseas.

Thank you all for your support, this is for you.

Victor Hugo Acevedo Donato

Trondheim, 28/06/2019

Contents

List of Figures

List of Tables

Chapter 1

Introduction

1.1 Motivation

The appearance of new diseases, the increase of chronic diseases and the aging of the population, together with the continuous technological advances, the miniaturization of devices, the new communication technologies and the boom that wearable devices are having in recent years, have raised challenges in the way in which institutions are taking charge of managing the health of the population [49].

The area that has had the most development and attention is the preventive medicine. In recent years, death rates from heart disease in the United States have been reduced by more than 25% as seen in figure 1.1; this is due to efforts made by the American Heart Association, with the aim of continuing to reduce mortality rates over the years. This has been thanks to advances in preventive medicine, e-health and continuous monitoring of the health of the individual, with the aim of pursuing healthier lifestyles and be able to improve early diagnosis, which will bring as a result an improvement in the effectiveness of the treatments. The key to further developing and improving these areas of medicine may be the use of wearable devices, which can help achieve a more proactive and accessible health system [36, 58].

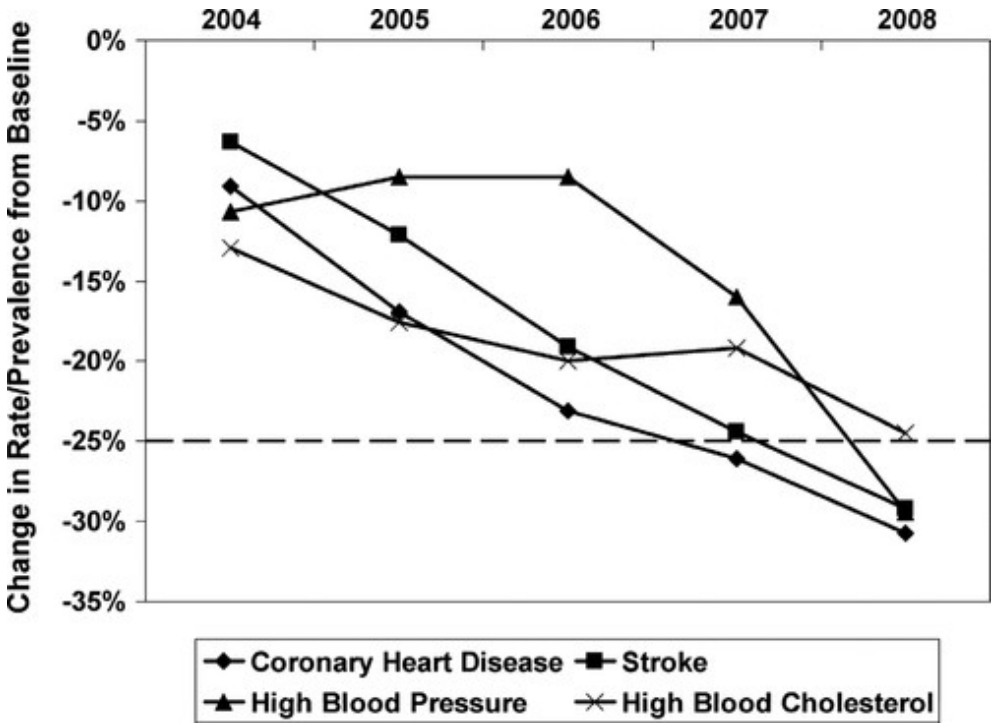

Figure 1.1: Drop in mortality rate from different heart conditions thanks to the improvement and development of new techniques in preventive medicine. Data obtained from the United States by American Heart Association (AHA) in the last decade. Figure taken from [36].

There is an increase in the number of wearable medical devices that are being developed, ranging from simple health monitors (Pulse monitors, activity monitors) to much more sophisticated systems of implantable sensors in the body [93].

With the aim of expanding the study of these devices, a new field of study has been defined in the area of communications networks: Body Area Network (BAN) and Wireless Body Area Network (WBAN). These are networks that consist of a variable number of sensor systems, which are going to be placed in different areas of the body, and depending on the function and purpose, they can be implanted, or weared. These devices communicate with other sensors placed in the body and these in turn will be responsible for sending biological signals to a doctor for the evaluation and diagnosis of diseases at an early stage for prevention [43, 8].

However, although these devices are very useful, they are still not widely accepted due to the limitations that they bring with them:

- The difficulty of communicating these devices using cables and the difficulty and disadvantages that these cables will bring in the body [48].

- In the case of using wireless communications, the devices will not have the best performance, due to the characteristics of the body as a channel for signaling or interference from other devices that use the same wireless channel for communication [27].

This thesis aims to explore the way in which the heart, in its natural functioning, makes use of electrical signals in which the cells (cardiomyocytes) that make up the cardiac tissue (myocardium) carry out the functions of systole and diastole, mechanical movements responsible for the heartbeat.

As well as exploring in the same way the models that describe these electrical behaviors of action potentials propagation within large scale networks of cardiomyocytes, we aim to propose a new model which is able to take advantage of the electrical properties of the heart to be able to use it as transmission channel. It is intended to use the electrical properties of the sub-threshold behavior of the heart.

The proposed model will be exploited considering the possibility of being used to propagate digital signals using cardiac infrastructure and metabolic energy, depending on the anatomical and electrophysiological properties of cardiomyocytes, with the purpose of replacing or improving in the future, the methods currently used in implanted devices and sensors close to the heart which may be harmful, uncomfortable, or not very viable for some types of communication.

1.2 Structure

In the second chapter of this thesis, we will initially explore molecular communications, their components, structure and functioning; the advances that have been made within the field and how these have been used in conjunction with the technological advances of implantable devices in the body.

In chapter 3, an introduction to the functioning and structure of the heart will be given, its electrophysiological characteristics can provide a very valuable tool that can be exploited to be able to communicate these devices; after reviewing its characteristics, an electrical and mathematical focus will be taken in order to begin the description of the functions of cardiac cells, and how they respond to stimuli, which are responsible of the generation of the APs that

propagate throughout the cardiac tissue.

In chapter 4 the main actors involved in this electrical propagation will be mathematically described and modeled, in order to generate a framework that is best suitable to work in the sub-threshold region of the cell, and can be used to perform computational calculations in order to analyze how different types of signals would behave in cardiac tissue, if it is feasible to use them to transmit information without affecting the heart rate, and the extent of them in a hypothetical system of molecular communications that use the heart as a transmission channel.

Chapter 5 will contain a review of the tools used to implement the framework, the characteristics of the system, languages and software used, it will also be discussed how and what different simulations will be implemented.

Chapter 6 Will contain the results of this simulations, corresponding first to the original Ten Tusscher model, to be able to present the results of the modified proposed model. Two different frameworks using a Delta Pulse Signal and a Square Wave Signal will be presented with the respective 1 cell, 1D and 2D simulations.

In chapter 7 discussion will be made about the results obtained in the previous chapter, to finalize with the conclusion in chapter 8.

Appendix A of this Thesis contains the parameters used to model and simulate the system, with the formulas that are being modeled. Appendix B contains the code generated to model the framework with some scripts that helped perform the simulations.

Chapter 2

Molecular Communication

The miniaturization of devices and the increase in the use of implants and medical devices, has brought with it a challenge, these devices must be able to communicate with each other, but what communication system is the ideal for them?

In the case of implantable sensors, miniaturization is a good thing, because its use has made the process less invasive in the body, but with its size comes a significant disadvantage, a device of this magnitude has a very limited energy capacity, and should take advantage of all the possible energy of the environment that surrounds them. In addition, these devices must operate without causing any inconvenience to the user, or damaging organs and tissues.

2.1 What are molecular communications

Molecular communications are a solution inspired by biology to deal with the problem of communicating these devices. There are two main ways of molecular communications taking advantage of biological functioning.

- Using the presence or absence of certain molecules to encode information.
- Using the molecular communications of a previously existing organ or tissue, for example, the electrical propagation originated in the brain by the neurons and in the heart by the cardiac tissue.

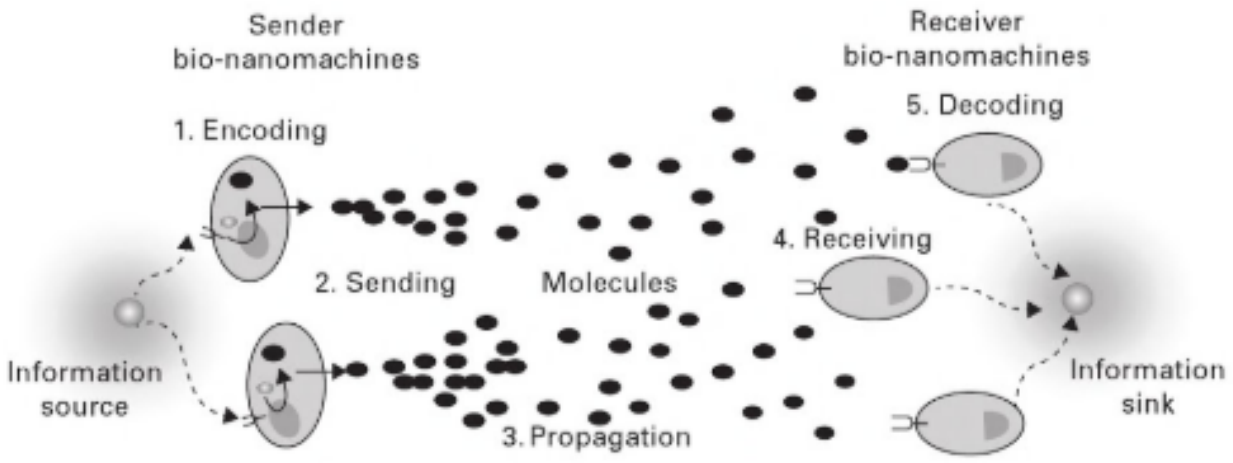

Figure 2.1: Example of how molecular communications are performed. the information comes from a source, and is encoded in a cell, this in turn use any means to transmit the information, in this case by signaling molecules where in the other side of the system will be decoded by the receiver. Image from [73].

A message to be transmitted in this type of system can be analog or digital, but in this investigation we will consider mainly digital transmissions. To communicate the transmitter must make a physical change in the environment, and for the receiver to identify the transmission, the receiver must associate the message with a type of molecular signal, this is, an easily distinguishable pattern, of which three can be mainly identified.

- Quantity: The receiver will identify a message based on the number of molecules that are received at one end, if a low number of molecules is observed, it means that a zero is being received. If we observe molecules at the end of the receiver, it means a 1 was meant to be sent.

- Identity: Multiple types of molecules are required in the system, in which the receiver can distinguish between these different molecules. In this system receiving an A type of molecule can mean receiving a 1 and receiving a B type of molecule a 0.

- Time: The receiver decides whether a 0 or a 1 is being received depending on the fraction of the time a molecule is arriving.

2.2 How a molecular communication system works

First, a cell in the system that is going to be used as a transmission channel, must be stimulated to initiate the communication, the message to be sent is going to be encoded in this cell. The cell will be responsible for transmitting in all directions by external (extracellular) or internal (intracellular) means. The message will be propagated so that at the other end it is detected by the receptors as pictured in figure 2.1.

2.3 Previous Work

The term molecular communications was used for the first time in the title of a research in the year 2005 [74]. This research focused on the implementation of communication systems that used the diffusion of chemical components which could be used to establish communication links.

Over time, several components of great importance in a system of this type have been identified, such as gap junctions, used by certain cells for the exchange of ions, where exists an opportunity for a message to be transmitted between cells through them [75].

In the present, multiple investigations are being carried out, which include:

- Nanonetworks, which will involve multiple devices of very small scale that communicate with each other and are currently being extensively investigated [3, 4].

- Modulation of Channel and noise analysis, channel models are being formulated, based on the additive White Gaussian noise channel, however there is still no model to describe the noise generated in the channel that is widely accepted.

- Theory of information, which is investigating the maximum amount of information that can be transmitted, and in which is still a question the capacity of the channel.

- Simulations and design of communications systems, although laboratory experiments are the most reliable tool to determine the functioning of a communication system of this type, they can not be used due to its difficulty and high cost.

2.4 Design of a molecular communication system

There are different types of components that can be used to design a molecular communications system which can be: molecular proteins, molecular DNA, liposomes and biological cells.

A molecular protein is a set of aminoacids that unfolds in a functional structure. Enzymes will be responsible of cataloging chemical reactions that modify the molecules so that they can act as encoders and decoders of information. Multiple types of enzymes can be used to implement Boolean logic operations such as AND, OR and XOR. In this case, molecules with multiple inputs can be combined and transformed into molecules with multiple outputs [52]. When a large number of molecules is available, the message to be transmitted can be encoded or decoded in the amplitude or frequency of the oscillations of a type of molecule, similar to an analog transmission.

The second approach uses DNA molecules, made from sequences of DNA bases, which can be prepared using enzymes to build these molecules in specific sequences. The chemical characteristics of DNA are well known; Adenine in conjunction with Thiamine, Guanine and Cytosine can be exploited to build a variety of structures that can be easily recognized by a decoder [82].

The third approach will be using liposomes to design bio-nanomachines and other key components to carry out molecular communications. The liposomes are accumulation of lipids in the cytoplasm of the cells, which constitutes their food reserve. Molecules such as DNA and RNA are encapsulated in the liposome to reproduce cellular behaviors. They are widely used in the area of drug delivery as carriers [26].

2.4.1 Biological Cells

The last class used to exploit molecular communications are biological cells, which are inherently capable of coding and decoding chemical messages, reason why they are important materials for the implementation of communication systems.

Guide cells

The cells can be used as media to transmit signals. The majority of animal cells establish gap junction to communicate with contiguous cells and exchange ions.

For example, a group of neurons in the body make up a circuit through which information travels by means of electric pulses, using the integration of gap junction; the brain in turn forms a large and complicated communication network that is capable of storing information.

In order to use a cellular biological network as a transmission channel for communications, mechanisms are necessary for the formation of this network using cells and their inherent characteristics.

2.5 Applications

The multiple fields of design of a communications systems that exist in molecular communications give rise to a large number of applications such as drug delivery, artificial tissue engineering, among others. However, the area of information technology and biomedicine will be the great beneficiary in a short term; the integration of sensors and medical devices, in the not too distant future may have incorporated systems that allow communication between them and with systems outside the body like a smart phone that will be able to carry out the health monitoring.

A display implanted in the skin which will require communication with other components implanted in the body. A large number of sensors distributed in the body connected to the internet of things, a network of nano devices [2, 7]. The exploitation of chemical and biological physical materials can bring a change in the design of computer structures and their algorithms.

Chapter 3

The Heart

In this section we will mainly review the various processes which the heart goes through and how all these are linked in their normal functioning, with the purpose of gradually introducing them into the specific elements and the importance of these in the model proposed in this document. Likewise, an anatomical and physiological background will be reviewed in order to provide the necessary context.

This will be done in the context that this organ is going to be used as a transmission channel, in the model proposed for the intra-body communications system of this thesis.

3.1 Characteristics

The heart is located in the center of the chest, below the sternum, between the lungs, in a thoracic division as seen in 3.1.

It is an organ composed of muscle tissue that acts as a pump, this pump, ensures that blood reaches the entire body through the circulatory system with the purpose of distributing oxygen and nourish the cells and tissues of the entire body [57].

In the Physiology of the heart you can find 2 areas of great importance for our study: structure and electrical functioning.

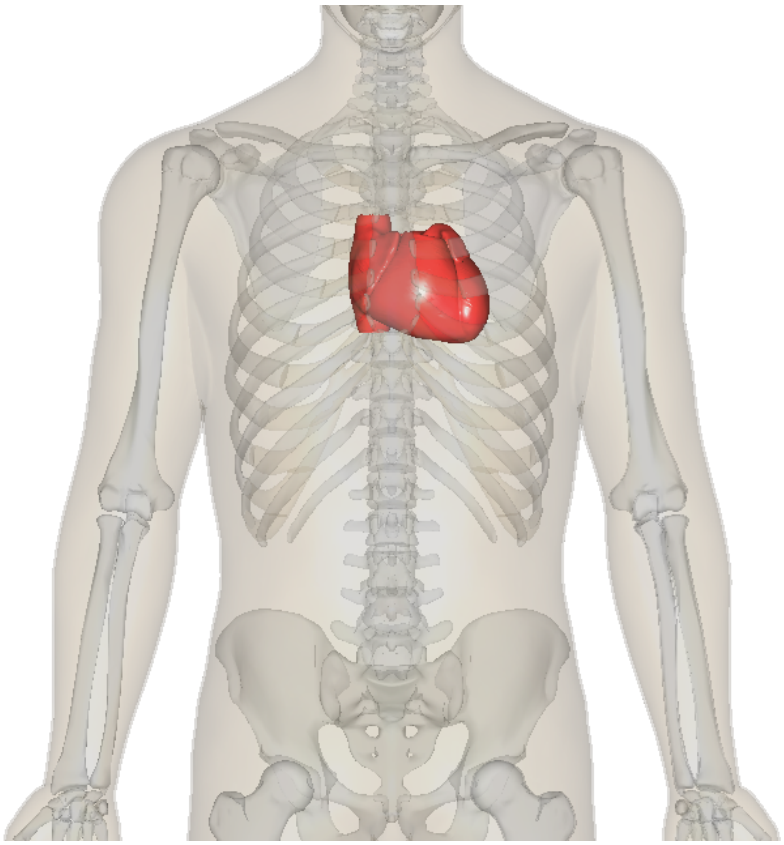

Figure 3.1: Exact location of the heart in the body, its found in a thoracic division a little bit to the left side of the body. Image taken from the database center for life science, which is a 3D generator of anatomical parts of the body [32].

3.2 Structure and Operation

The heart is divided into 4 parts, two chambers called atria, and two chambers called ventricles. The atrial chambers are located in the upper portion of the heart and receive poor oxygen blood. On the other hand, the ventricles are chambers found in the lower portion of the heart; and they pump blood enriched with oxygen [31].

The function of the heart is to pump blood to all corners of the body. The blood collects oxygen as it passes through the lungs and circulates to the heart to be propelled throughout the body.

In order to push the blood through the vessels of the whole body, the heart contracts and relaxes rhythmically. The phase of contraction is called systole, it corresponds to the expulsion of blood out of the organ. This phase is followed by a muscle relaxation called diastole [44].

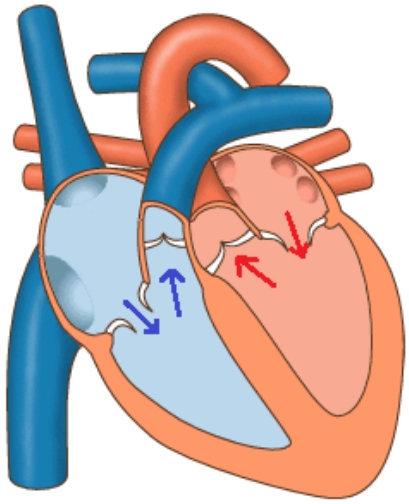

Figure 3.2: 4 chambers are distinguished in the heart, in these chambers the blood comes in, stays for a moment inside the heart, then gets pumped to continue its travel around the body. Image taken and modified from Revista Medica [46].

The heart rate, intensity and force of contraction are regulated by the brain, which is responsible of transmitting nerve impulses, as well as chemicals that act on the heart.

The cellular structure of the heart consists of a wall composed of four layers: the epicardium, which is the outside of the heart, the pericardium, the myocardium, which is the central layer, and the endocardium, the deepest layer of the wall.

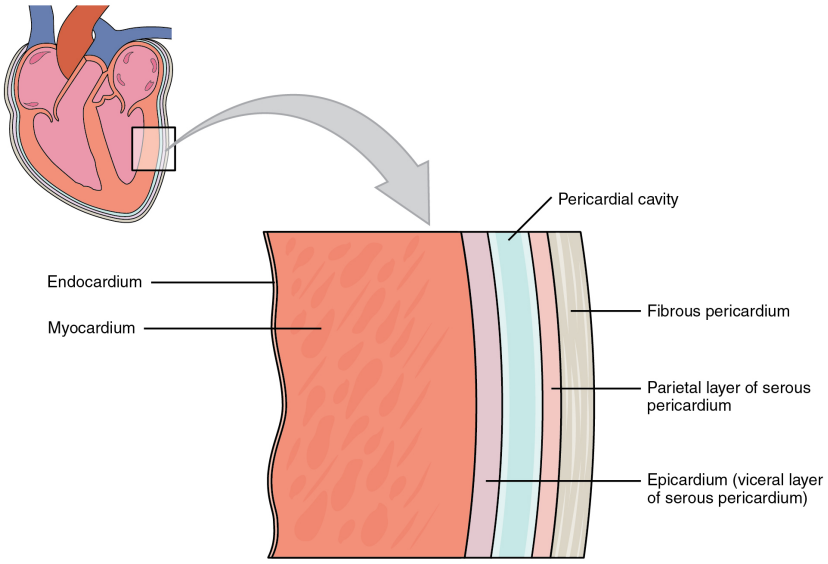

Figure 3.3: Illustration of the layers composing the heart structure. Epicardium, endocardium, pericardium and the center of out study: the Myocardium. Image taken from OpenStax Textbooks [94].

3.3 Myocardium

The myocardium is a muscle tissue by which most of the heart is formed. This tissue, as a whole, is responsible for the previously mentioned involuntary movements of systole and diastole with which the heart keeps pumping blood [51].

The myocardial cells known as myocytes, also be known as cylinders, have a length in between 80 and 100 μm and a diameter of between 10 to 20 μm; these cylinders are connected by interleaved discs [10].

The tissue of the myocardium is not uniform or continuous, it is composed of several layers of fibers called sheets.

According to Hunter, Nash & Sands (1996): "... is represented as an interconnected hierarchy of muscle layers whose three-dimensional orientation varies through the ventricular wall ..." [76].

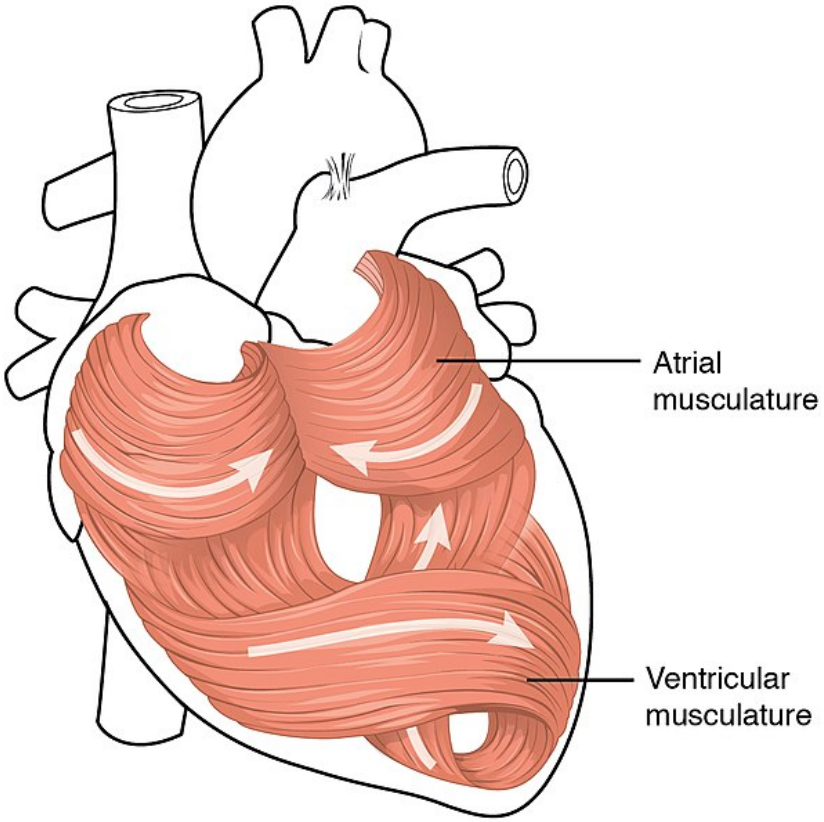

Figure 3.4: Myocardium tissue surrounding in the heart, this tissue will be used as a transmission channel for the communication system, but more specifically the cells that compose it, the myocytes. Image taken from OpenStax Textbooks [94].

The electrical impulses that regulate the movements of relaxation and muscular contraction are originated in specialized cells called cardiomyocytes, and, are caused by the flow of ions through the membrane of these cells. These have as consequence the emergence of an electrical signal of excitation that spreads throughout the myocardium. When this electrical signal propagates through the myocardium, it coordinates the contraction of cardiac cells and their relaxation when passing through them; resulting in the pumping of blood in the heart [69].

3.4 Cell Physiology

The cell membrane is constituted by a lipid bi-layer that acts as a barrier that separates two sections, in this case the cell can be divided into two sections for our convenience, extracellular space (denoted in the future with $\boldsymbol{e}$), which is the space that covers outside the cell membrane and intracellular space (denoted in the future with $\boldsymbol{i}$), considering the inside of the cell.

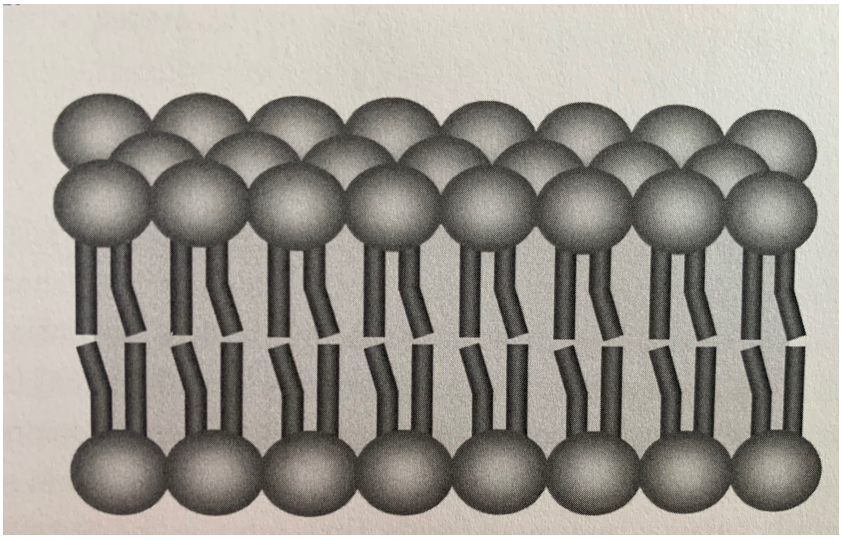

Figure 3.5: Illustrating how the membrane of the cell is composed, every segment of circles represent the 2 layers of lipid material, which makes it permeable to the ions. Image taken from [79].

Within the cell we can find proteins that combine to form small holes in the cell membrane, these holes, which we are going to refer to as ion channels, will be responsible for allowing the passage of ions through the cells in certain conditions. This will result in a difference of potential between the $\boldsymbol{e}$ space and the $\boldsymbol{i}$ space.

3.4.1 Ion Channels

These are called like this because the proteins that make them are of tubular structure and are embedded in the double lipid layer of the membrane. They are integral proteins that cross the membrane of the cell side by side, that is why they are also known as trans-membrane proteins [96, 5]. These channels regulate the passage of ions to the cell membrane.

The permeability of the cell membrane will depend mainly on the following points [60]:

- Number of channels present in relation to the surface of the cell membrane.
- Relation between the diameter of the ion and the diameter of the channel.
- Ion electric charge.

The trans-membrane proteins are going to be in charge of making the cell membrane selective with respect to the permeability to different ions, thanks to the presence of gates that open or close to allow the passage of ions, which is why we can say that they are voltage dependent, they can allow the passage of ions at some point in the cardiac process or prevent it at another time [50, 61, 9].

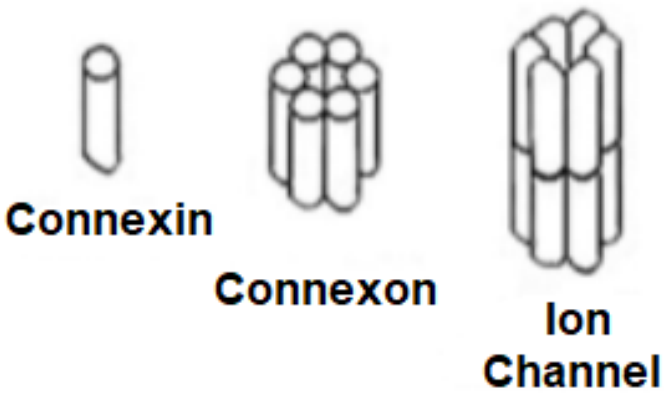

Figure 3.6: In order of how they are composed, we can see from the most basic element conforming an ion channel, a connexin, a group of 6 connexins making a connexon, and an union of these to make the ion channel, where the change of ions is going to take place.

The ions that will be of our interest in the model to be developed are N_a+ (Sodium), $K+$ (Potassium), and C_a^2+ (Calcium).

According to a recent model proposed by Luo & Rudy in 1994, the concentrations of ions in the cells when they are at rest are the following [65]:

Table 3.1: This table shows the ion concentration of the 3 main acting agents in the cell, this 3 elements will be responsible of the variations of electric potential in the cardiac tissue [65].

Ion	Concentration (nm)
N_a+i	10
N_a+e	140
$K+i$	145
$K+e$	5.4
C_a^2+i	0.00012
C_a^2+e	1.8

Ion channels are proteins that can be found in all cells that have a membrane; there is no way for ions to cross the cell membrane if it is not through these channels. These are not structures that are open all the time, they can be opened and closed as required, and this opening or closing can be modulated. These structures can respond to stimuli according to [38].

3.4.2 Gap Junctions

Gap junctions are closely connected with the previously mentioned channels, these are communication systems of the cell membrane formed by the coupling of protein complexes, (based on the proteins called connexins), on the cells that are attached; that is, they are group of ion channels that communicate to contiguous cells in the tissue. These gap junctions are responsible for allowing the passage of water, ions and small molecules between cells through their channels [87].

Functions

- Participate in rapid communication between cells.
- They can be found in the skin, nervous tissue of the heart and muscle tissue.
- Allow the passage of small molecules between cells.
- They mediate the ***i*** communication by allowing the passage of inorganic ions, and other small water-soluble molecules, such as sugars, aminoacids, etc.
- They are the foundation of the electrical synapse.

At the cardiovascular level, cell-to-cell communication is essential, so gap junctions allow rapid coordination of the cells under normal conditions, to enable transmission of the electrical impulse and the synchronization of cardiac contractile activity [30].

The connexins mentioned above, are in groups of 6, these surround a pore of the membrane forming the channel or connexon. 2 connections of adjacent cells are aligned and anchored to each other to form a channel as seen in 3.6 [90].

The gap junctions are not perfect connections between the membranes of the cardiomyocytes, they are organized in intercalated disks, which affects each cell in different ways, each one will have a small variation with respect to the others at the moment of transmission of the electric impulse [83, 39].

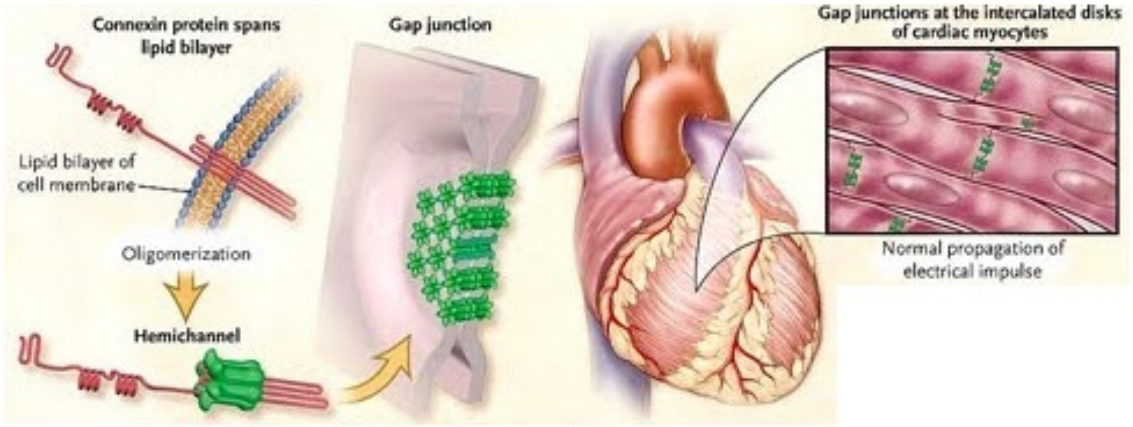

Figure 3.7: The gap junctions are going to interconnect neighbouring cells, but these connections are not going to be perfect, they are going to be intercalated, presenting different properties in each cell.

3.5 Electrical Characteristics

All the electrical activities that are going to affect the heart naturally, more specifically, the cells that are responsible for its functioning, are based on the distribution of ions on both sides of the cell membrane, and this distribution in turn, is caused by the permeability of the cell membrane for the different types of ions and kept stable by a process called pump N_a+ / $K+$ [66, 24].

The unequal distribution of ions will establish difference of potential in the membrane, and the movement of these between $\boldsymbol{i}$ space and $\boldsymbol{e}$ space, this flow will cause electric currents to move in the cell.

When the cardiac cell is in a resting state, it can be observed that the ***i*** concentration of potassium is $(K + i > K + e)$ as seen in table 3.1, and since the membrane is permeable, it tends to flow outward following its chemical gradient. The output of very small amounts of $K+$, even though it does not influence the previously mentioned amounts, as this is an element with positive electric charges, it will cause an increase in positive charges in the ***e*** part of the membrane, and consequently, it will leave a higher percentage of negative charges in the ***i*** space [62, 54].

The output of $K+$ will not be accompanied by a proportional input of another element. Since the permeability of the membrane for sodium, N_a+, will be of an order 100 times less than that of $K+$, the $K+$ that goes to the ***e*** space, will represent a domain of positive charges in the outer space of the cell causing a polarization. That point of balance between the inclination of the ions to move to the ***e*** and to the ***i*** will represent a Resting Equilibrium Potential [55].

The Nernst equation expresses that this equilibrium, where there will be no greater force in any of the two directions, and consequently, there will be no transfer of charges [81].

The Nernst potential E_x for an ion x can be written as:

$$E_x = \frac{RT}{z_x F} log_e \left(\frac{x_e}{x_i} \right) \tag{3.1}$$

Where:

R is the universal gas constant.

T is absolute temperature.

z_x is the valence of ion.

F is Faraday's constant.

x_e and x_i are the ***i*** and ***e*** concentrations for the ion x.

The Nernst equation states that, for certain concentrations of ions somewhere on the cell membrane, there will be an electrical potential that can maintain these concentrations without variation.

The existence of increased potassium levels in the body is possible; hyperkalemia is a condition that increases potassium levels in the blood, causing poisoning and kidney failure. This increase will cause the resting potential of the cell to be different to the normally seen in experiments or studies, this will cause that the resting potential will be more negatively charged, and because the chemical gradient is reduced without being accompanied by an equivalent decrease in the electrical gradient, it will facilitate the passage of $K+$ ions into the cell with the effects of its respective charges [95, 67].This will mean that the magnitude of the potential is directly related to the output of potassium.

Using the values of the table 3.1 it can be solved based on the Nernst equation that the potentials for $N_a = 70\ mV$ $K = -88\ mV$ and for $C_a = 128\ mV$, at body temperature[79].

The resting potential is not equal to the equilibrium potential of potassium, although it can be observed that it is very close to it, this is because the membrane of the cardiac cell is not permeable only to this ion. Although the membrane is less permeable for ions of N_a+, this ion will be able to pass into $\boldsymbol{i}$ space following its chemical and electrical gradient making the resting potential less negative [21, 45].

In conclusion, it can be observed that the resting potential is determined by the flow of potassium towards the $\boldsymbol{e}$ part of the cell membrane, it is dependent on the permeability of the membrane and will be maintained by the previously mentioned process, the pump N_a+ / $K+$, which will be responsible for transporting these two types of ions between cell spaces [24].

3.5.1 Action Potentials

The cardiac muscle has a protection, with which, upon receiving any external stimulus in the difference of potential of the cell membrane, it will yield a small response. After this response to the external stimulus, the membrane potential will return to its natural state of rest.

But, if a stimuli of enough magnitude reaches the cardiac muscle, the potential that remains in the resting state will surpass a critical point known as threshold level, and consequently, a response to the stimulus will be displayed [23]. This response is known as Action Potential.

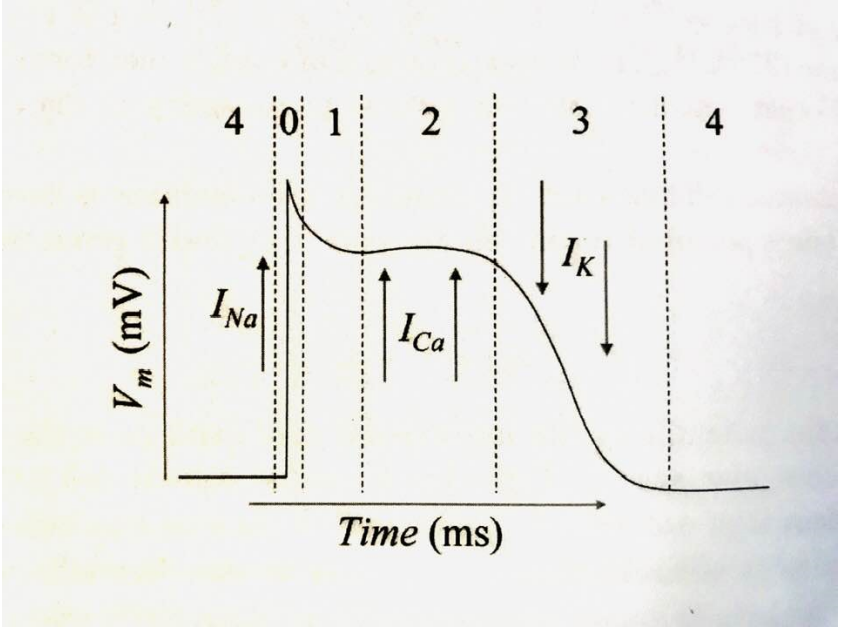

Figure 3.8: A normal action potential with all its phases shown, we can appreciate how and what currents are acting at each point of the signal, i_{Na}, I_{Ca} and I_K are the main actors to give shape to the response. Image taken from [79].

At the beginning, the membrane is in a resting state also known as polarized state, the increase in potential, causes the membrane potential to move towards a more positive voltage, which is known as depolarization. When the cycle of action potential ends and the cell recovers its original potential, this is, returns to the negative value, it is said that the membrane of the cell is repolarized. If the membrane potential exceeds the resting value, the cell is said to be hyperpolarized.

The normal amplitude of an action potential in a cardiomyocyte goes around 130 mV, that is a positive potential in the cell membrane of around 40 mV and 50 mV.

Based on the previously mentioned text about the Nernst potential, this value is close to the sodium value, this means that around this potential the cell membrane is permeable to sodium ions [1].

Phase 0

The rapid rise that can be observed at the beginning of the action potential is due to the flow of the sodium ions through the cellular membrane, creating a sodium current I_{Na}. This slope is best known as phase 0 of the action potential.

Phase 1

The conditions in which the cell is maintained with a positive action potential are not able to be kept for a long time, as soon as a sudden entry of N_a+ ions occurs during phase 0, due to the conditions existing at that moment, the cell membrane begins to return to its polarity that it had before the arrival of the stimulus that caused the action potential to go off, in other words, it is going to start its repolarization, at the first moment it is fast so that a peak can be observed which will receive the name of Phase 1.

Phase 2

The repolarization initiated during phase 1 does not proceed immediately, this is followed by a prolonged delay, named phase 2, during this, a balance will be observed between the input and the output of charges in the membrane. The main actors in this phase are the calcium currents I_{Ca}.

Phase 3

In order for the membrane potential to return to its resting state, the potassium currents I_k will be the next to flow through the cell membranes. Phase 3 is going to be in which the calcium currents cease their flow; at the end of this flow of calcium ions into the cell, which were responsible for maintaining the membrane potential in depolarization. The potassium ions are going to be the new occupants of the channels, which will now be responsible for returning the membrane potential to a state of rest.

Phase 4

At the end of phase 3 the cell membrane will acquire the same potential that it had in its resting state.

In summary, the action potential is a signal that will represent the changes in the membrane potential, and thanks to it we can observe the flow of ions through the cell membrane.

But what happens if the applied stimulus is not enough to activate an action potential? There is a time between action potentials in the cells that carry the heart rate, it is possible to take advantage of this time to carry out some type of communication using the electrical properties of these cells as a transmission channel in our communications system. If signals with an intensity lower than that needed to trigger an action potential are used, it is possible to use that signal and propagate it through the cell membrane, to establish a communications system [77, 56].

3.5.2 Subthreshold Behavior

An external stimulus in the cell membrane will cause a change in the permeability, and will predominate the entry of ions of N_a+ to it, it will alter the potential of the membrane making it less negative, in other words, causing a degree of depolarization until reaching a certain level previously called Threshold level, from this threshold, the action potential is going to trigger in an explosive way and it will act in the cell, now, independently of the stimulus that has been applied to trigger it, once this threshold has been reached, any change to the intensity of the stimulus will not be reflected in the action potential.

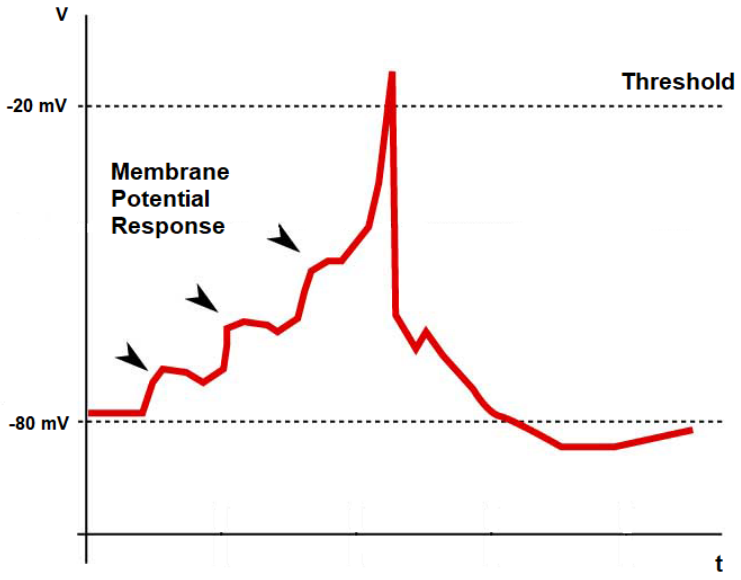

Figure 3.9: In the figure, it is observable that from the resting phase, when an external stimulus not strong enough to trigger the action potential, small responses are going to be shown in the membrane potential, where these are not triggering the actual action potential, but if the potential is taken beyond the threshold point, an action potential is going to present.

For a given stimulus, it is possible to have 2 responses, the cardiomyocyte will respond with an action potential, or the threshold is not going to be reached and there will be no action potential, just an small response. From the threshold level, the cell will have an all-or-nothing behavior regarding action potentials.

If the applied stimulus is in the subthreshold level, this is, it only manages to change the membrane potential a few mV, it will not produce an action potential, in this case the cell membrane will recover its original polarization level after having undergone a slight displacement, but if the stimulus to be applied is of sufficient intensity to reach the threshold level, an action potential will undoubtedly trigger, which will lead to a chain reaction that will spread to the entire cell membrane activating also in the other cells the action potentials in the same way [68, 84].

From the electrical point of view, the stimulus will cause the opening of the channels dependent on the ion N_a+, this will increase the permeability of the membrane in addition to its conductance, which in turn will cause greater depolarization and opening of new channels thus perpetuating the process. Simultaneous to the activation of the N_a+ channels, depolarization will also trigger its inactivation, but in a slower manner [15].

This is an important part in the development of this thesis, because, this behaviour is intended to be used to be able to transmit signals using the heart cells as a transmission channel. We want to be able to take advantage of the small fraction of times in which the heart cells are not involved in the pace keeping process. While these cells are in their resting phase, it is intended to give as input a small signal, not strong enough to surpass the threshold level and trigger an action potential, but instead, be able to just observe an small response in the cell, and this response could be able to propagate between more cells of the tissue. We are studying the possibility to transmit these signals, their reach and characteristics after being transmitted in the tissue [80].

Chapter 4

Modeling

4.1 Mathematical Modeling

A model is an abstract representation of a certain aspect of reality, essentially formed by the elements that characterize this aspect and the relationships between those elements. Generally speaking, a good model is going to adjust to the real phenomenon that it plans to represent in a way that allows us to better understand its properties and thus, expand knowledge of it. The following figure shows the highlighted phases to build a good model.

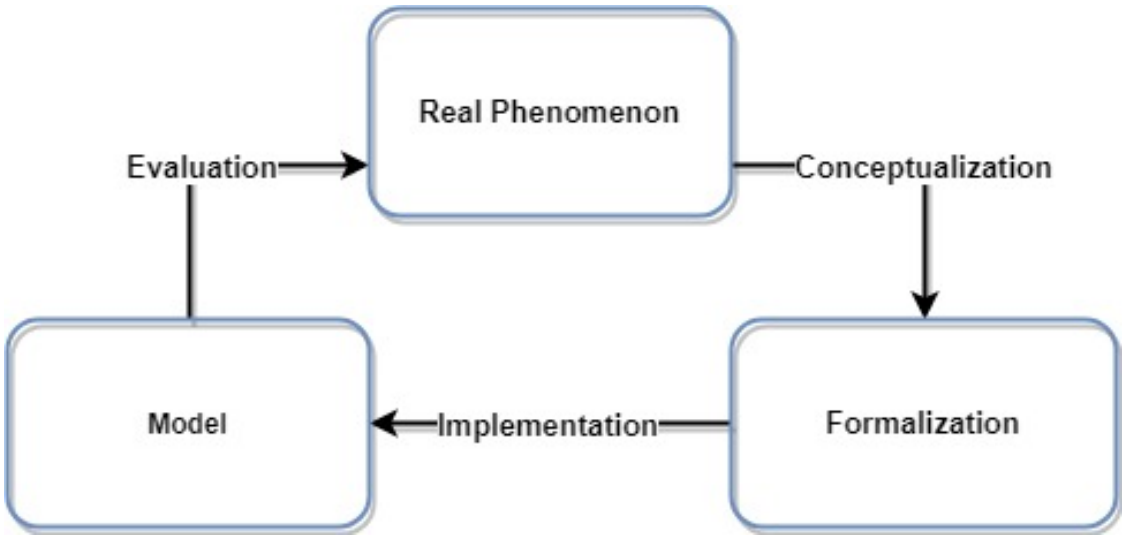

Figure 4.1: How to build a good model, first we have to analyze a real phenomenon, and conceptualize the information to formalize it, when a formalization of the description of the model exists we can now make the implementation to evaluate it. Image modified from [17].

Mathematical modeling will stand out for its effectiveness and properties when trying to explain phenomena. It is presented in different ways: mathematical theories (based on systems of axioms and demonstrations), numerical models (based on linear equations, differential equations, stochastic calculus); or the computational models (based on systems of agents and their interactions, particle systems, evolutionary algorithms), which are becoming important in consequence of the technological capabilities achieved.

Mathematical modeling of processes has many advantages: during the modeling process, relationships are often revealed that are not obvious at first glance, so the task will produce a better understanding of the studied phenomenon; once constructed, it is possible to extract the characteristic properties of the relationships between the elements of the model that would otherwise remain out of sight; it will allow us to represent complex situations that in some other way would not be possible in other types of models, and, will provide a resolution of the problem, although it is not an analytical solution but a numerical made by a system[17].

For our area of study, it will be defined as the process of using quantitative information in conjunction with a qualitative understanding to be able to produce a tool that has a behavior very similar to the system that is intended to explain or model. It is very difficult to make an exact model of a system as it is.

This process must be, by obligation, iterative and improved with each of these iterations, the figure 4.2 will explain the process.

The first step to be done is to identify the main problem, then this or these problems must be described using mathematics, it is necessary to identify all the important points to describe, in order to formulate equations and variables correctly. By having the equations at hand these must be solved, to obtain a mathematical solution to the problem, which in turn must be interpreted to relate the numerical meaning with the behaviors that are planned to study. These results must be compared with the reality, it is passed trough a process of validation and verification. It is possible that there is room to make modifications, or improvements in the mathematical models initially proposed so that they better describe the desired process.

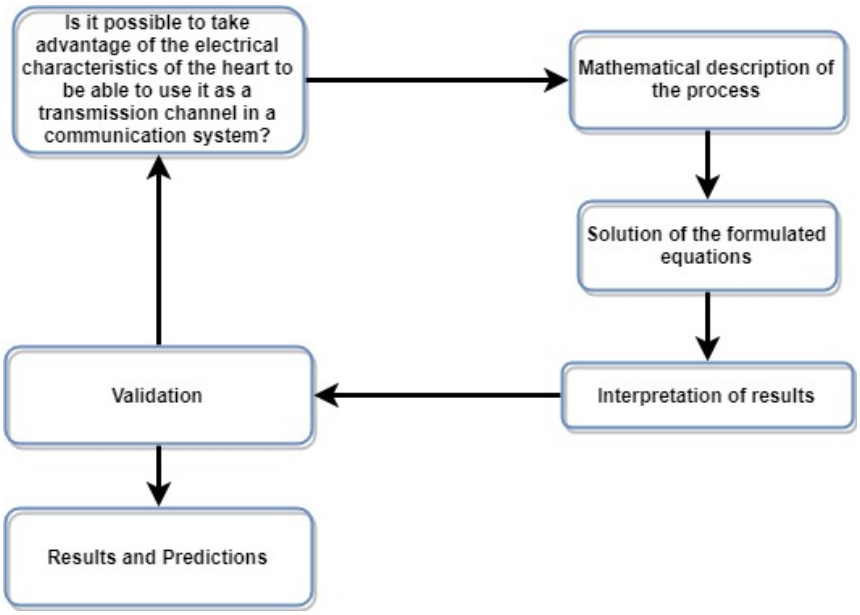

Figure 4.2: How can we utilize the subthreshold region of the cardiac action potential to be able to transmit information using that region and the idle times where not pacemaking functions are being held. This is the process that we are going to follow to create our model, beginning with the mathematical description of the functioning, to the solution of the mathematical formulas, to finalize with the interpretation and validation of results. Adapted graph from [79].

In the area of biomedicine there is a great diversity of types of variables, but, specifically for the area that is being developed in this thesis, which is the modeling and behavior of the heart and its cells as a transmission channel for a communications system , it will be necessary to consider the information from an anatomical, physiological, biological point of view, and from previous clinical experimentation data [79].

4.2 Units

There is no official standard on which units should be used for a mathematical model of the electrical functioning of the heart, and neither can we speak of a correct or incorrect set of them. However, mention can be made of a system that is under development, to solve the problems that exist associated with the transcription and interpretation of different types of models, CellML. However, a set of units for the electrical modeling of cellular physiology have been proposed, which can be found in tables 4.1 and 4.2.

By adopting a consistent system of units, the aim is to avoid the problem associated with the translation and interpretation of different types of models described by different authors.

Table 4.1: Units of the SI and their multipliers used in the development of the framework.From [79].

Parameter	SI units	Multiplier	Cell units
Lenght	metre, m	10^{-3}	millimetre mm
Mass	kilogram, kg	10^{-12}	nanogram, ng
Time	second, s	10^{-3}	milliseconds, ms
Electric current	Ampere, A	10^{-6}	microampere, μA
Temperature	Kelvin, K	10^{0}	Kelvin K
Amount of substance	mole, mol	10^{-9}	nanomole, $n$mol

Table 4.2: Derived units used in electrophysiological models based on multipliers of the SI V = Volts; S = Siemens; C = Coulombs; F = Farads; M = Molar; N = Newtons; Pa = Pascals; J = Joules; W = Watts. From [79].

Parameter	Basis	Units
Area	mm^2	mm^2
Volume	mm^3	mm^3
Voltage	$mm^2\ ng\ ms^{-3}\ \mu A^{-3}$	mV
Conductivity	$mm^{-2}\ ng{-}1\ ms^3\ \mu A^2$	mS
Membrane Conductance	$mm^{-4}\ ng{-}1\ ms^3\ \mu A^2$	$mS\ mm^{-2}$
Tissue conductivity	$mm^{-3}\ ng{-}1\ ms^3\ \mu A^2$	$mS\ mm^{-1}$
Current density	$mm^{-2}\ \mu A$	$\mu A\ mm^{-2}$
Volume current	$mm^{-3}\ \mu A$	$\mu A\ mm^{-3}$
Charge	$ms\ \mu A$	nC
Capacitance	$mm^{-2}\ ng{-}1\ ms^4\ \mu A^2$	μF
Specific Capacitance	$mm^{-2}\ ng{-}1\ ms^4\ \mu A^2$	$\mu F\ mm^{-2}$
Concentration	$mm^{-3}\ nmol$	mM
Concentration rate	$mm^{-3}\ ms^{-1}\ nmol$	$mM\ ms^{-1}$
Force	$mm\ ng\ ms^{-2}$	nN
Stress (pressure)	$mm^{-1}\ ng\ ms^{-2}$	mPa
Energy	$mm^{-2}\ ng\ ms^{-2}$	pJ
Power	$mm^2\ ng\ ms^{-3}$	nW

4.3 Modeling the membrane

An action potential, or stimulus applied to a cell which will not trigger the action potential, this is, it will stay below the threshold level, will mean changes in the cell membrane, more specifically in the membrane potential, these changes can be illustrated with an electrical circuit as seen in figure 4.3.

The cellular membrane, by its characteristics, will act as a capacitance, (due to its bi-lipid membrane and the flow of currents through it) which will be connected in parallel with a series of resistances, and these at the same time are dependent on the membrane potential and time, they will represent the currents that flow through the cell, and these currents will vary depending on the type of ion that is being formulated [34].

The difference between the membrane potential and Nernst potential of each ion will indicate in which direction of the cell membrane the currents are flowing.

$$I_x = g_x(V_m - E_x) \tag{4.1}$$

Where:

E_x: Nernst potential for ion x.

g_x: Conductance of the channel for ion x.

(Conductance is the inverse of resistance so $g_x = 1/R_x$).

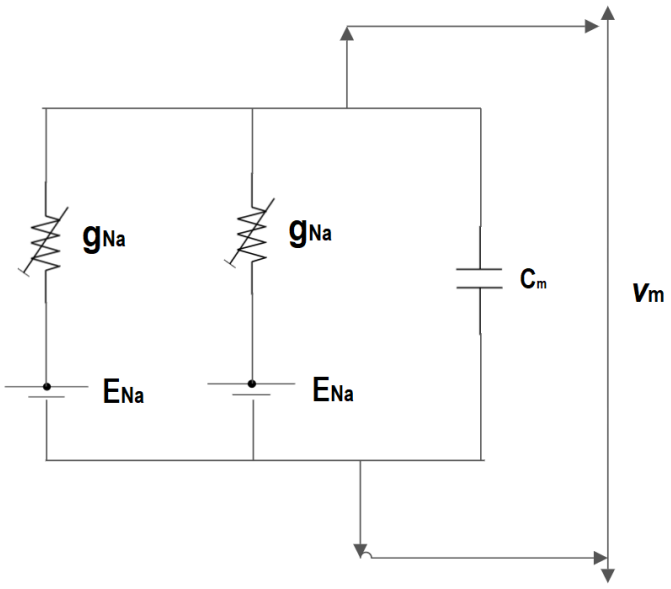

Figure 4.3: This electrical circuit will represent the flow of electrical currents through the cell, which will depend on the conductance of the channel, and the direction will be tied to the difference between V_m and the Nernst potential that acts as voltage source in the circuit. The current passing through the bi-lipid membrane of the cell is modeled as a capacitance C_m in parallel with the currents of the ion channels. Note: the circuit illustrates only two currents in the cell, but the amount of these will vary depending on the model. From Huxley model [42].

Having the conductances in parallel in the electric model of the cell will mean that the currents that interact in the ion channels can be summed, so we can call I_{ion} to the total sum of currents that will interact with the cell through the ion channels.

$$I_{ion} = \sum_{x} I_x \tag{4.2}$$

Where:

I_{ion}: Sum of all currents interacting in the membrane.

I_x: Current of the ion x.

The number of ion channels and currents that will interact in the membrane potential to form the total current I_{ion} will vary depending on the experiments performed and data obtained by each author in each electrical model of the heart.

The total flow of currents through the membrane over a certain time t, will be determined by placing this current in parallel to the current passing through the capacitance of the membrane C_m, which will yield the following expression .

$$I_m = C_m \frac{dV_m}{dt} + I_{ion} \tag{4.3}$$

Where:

C_m: Capacitance of the membrane.

I_m: Current trough the cell membrane over time t.

I_{ion}: Ionic currents acting in the membrane.

Vm: Difference of potential across the cell membrane.

The action potential of a cell will be given by the following formula.

$$\frac{dV_m}{dt} = \frac{-\left(I_{ion} + I_{stim}\right)}{C_m} \tag{4.4}$$

Where:

I_{stim} : External stimulus required to trigger the movement of ions in the cell.

Due to the non-linearity of the terms, it is difficult to find a solution where the equation 4.4 can be solved analytically, this means, it will be required an additional approach to solve via numerical integration. For this step, a set of solvers are available to deal with these formulations, which will be reviewed later in the document.

4.4 Modelling Gap Junctions Connectivity

We have already talked about different important elements that act in the structure of cardiomyocytes: channels that connect the membranes, formed by connexins, (these so called gap junctions) that are responsible for propagating the current between cells (action potentials), as well as the capacitance in the membrane of the cell that regulates the displacement of current.

Now, it is important to mention the behavior of the gap junction, we are interested in obtaining a real measure of transmission velocity in the tissue, so it is important to model all the affecting variables.

As seen before the myocardium is not a nice and planar tissue where everything is connected perfectly, (refer to Figure 3.7) gap junctions are not perfectly formed through the tissue. So, we can propose a model where the gap junction connectivity affects the transmission of the signal presenting a resistance opposing this electrical signal, depending on the alignment of the cardiomyocytes, where this resistance will go up if the alignment is not perfect or it will present less resistance if it presents better alignment; meaning that when the cardiomyocytes are better aligned, more ion channels will be present between the membranes of the contiguous cells [63, 25].

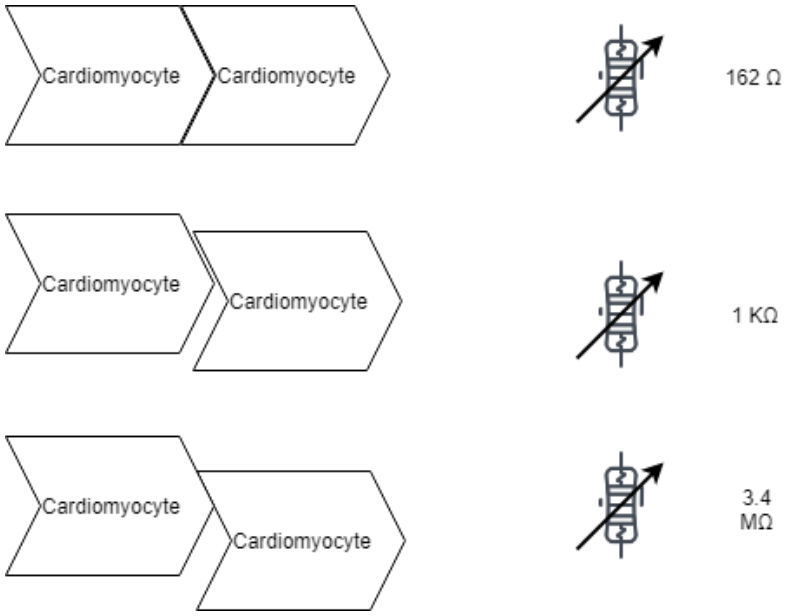

Figure 4.4: Depending on the alignment of the cardiomyocytes, more ion channels will be present that will allow the flow of ions through the membrane of the connecting cells. Made after [91, 11]

To achieve this optimal transmission velocity, a model of Taggart et al. will be used for the resistance of the gap junction where a very wide range of the cells will require a resistance of $162\Omega cm$. In comparison, other studies made by Bernus et al. a resistance of $180\Omega cm$ [91, 11].

This model illustrates the connection between cardiomyocytes as a variable resistance as shown in Figure 4.4, depending on the number of channels that exist between the membranes of two cells. It is intuited that these are aligned or misaligned, observing the value of resistance between them. The greater the alignment between cardiomyocytes, the less resistance, and viceversa.

4.5 Cardiac Cell Models

There are many models of cardiac cells, most of them structured based on the Hodgkin-Huxley model of a giant squid axon [42]. Departing from this point, passing through the DiFrancesco model of Purkinje Fibers, to the most recent ones such as the one proposed by Luo & Rudy in 1994 [65].Each model that has been appearing in scientific publications, is making the description of cardiac cells increasingly complex, in which every single one of the variables that intervene in the functioning of these are added with the passage of time [85].

In the development of this thesis, it was considered to use the cell model proposed by Dokos, Celler & Lovell in 1996, describing the cardiac cell of a rabbit based on scientific experimentation in conjunction with a more recent model proposed by Kurata, Hisatome, Imanishi & Sibamoto in 2002, in which data from experiments on cardiomyocites of rabbits are used in the same way, but with many added variables [28, 59].

4.6 Ten Tusscher Model

For the purpose of this thesis, and to carry out the model corresponding to a communication system using the cells of the heart as a transmission channel, the model described by: Ten Tusscher, D. Noble, PJ Noble, and AV Panfilov in his paper entitled: "A model for human ventricular tissue" will be used as a basis [92].

This model was formulated, in the beginning, to have the possibility to study cardiac arrhythmias in the myocardium. In this study, a mathematical model is proposed on how action potentials are generated, with a very high level of electrophysiological detail, which makes it very intensive to simulate.

The model formulated by Ten Tusscher is based mainly on data obtained through recent animal experimentation, because the possibilities of conducting experiments and obtaining data from human hearts is very limited. One of the limitations is that the behavior of a heart other than the human heart, will make the results obtained, to have a variation compared to results that can possibly be obtained with human heart data, due to obvious variations such as the size, however, this is a very extensive model that includes 12 currents which will interact with the cellular membrane to generate an action potential in contrast to the two currents with which this phenomenon was being modeled in previous pages of this document.

This model is based on a previous and more basic model formulated by Luo & Rudy, with data obtained from guinea pig heart cells, and it shows an important problem, the duration of the action potential is about 360 ms, duration that is much higher than the human measure which is close to the range of 270 ms [65].

The most important ionic currents are taken into consideration, such as I_{Na} based on the sodium ions that cause the magnitude of the action potential to rise in phase 0, the current I_{CaL} corresponding to the calcium ions and the slow delayed rectifier current I_{Kr} corresponding to the potassium ions which cause the potential in the membrane to return to the negative side, in other words, to its resting state.

As was analyzed in previous pages, the model explains that the electrophysiological behavior of an action potential will be governed by the following equation.

$$\frac{dV}{dt} = -\frac{I_{ion} + I_{stim}}{C_m} \tag{4.5}$$

Where:

V: Voltage.

t: time.

I_{ion}: Sum of al ionic currents in the membrane.

I_{stim}: External stimulus.

C_m: Cell capacitance.

The sum of all the currents that will interact in the membrane, this is, I_{ion} will be formulated by all the currents that describe the operation of the action potential, as previously mentioned, these will be 12, it is given by the following formula.

$$I_{ion} = I_{Na} + I_{K1} + I_{to} + I_{Kr} + I_{Ks} + I_{CaL} + I_{NaCa} + I_{NaK} + I_{pCa} + I_{pK} + I_{bCa} + I_{bNa} \quad (4.6)$$

Where:

I_{Na} : Fast $Na+$ current.

I_{K1} : Inward rectifier $K+$ current.

I_{to} : Transient outward current.

I_{Kr} : Rapid delayed rectifier current.

I_{Ks} : Slow delayed rectifier current.

I_{CaL}: L-type Ca^2+ current.

I_{NaCa} : $Na+/Ca^2+$ exchanger current.

I_{NaK} : $Na+/K+$ pump current.

I_{pCa} : Plateau Ca^2+ current.

I_{pK} : Plateau $K+$ current.

I_{bCa} : Background Ca^2+ current.

I_{bNa} : Background $K+$ current.

The rest of the formulas that conform the model and the initial conditions of it can be found in the appendix of this document and the experiments conducted when building this model in [92].

4.6.1 Modifications to the Model

As previously mentioned, it is required to use the part of the subtreshold behaviour of the cardiac cells to transmit information using this medium as a transmission channel. For this it is necessary to modify the model and make it more suitable for it to be able to work in this region.

Hyperpolarization

As it is defined textually in the medical dictionary: "Hyperpolarization: is the increase of the internal negativity of the membrane, so it becomes less sensitive to stimuli" [48].

In order to keep the potential below the threshold level, we will exploit the hyperpolarization phenomenon in the cell membrane.

Hyperpolarization is going to be observed, when the membrane becomes more negative at a particular point, this occurs when the ion channels of the membrane open or close, and will alter the ability of certain types of ions to enter or leave the cell [86].

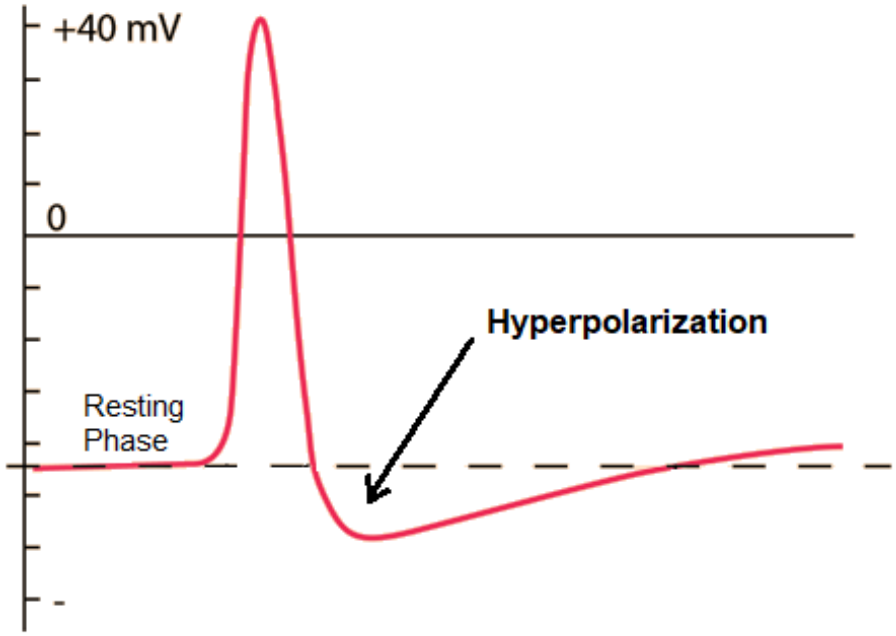

Figure 4.5: Hyperpolarization can be observed, the voltage of the cell goes below it is normal resting state level, effect of $K+$ ions.

The opening of the channels that allow the flow of positive ions out of the cell can cause hyperpolarization. These channels will be, the ones that let the $K+$ ions out of the cell [72, 71].

The opening and closing of these channels may depend on the binding of signaling molecules, such as neurotransmitters, or on the voltage across the membrane [14].

According to previous research produced by William A. Caterrall, ion channels can be voltage-gated, in other words, gates that are a characteristic part of these channels and allow the passage of ions outside and inside the membrane can be controlled by an stimuli voltage, with these stimuli you can achieve the opening or closing of these channels to a certain degree [18, 19, 97].

This means that it may be possible to control the opening of the sodium or potassium channels, which are where the ions, that have the most influence on the positive or negative charge of the cell membrane are flowing. As it was seen before, the ion of $K+$ is the one that influences the repolarization of the cell, making it more negative [29].

There are conditions that can occur in the heart, and will affect its electrophysiology, such as Hyperkalemia, this refers to a high level of potassium in the blood.

Based on a study by James N. Weiss, these high potassium levels can come combined with an increased arrhythmia condition. The electrophysiological effects of this condition will be [95]:

- Shortening of the duration of the action potential.
- Increase of $K+$, which will increase the conductance of $K+$ ions.
- Less amount of channels of N_a+ will be available, which will mean that there will be less contributions to the upstroke of phase 0 of the action potential.
- Produces arrhythmia mechanisms.

Formulas

Based on studies in neurons, where the action potentials are also present, we will increase the total amount of currents that will describe the membrane potential to 14 currents. Two currents will be added to the model: hyperpolarization-activated current, I_f, and a sustained potassium current, I_{sus} [35, 78, 53, 12].

The purpose of these currents is to give the $K+$ potassium channels a wider participation in the electrical potential of the membrane, which will help the cell membrane to be less vulnerable to the rise of the action potential, and more viable to its functioning in the subthreshold area.

The new description of I_{ion} that arises with the 14 currents would be as follows:

$$I_{ion} = I_{Na} + I_{K1} + I_{to} + I_{Kr} + I_{Ks} + I_{CaL} + I_{NaCa} + I_{NaK} + I_{pCa} + I_{pK} + I_{bCa} + I_{bNa} + I_f + I_{sus} \quad (4.7)$$

Where:

I_{Na} : Fast $Na+$ current.

I_{K1} : Inward rectifier $K+$ current.

I_{to} : Transient outward current.

I_{Kr} : Rapid delayed rectifier current.

I_{Ks} : Slow delayed rectifier current.

I_{CaL}: L-type Ca^2+ current.

I_{NaCa} : $Na+/Ca^2+$ exchanger current.

I_{NaK} : $Na+/K+$ pump current.

I_{pCa} : Plateau Ca^2+ current.

I_{pK} : Plateau $K+$ current.

I_{bCa} : Background Ca^2+ current.

I_{bNa} : Background $K+$ current.

I_f : Hyperpolarization-activated current.

I_{sus} : Sustained potassium current.

The equations that describe these two currents can be found in the appendix.

As reference points for this model, it should be highlighted that the voltage in the resting state of the cell will be around $-84\ mV$ and the threshold point will be in the $-20\ mV$ mark [13].

4.7 Myocardium Propagation

4.7.1 Boundary Conditions

It is impossible to model myocardial tissue if it is intended to model cell by cell the functioning of it, this is because there is a huge number of cells in the tissue, and, in addition, a simulation of this type would be very computationally intensive and impossible to perform.

For this it must be considered that the cells are connected, and this set of interconnected cells, should be considered as a whole. The tissue of the heart can then be seen as it was previously mentioned in this document: as two continuous spaces, the $\boldsymbol{i}$ and the $\boldsymbol{e}$. Each of these domains being extremely complex to be able to be represented individually in its entirety.

For these reasons, these two domains are modeled in a single concept, both interacting in the same space and covering the entire space of the myocardial tissue at the same time. So we can say that each point of the myocardial tissue belongs to both spaces, the $\boldsymbol{i}$ and the $\boldsymbol{e}$.

This formulation is known as the Bidomain model and is responsible for explaining the electrical properties that the tissue will have in a whole, making use of the cellular behavior $\boldsymbol{i}$ and $\boldsymbol{e}$, therefore there will be no necessity to make the individual computation of the behavior of each cell; in addition, this model in conjunction with a different one called Monodomain, will take into consideration the electrical potential around the tissue that is planned to be studied [40, 41].

The tissue intended to be used as a transmission channel in this study, is an excitable tissue, it will give a response when it enters in contact with an electrical stimulus, but, the tissue that surrounds it, and is not part of the heart, is a tissue that is mostly non-excitable, in other words, the cells around this tissue are not going to present affectations in their electrical characteristics when they encounter an stimulus of the same type.

This is why we must define in the model, a set of boundary conditions, that will take into consideration these two spaces, by making the cells and tissue, that are different from the myocardium, function as a passive conductor.

Assumptions made in the Bidomain model

- Assume that the body is insulated from its surroundings.
- $\boldsymbol{i}$ is insulated from the myocardium, and the rest of the heart tissue.
- $\boldsymbol{e}$ is going to connect directly to the neighboring tissue.

The bidomain model is a very complex system of equations, and is used when it is intended to include in the simulations the rest of the body, which will provide various factors affecting the system. For the simulations conducted in this research, both models are used to perform simulations; but when using the monodomain model, it will be because the objective is to analyze what is happening considering only the tissue and the affections in the heart, but not the whole body. The disadvantage of this model is that it can not be immediately coupled to the rest of the body. For more information about the equations that make up this model [40, 41].

Chapter 5

Implementation

5.1 Tools

5.1.1 System characteristics

The implementations, simulations and solutions of the model proposed in this thesis were made using an MSI GT72VR computer with Microsoft Windows 10 Home 64-bit OS, a GeForce GTX 1070 GPU, Intel® Core™ i7-6700HQ processor CPU @ 2.60GHz, RAM of 23.96 GB.

5.1.2 Solvers

Each model mentioned, which will be responsible for describing the electrophysiological functioning of the heart, is formulated as an ordinary system of differential equations (ODE). From this system it is intended to obtain a result over time to be able to observe the response and behavior of electrical signals, i.e. the action potential. Most of the first formulated models were solved by the forward Euler method, using a time step of microseconds [37].

In more recent and complex models that have a large number of differential equations, it was necessary to use a more effective integration method; in these new models the method of Runge Kutta is used. This method has greater precision, by including higher order terms belonging to Taylor series. In short, when solving using this method, another evaluation function is added between two-time fractions, in order to update the time step [47]. This method is also known as the improved Euler method.

In all systems of integrators that exist, there is an adaptive time-stepping scheme, and variable polynomial orders implemented. In the end the choice of integrator to use will depend on the personal preference of the available tools, and which of them delivers an optimal solution to the system of equations in a shorter amount of time.

An extra factor to consider in the choice of the solver, especially in the formulation of our model, due to the complexity and number of equations, is the stiffness of the system, this is, the measure of how difficult it is to solve numerically, and it is going to be characterized by a disparate scale of times. If a cell measurement is operating on a time scale, for example, in milliseconds and another characteristic is operating in microseconds, as can be seen in the table of units to be used in our system; then a time step of the microsecond order will take a thousand times longer than necessary to solve the slower characteristic, this will lead to an accumulation of errors. On the other hand, a time step of the millisecond order will cause instabilities in the fastest features of our model. All these problems are very recent in electrophysiological modeling, due to the gradual increase of characteristics in the new models as they are being formulated. These stiff solvers will be responsible for using implicit integrated schemes that are more stable [16].

The tool used to solve these ODEs, uses an integrator that is capable of dealing with this stiffness in the model, this is going to be fundamental because the model used as a basis for the simulations of our communications system, is one of the most recent and complex electrophysiological models, in addition, modifications have been made to be able to handle potassium ions more effectively, adding a broader description in its equations and therefore making the model that will describe the behavior of the action potential and the subthreshold behavior more complex.

5.1.3 Myokit

As it is explained in its website, Myokit is an open source simulator, based on Python programming language, and is designed to facilitate and simplify the use and numerical modeling that aim to describe the electrophysiological activity of the heart [20]. Created by the University of Maastricht, is a software that is currently being optimized by the University of Oxford.

Myokit is a software that allows the modeling of cellular characteristics using ODEs that describe these processes, we are be able to perform simulations in which the behavior of a single cell can be observed, with a possibility of performing also a simulation in one dimension or in two dimensions; the simulator has the ability to make use of the CPU and GPU of the system where it is implemented to accelerate the simulations.

When the model is implemented, this simulator has the ability to export or import the implementation to a set of different programming languages, which facilitates standardization with models proposed in languages other than Python or in other types of software. It is possible to export to CellML, the standard language for cell modeling, which will be discussed in the following pages; to C, or Matlab, which are the languages most used for this type of modeling. These facilities are possible thanks to the separation of the code that is in charge of all the description, and the base of the software, where the libraries and solvers that give solution to the systems of equations are implemented.

The software has a GUI that makes the simulation work simple, by allowing to observe graphs in specific fractions of time, as well as to observe different types of responses in a same screen, in different sections of the cell.

To make use of this tool it is necessary previously to have installed on the PC other third-party software, for the correct functioning, among which are: Python, SUNDIALS, CUDA, OpenCL.

5.1.4 CVODE

To solve the differential equations systems, Myokit uses a tool developed by SUNDIALS (SUITE of Nonlinear and Differential / ALgebraic Equation Solvers).

As explained on the website, CVODE is a solver designed for stiff and nonstiff Ordinary Differential Equations (ODE) systems (with initial value problem). The methods used by CVODE to solve are variable-order and variable-step multistep methods. For either choice of formula, the resulting nonlinear system is solved (approximately) at each integration step [88].

The installation of the SUNDIALS CVODE library was required in the PC used for the modeling and simulation explained in this thesis [89].

5.1.5 OpenCL

When performing 2D simulations of tissue, libraries of OpenCL had to be installed. As the process of simulating 2D tissue is very computationally intensive, it cannot run in the CPU, so it had to be parallelized in the GPU of the computer.

OpenCL NVIDIA packages where used along for the simulations, found at [22].

5.1.6 Python

Python will act as the programming language and base of the myokit software, which will allow the implementation of the model to be simple and flexible, this due to the possibility of creating scripts that are going to allow the automation of certain functions of the simulations in a fast way.

To make possible the use of Myokit, it was required to install in the PC the Miniconda 2.7 (64bit) package that can be found in [6].

In addition, the Microsoft Visual C / C ++ libraries required as a compiler for Python 2.7 were installed, which can be found in [70].

5.1.7 Language

The language in which the described model was implemented was Python since it is the basis of the Myokit implementation as previously mentioned. Several documents were generated describing systems of equations, and scripts to implement behavioral simulations of either action potential or subthreshold behavior in one or more cells. The choice of this language was made considering the easy standardization with other languages commonly used in electrophysiological modeling such as Matlab, C and CellML [33].

5.1.8 CellML

The importance of the model being easy to import and export to the CellML language is that this language is rapidly becoming a standard, in an effort to reduce the problems associated with the transfer and transcription of cellular models [64]. Although it is not yet considered a standard, there is a proposal from the Bioengineering Institute of the University of Auckland to incorporate in this language the collaborations of various groups working on molecular communications. This proposal makes use of the markup language XML (eXtensible Markup Language), which is employed to define the standard of tags that can be used to describe a cell from its geometry to its electrophysiological behavior. It is intended that an implementation in CellML, regardless of the author can be interpreted and used incorporating a quick modification of the model, as well as the ease of sharing the information.

5.2 Simulations

5.2.1 1 Cell Simulation

The first step was to simulate the response that causes an electrical stimulus in a cell of our model, first with the objective of observing an action potential, to compare the form of this action potential generated with the new model proposed against the action potential generated by the model established by Ten Tusscher, in order to corroborate the correct operation of the model.

After making sure of the correct functioning, the next step was to reduce the electrical stimulus used to generate the response in the cell, in order to obtain a response below the threshold level, because the purpose of this research is to be able to use the generated model to simulate a communications system using cardiac cells. It is fundamental that, upon receiving these stimuli, the response does not exceed the threshold level for any reason, exceeding it would imply the generation of an action potential, meaning an alteration of the heart rate.

The signals used to observe the response of the cell and the rest of the simulations, are signals used in the field of digital communications, in the first case, a square signal with an amplitude of 50 mV and a duration of 5 ms and a second signal consisting in a Dirac delta function of the same amplitude of 50 mV and a duration of 5 μs.

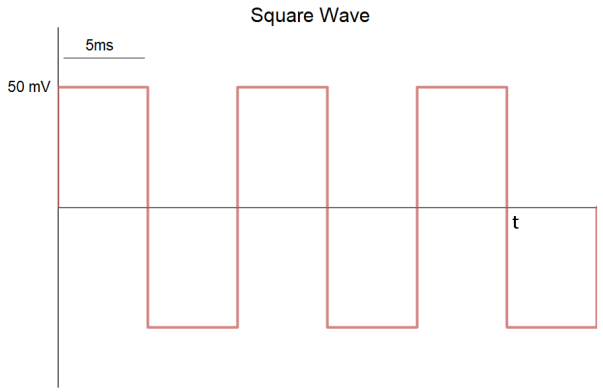

Figure 5.1: The square wave signal used to stimulate the tissue will have an amplitude of 50 mV and a duration of 5 ms.

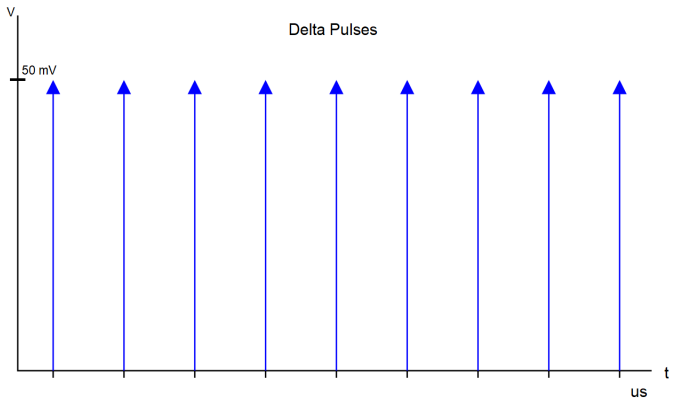

Figure 5.2: The Dirac pulse function used to stimulate the tissue will have an amplitude of 50 mV and a duration of 5 μs.

5.2.2 1D Simulation

After implementing the system of differential equations corresponding to the Ten Tusscher model in conjunction with the respective modifications previously made in the document, and having performed the simulations to observe the electrical behavior in a cell, a script was generated in order to perform simulations in one dimension, this is, a scenario was set up in which the functioning of more than one cell of the system could be observed in a cable arrangement. The cells are going to be connected one behind the other in a line, there will be a resistance of 162 Ωcm between cell connections.

At the beginning of the cable arrangement, it is intended to introduce a signal previously described, with enough intensity for it to provoke a response in the membrane potential, but taking care not to activate an action potential. With this we want to observe the behavior of the signal when it is introduced into the transmission channel, and how it propagates between cells assuming that it only has one direction to propagate. It is necessary to observe the duration of the signal in the cell, and how it will change between cells.

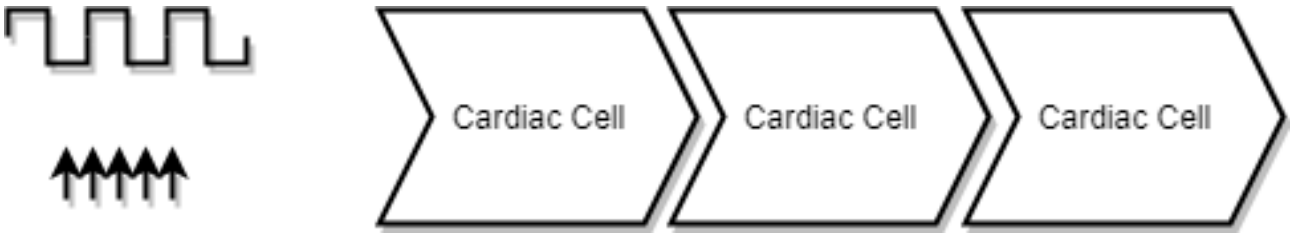

Figure 5.3: Cell arrange to simulate a cable of connected cells, the input signal will be fed into the first cell to observe the propagation in the rest of the arrange.

5.2.3 2D Simulation

2D simulation requires special software and hardware functionalities to function correctly. It is necessary to use a new aspect of Myokit to perform parallel simulations, since the 2D simulation involves an array of a large number of cells we are going to use OpenCL for this implementation.

We are going to generate a square structure of tissue composed of a large number of cells connected in two ways; on in which the cells have the same conditions of connection between them, present in all the tissue towards any of its axes, and, one in which the tissue is composed of arbitrarily connected networks of cells.

The 2D tissue model will be modeled by the following equation:

$$\frac{dV}{dt} = -\frac{I_{ion} + I_{stim}}{C_m} + \frac{1}{p_x S_x C_m}\frac{d^2V}{dx^2} + \frac{1}{p_y S_y C_m}\frac{d^2V}{dy^2} \tag{5.1}$$

Where:

p_x : Resistivity in x direction.

p_y : Resistivity in y direction.

S_x : Surface to volume ratio in x direction.

S_y : Surface to volume ratio in y direction.

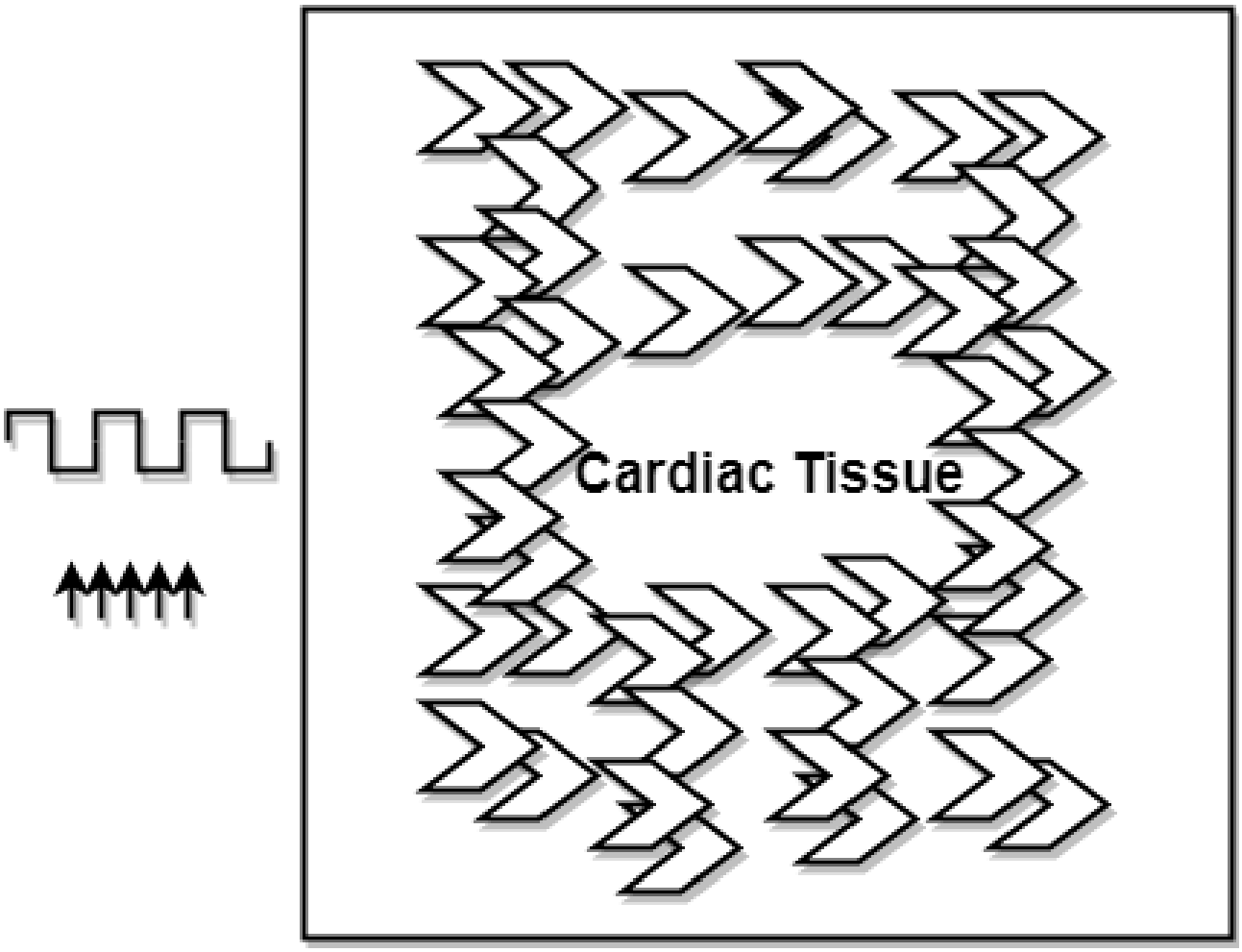

Figure 5.4: Figure used to represent how the 2D cardiac tissue will be arranged in the simulations, it will not be all homogeneously connected like the cable simulation, but the cardiac cells will be all around the tissue.

Chapter 6

Results

Throughout this chapter we will provide the results of all the simulations carried out, we will begin by observing and analyzing the baseline of our system, the Ten Tusscher model, we intend to observe the correct operation of the model, in order to give the go-ahead to begin to make the modifications in which the description of the currents that are going to interact with the membrane are going to be extended adding a wide description and participation of the $K+$ ions as it has been mentioned before.

After checking the operation of the original model, and observing how the modified model works under the same conditions, this is, when generating an action potential, we will proceed to observe the operation of the new model under subthreshold conditions, this is necessary because it is intended that our communications are carried out at this voltage level in the cell membranes. This behavior is intended to be analyzed by introducing the previously stated signals to perform the stimulation of the cell membrane.

The response will be observed in simulations of 1 cell, 1 dimension arrange and 2 dimensional tissue.

6.1 Ten Tusscher Model

6.1.1 Action Potential Response

In this first image we can observe the implementation of the equations system that will describe the original model of Ten Tusscher which is used as the baseline of this thesis. In the graph each of the phases of the action potential can be clearly distinguished, starting from a resting state in which the cell remains, to the sudden change of potential which corresponds to phase 0, passing through the phase 1 which corresponds to a rapid fall in voltage level belonging to the repolarization, phase 2 will be observable thanks to the plateau, it has to be remarked that the plateau is not very prolonged in this model. Following with phase 3 it can be observed how the repolarization of the cell continues, which is going to stop until the cell reaches its resting state in phase 4.

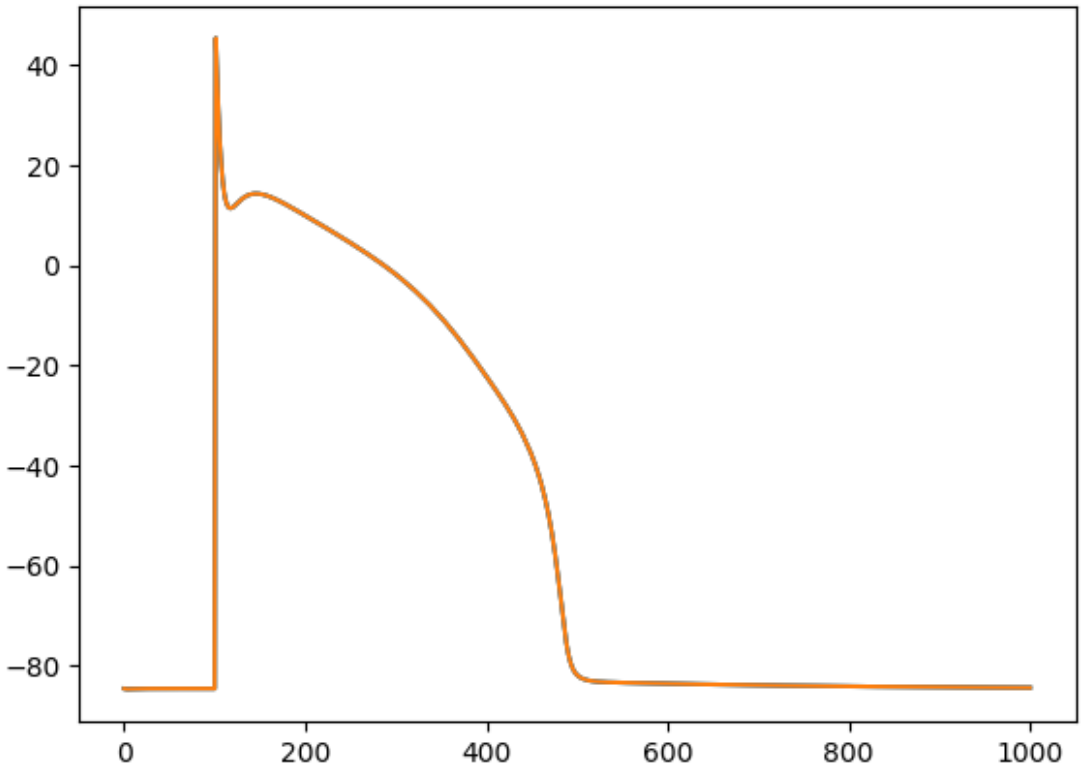

Figure 6.1: Action Potential response after having implemented the Ten Tusscher model. X-axis represented in ms, Y-axis represented in mV.

6.2 Proposed Model

After having checked the normal operation of the Ten Tusscher model as stipulated in the paper that describes it, and having made the changes proposed in the document to generate the new model, the result is shown in the following graph [92].

This image shows an action potential generated after having stimulated the cell. It can be observed unlike the result of the unmodified model, that the increase in phase 0 of the action potential at the beginning is going to be gradual, after phase 0, the rest of the action potential develops without any anomaly, until reaching the point between the phase 3 and phase 4. In this region it can be observed that the potential drops much more to the registered resting potential, this is due to the fact that the model will have more $K+$ ions present thanks to the modifications, and this will cause an increase in the conductances of the $K+$ channels. As explained in previous chapters, these ions are the ones that will contribute to the repolarization of the cell. By having a greater conductance in these channels, the hyperpolarization that was being sought when modifying the model is going to be present.

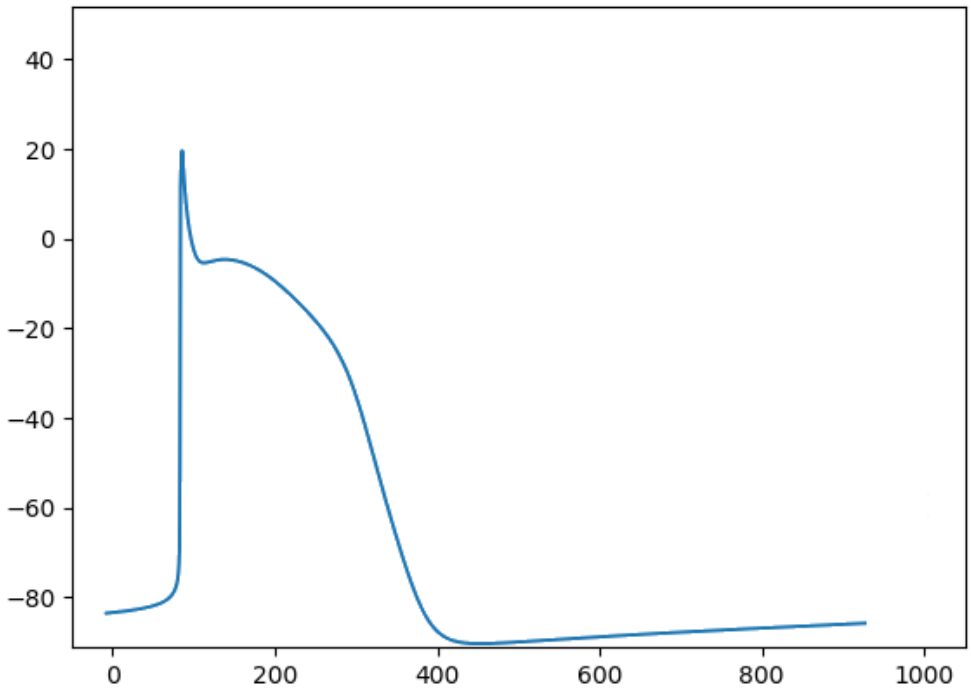

Figure 6.2: Action Potential response after having implemented the modifications to the Ten Tusscher model. X-axis represented in ms, Y-axis represented in mV.

6.2.1 Comparison

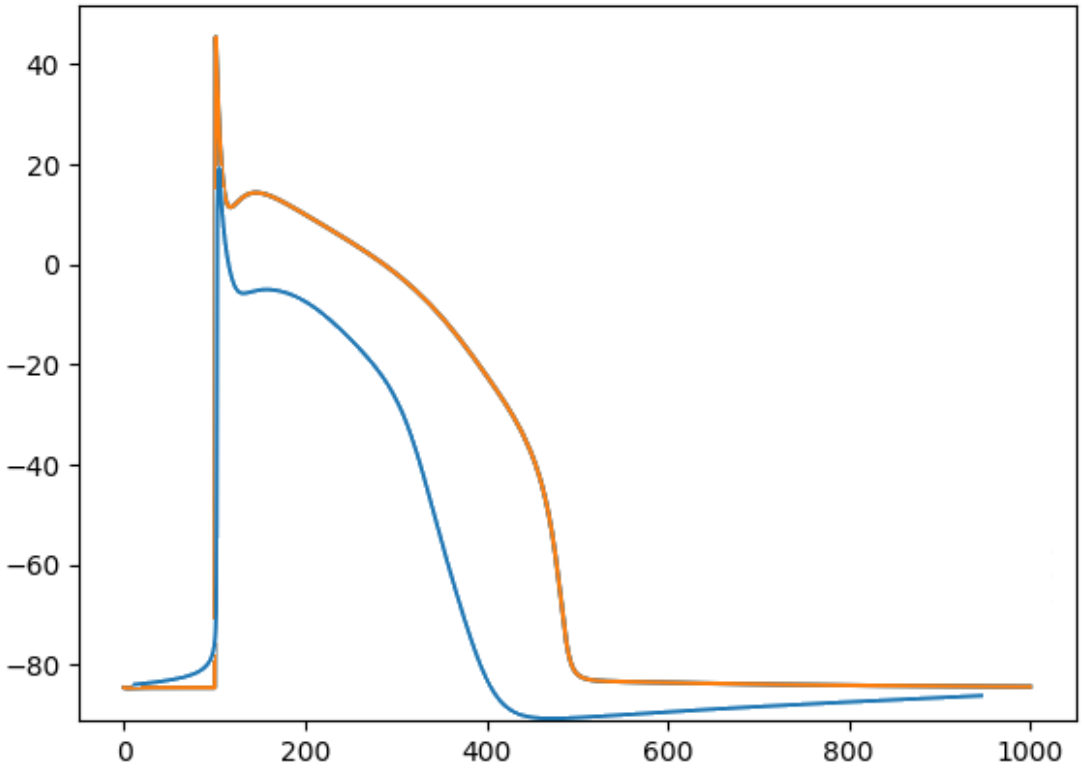

Figure 6.3: Action Potential response comparison of the original model and proposed model. Ten Tusscher model in orange, modified model in blue. X-axis represented in ms, Y-axis represented in mV.

By comparing the action potential responses in the Ten Tusscher model with the model proposed in this document, certain differences can be seen.

The increase in phase 0 of the action potential in the case of the Ten Tusscher model is sudden, it happens in a small fraction of a second, in which the time scale of the graph can only detect a straight rising line, whereas the modified model presents a gradual rise in a start to then continue with this sudden rise. This is because after carrying out the modification adding the potassium and hyperpolarization currents, there will be less available channels of $Na+$ to be activated, these channels are the ones that contribute to the rapid rise in phase 0.

The lower availability of these channels will bring the following characteristic in the action potential of our proposal, since it can be seen that it has a smaller amplitude compared with

that of Ten Tusscher; less channels of $Na+$ less contribution to the depolarization of the cell.

One of the problems that Ten Tusscher enunciates in its model is the duration of the generated action potentials; in its document states that the duration of the action potential is around 360 ms, when the measurements in real hearts show a duration of around 270 ms, it can be seen in the graph that the proposed model reduces the duration of the action potential and approaches the actual measures in real hearts. The last notable difference is the presence of the hyperpolarization curve.

6.3 Dirac Delta Function Results

6.3.1 Phase 0 Analysis

After checking the behaviour of an action potential in the new model, we proceeded with the simulations, now using as the stimulus for the cell the proposed digital signals used in normal communications system.

Making use of the Dirac delta function, as mentioned above, this signal will have an amplitude of 50 mV and a duration of 5 μs, in the figure 6.4 we can observe how the rise will be in the cell membrane potential. It can be seen that, due to the characteristics of the cell, the rise is not sudden as the original signal, at the beginning a sudden rise can be observed, but then it becomes constant until reaching the peak; the time scale in the graph is enhanced to be able to observe the slope.

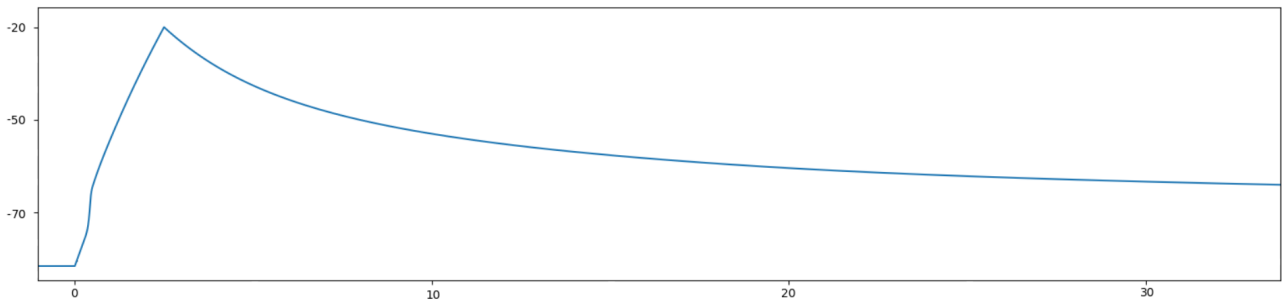

Figure 6.4: Close up of the response observed in a cell membrane after receiving the Dirac delta function. X-axis represented in μs, Y-axis represented in mV.

6.3.2 Sub-threshold results in individual cells

Making use of the Dirac delta function, and decreasing the resolution of time in the graphs, we will be able to observe the behavior when introducing the signal in an array of two cells, connected one after the other.

In the upper part of the graph we can see the response in cell number 1 of the arrangement, the numbers that are on the side of the signal will represent the duration that the response has until returning to a level of 10 % before its resting state, the duration of the recorded signal was 92.757 μs and in the second cell it was 92.450 μs. This decrease in the duration of the signal is due to the fact that as the signal travels between cells an attenuation will be present, an effect produced due to the characteristics of the transmission channel; there is not a drop in the potential to be considered between cells number 1 and cell number 2, and there is also no appreciable delay in the time of both signals, so it can be noted that the signal travels at high speed.

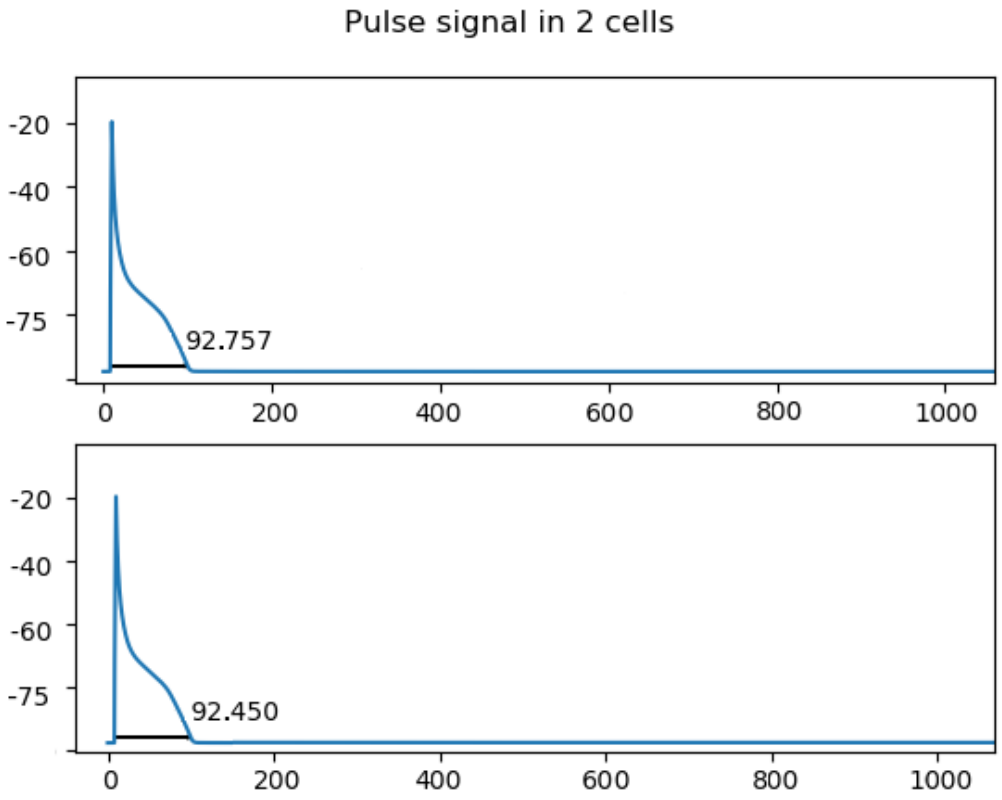

Figure 6.5: Sub-threshold response observed in 1 and 2 cells after receiving the dirac delta function. X-axis represented in μs, Y-axis represented in mV.

6.3.3 1D Results

The figure 6.6 was obtained in a 3D graph so that 3 dimensions that are intended to analyze which are: voltage, time and number of cells were appreciable. An array of 100 cells was made in cable, as it was explained in the previous chapter, in order to observe how the signal propagates not only in two connected cells, but over a long distance.

It can be seen that, like the results obtained in the response in two cells, there is no considerable attenuation between the first two, but, using this type of signal, it is not possible to transmit over long distances within our channel.

The signal begins to dissipate rapidly after a pair of cells traveled exactly before reaching the cell 20, the other components of this array will no longer have any alteration which will mean that they remain in a resting state. There is no delay to consider as the signal does not get very far.

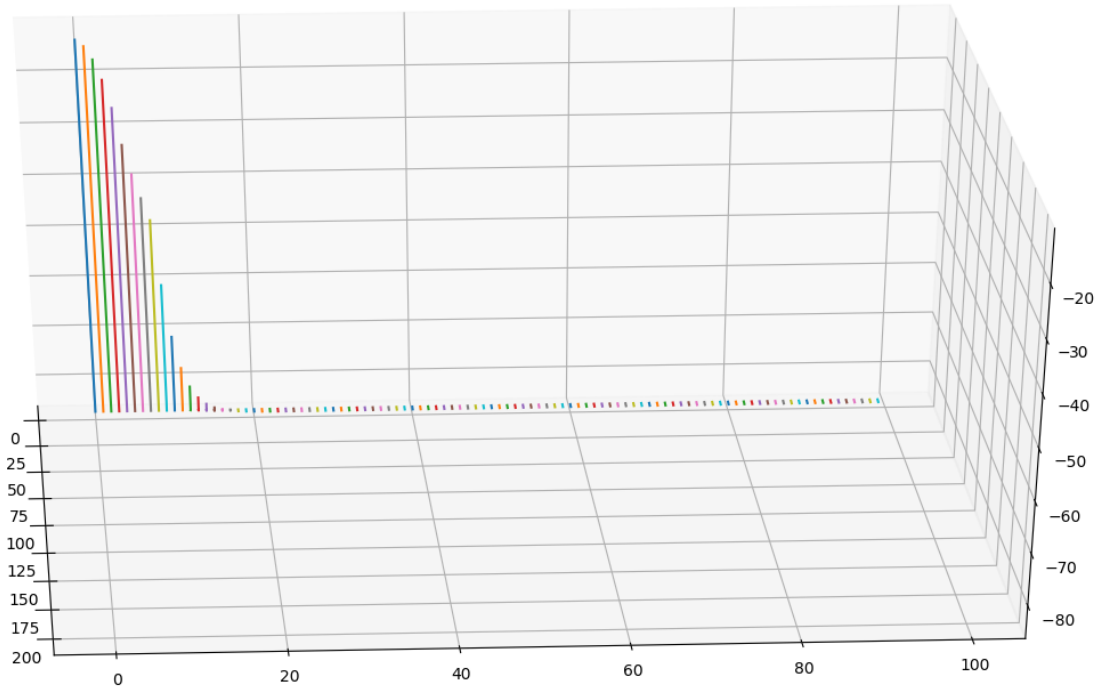

Figure 6.6: Cable simulation, result observed in a cable composed by 100 cells with the previously stated specifications. As this is a 3D graph to be able to observe the number of cells also, X-axis will represent the number of cells, Y-axis will represent potential in mV, Z-axis will represent time in ms.

6.3.4 2D Results

The first simulations of the 2D tissue were made without considering a limit in the tissue, this is, a fragment of the tissue was generated, but the cells at the ends of the tissue did not consider what was in the limit. The cells continued to have a conductive behavior as if there were still more cells beyond this limit, the following graphs correspond to these simulations.

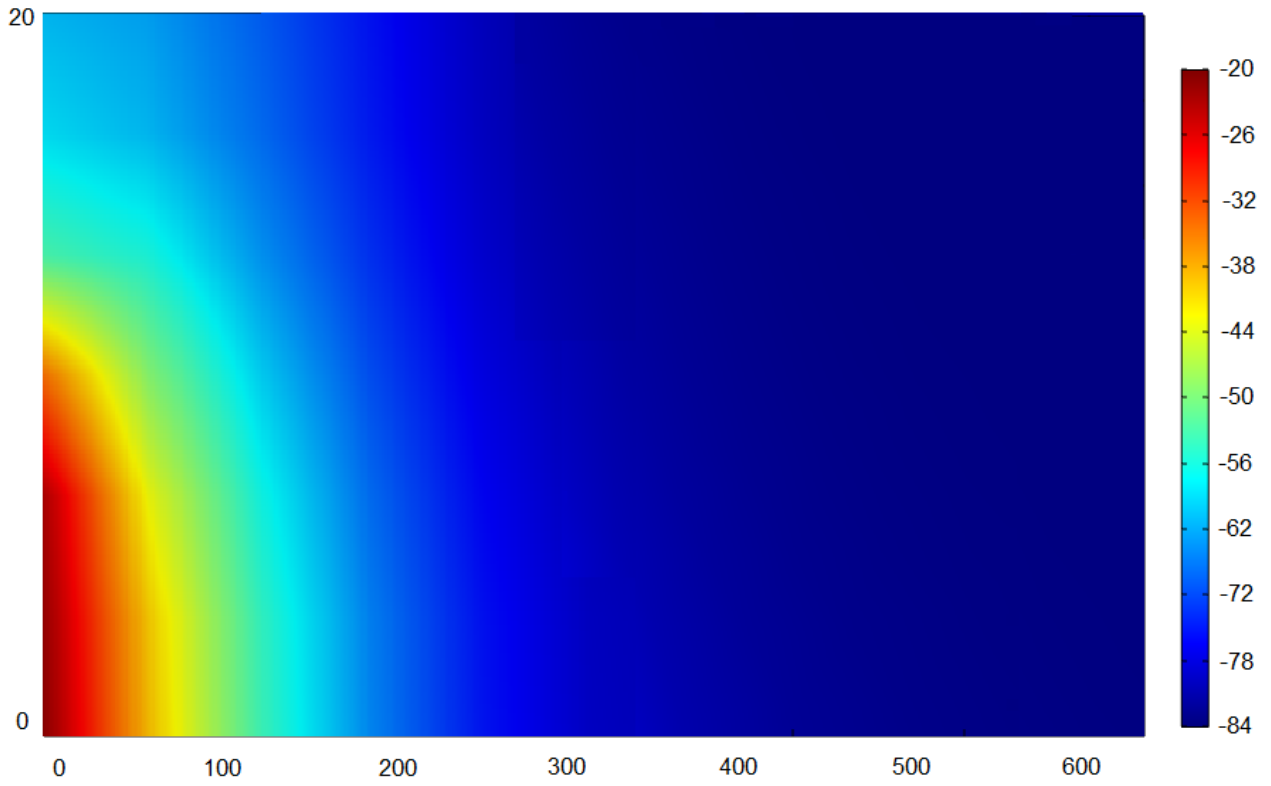

Figure 6.7: 2D graph representing the cardiac tissue, different color represent different levels of potential. X-axis represents time in μs, Y-axis represents cell index.

In this figure we can see the tissue generated in two dimensions, the scale of colors located on the right of the figure will represent the potential in that specific region of the tissue. We worked with a geometric shape for the ease of its design, and the ease to observe the behavior of the signals.

In these first graphs in which no boundaries were generated for the tissue, it can be seen to the left of the tissue the starting point where the signal is propagating, it tries to follow its path to the left because there is no type of limiter that tells the model that it can not continue in that direction.

In the case of the Dirac delta function, a tissue with a low cell index was generated due to the fact that in 1D results it was discovered that the signal was not going to propagate over long distances.

Due to the resistance conditions given by the formula 5.1. In this first example it can be seen that the signal is propagating mostly towards one side of the tissue, due to the different resistance in the other cells, the signal does not get very far in spite of being a tissue with a very small cell index.

Same conditions as the previous figure, different simulations are being carried out in which the resistance in the tissue is randomly varied, in Figure 6.8 it can be observed that the behavior continues being towards a single direction, with a more linear attenuation of the signal. The signal reaches further in the tissue in one direction, but its propagation towards the center of the tissue is almost non existent.

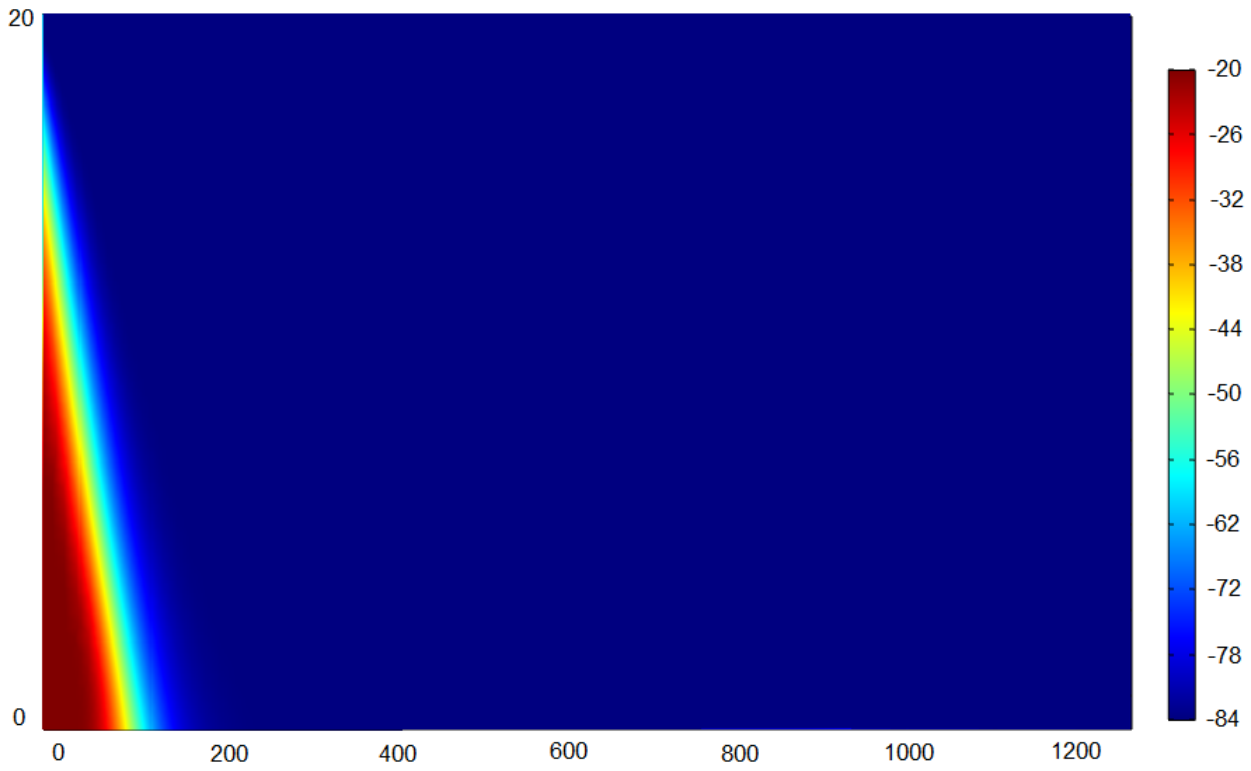

Figure 6.8: 2D graph representing the cardiac tissue, different color represent different levels of potential. This simulations don't consider limits in the tissue. X-axis represents time in μs, Y-axis represents cell index.

In order to better observe the propagation behavior of the signal, a tissue with a lower cell index was generated, this tissue is half the size of the previous ones. It can be seen that the signal moves almost completely throughout the entire tissue, however, in the absence of a limit, this signal tries to move in the same way outside the tissue, in the absence of limits the signal does not attenuate as it should.

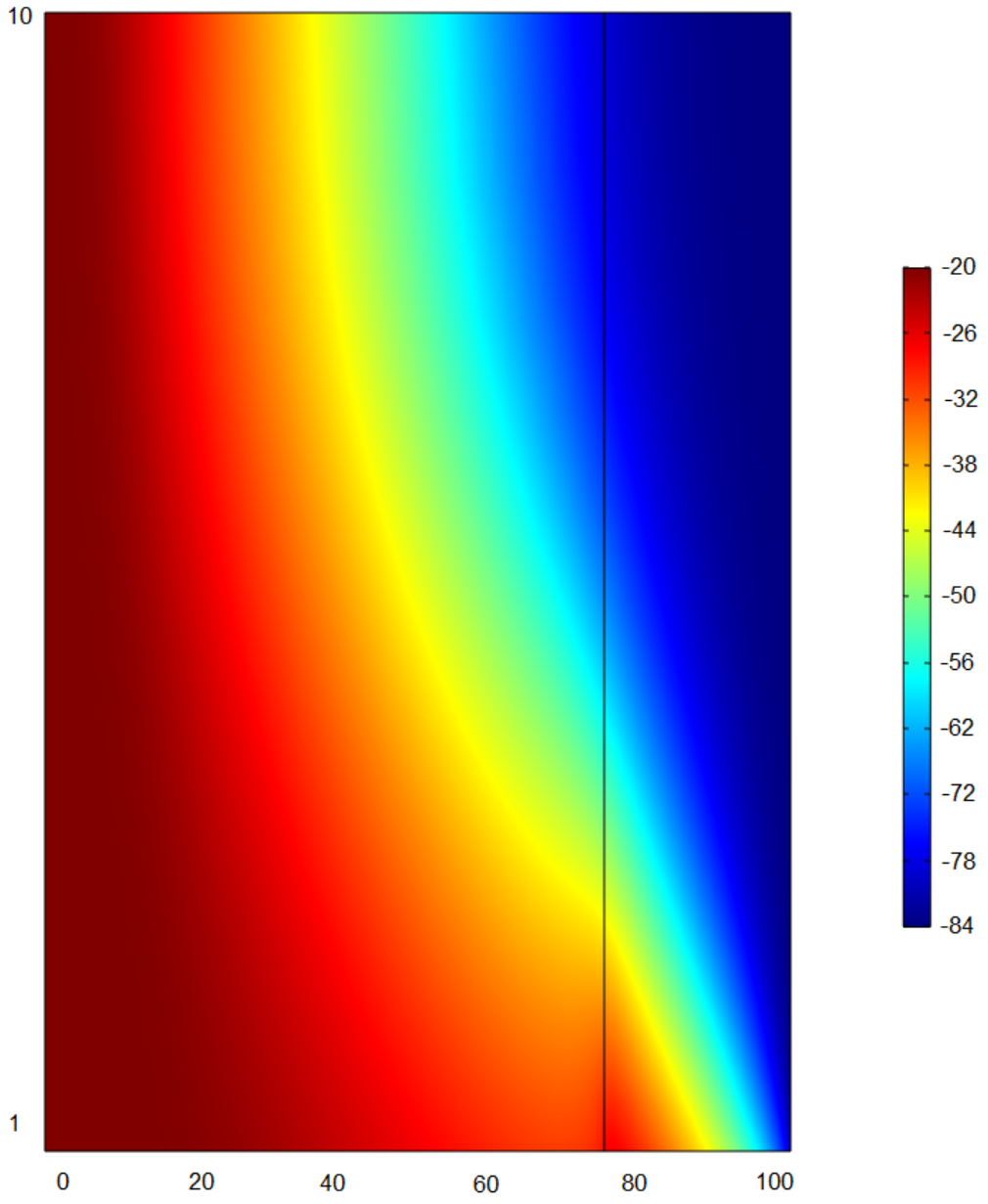

Figure 6.9: 2D graph representing the cardiac tissue, different color represent different levels of potential. In this simulation the size of the tissue was reduced. X-axis represents time in μs, Y-axis represents cell index.

Applying a Boundary to the Tissue

From this figure the description of the boundaries are now applied. It will be considered that a material that is not excitable as the cardiac cells exists in the limits of the tissue, and for effects of this investigation it will perform as an electrical insulator.

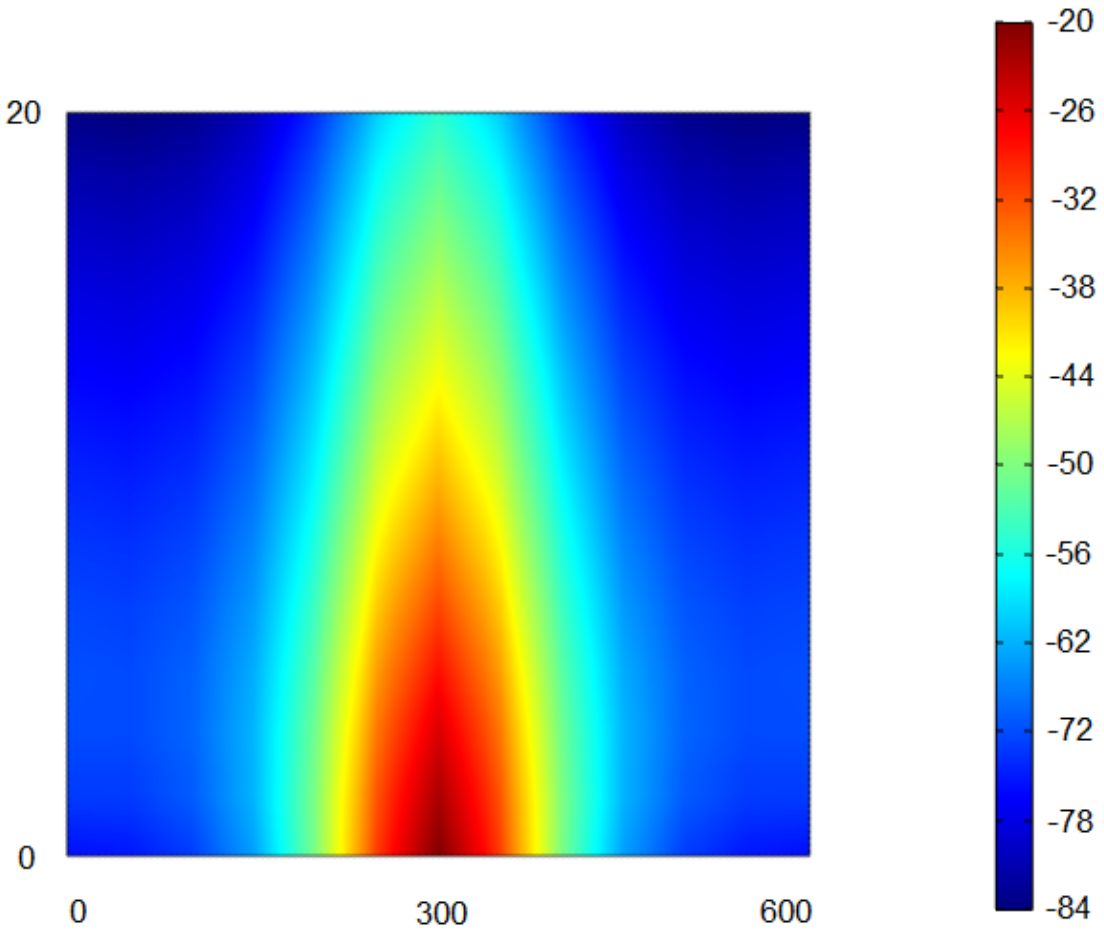

Figure 6.10: 2D graph representing the cardiac tissue, different color represent different levels of potential. In this simulation boundaries in the tissue are now considered. X-axis represents time in μs, Y-axis represents cell index.

To vary the conditions with respect to the previously generated tissues, starting with figure 6.10, an index of 20 cells is considered again, in addition, the initial point where the digital signal will begin to be transmitted will be in the middle of the tissue, in the lower part , we can observe how the signal propagates towards both sides of the tissue in the same way, however, despite having a good reach considering the geometry, it dissipates rapidly towards the sides. It should be noted that now that an insulator is considered at the limits of the tissue, the signal does not propagate indefinitely at the ends.

Now, increasing the tissue index to 100 cells for the next experiments, we can see that it is a propagation very similar to the one observed in the previous figures, however, this tissue, being of a higher index, in other words, composed of a greater number of cells, we can realize that as was observed in the 1D simulation, the signal does not travel very far without it attenuating.

In the following figures 6.11 and 6.12 the simulations will have conditions practically equal to the past, with the difference of the random variation of the resistance in the directions of the tissue. In the figure 6.13 the initial signal will be on a different side of this tissue.

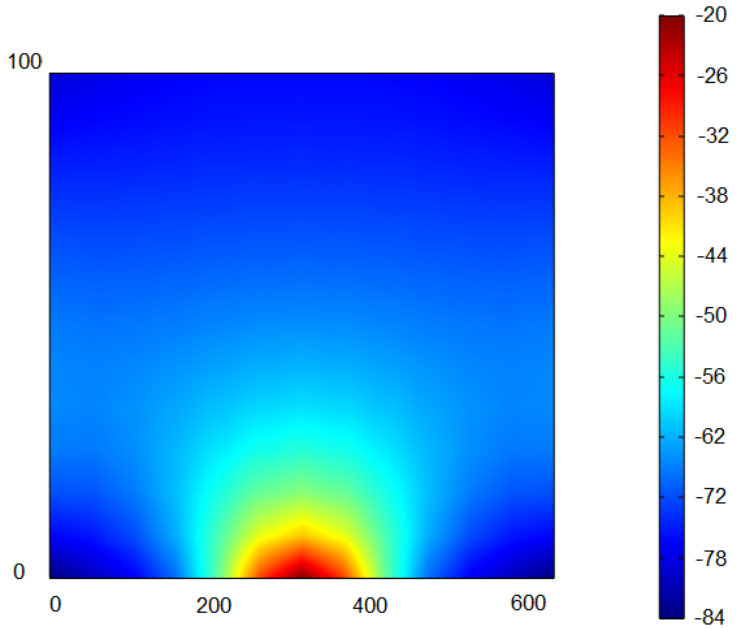

Figure 6.11: 2D graph representing the cardiac tissue, different color represent different levels of potential. X-axis represents time in μs, Y-axis represents cell index.

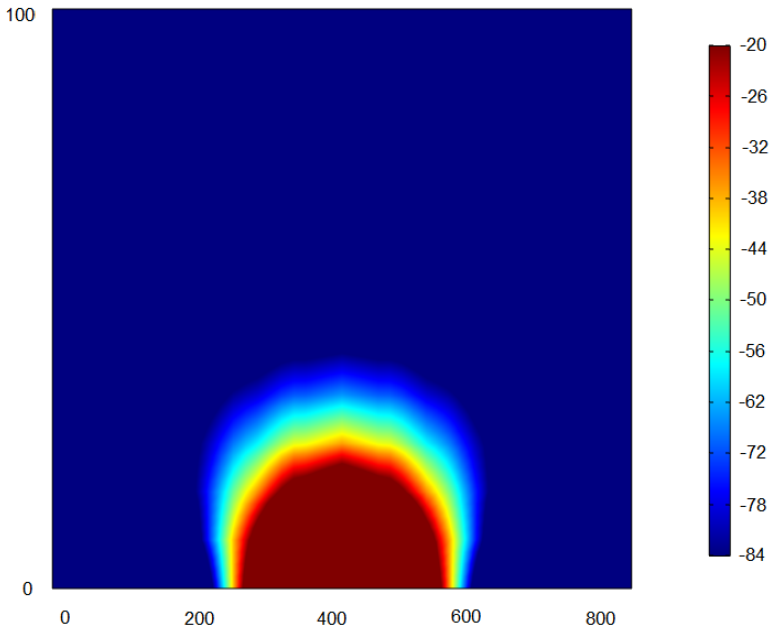

Figure 6.12: 2D graph representing the cardiac tissue, different color represent different levels of potential. X-axis represents time in μs, Y-axis represents cell index.

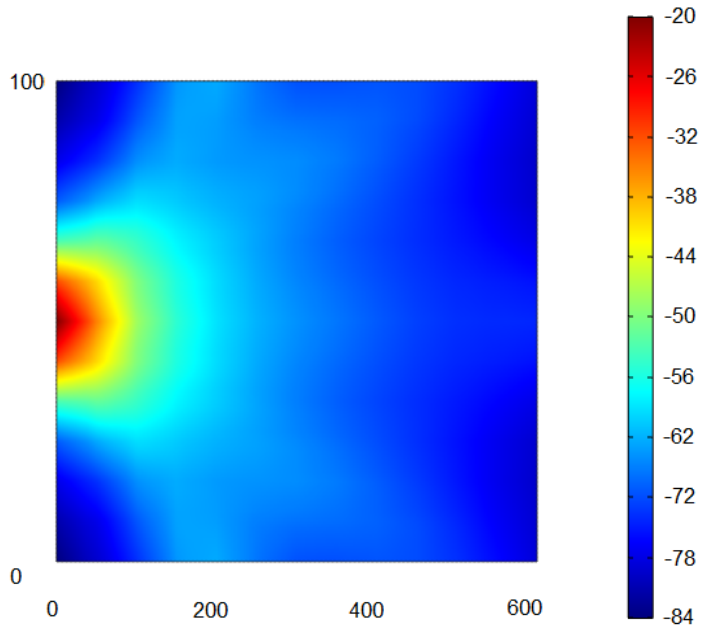

Figure 6.13: 2D graph representing the cardiac tissue, different color represent different levels of potential. Initial signal will be at the left of the tissue. X-axis represents time in μs, Y-axis represents cell index.

Moving away from the boundaries of the tissue, now the signal is being initiated in the center, this, to be able to observe how the propagation is without the ends coming into play. In the same way, given the short duration of the signal and the characteristics of the cells, it is rapidly attenuated, and in spite of observing a more uniform propagation, it dissipates rapidly, not reaching most of the tissue with an index of 100 cells.

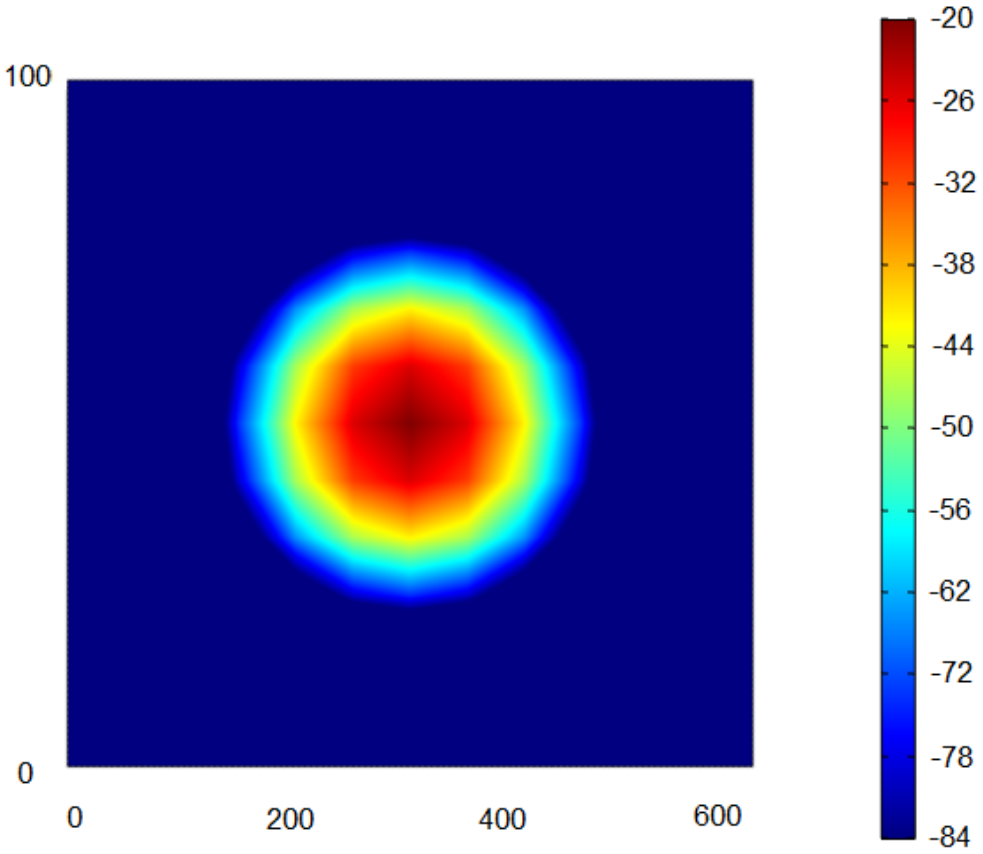

Figure 6.14: 2D graph representing the cardiac tissue, different color represent different levels of potential. In this graph the initial signal will be in the center of the tissue. X-axis represents time in μs, Y-axis represents cell index.

6.4 Square Wave Signal Results

In this section, the simulations that were previously performed will be repeated, however, the analysis of a square wave signal, commonly used in digital communications, will be performed as input and stimulus for our cell. Simulations were also carried out in a cell, in a cell cable arrangement, in 1D and 2D tissue. The signal used will have an amplitude of 50 mV and a duration of 5 ms.

6.4.1 Phase 0 Analysis

As with the Dirac delta function, in this signal we also have to observe how is the rise in phase 0 of the cell when excited by our digital signal. As the square signal is much longer than the pulse, this rise will take about 2 ms for the cell to be depolarized at its highest point.

It can be seen in a start that the rise has a linear behavior, then, it haves a sudden upstroke corresponding to the operation of the channels of $Na+$, remembering that, as less channels are present, less sudden will be the rise.

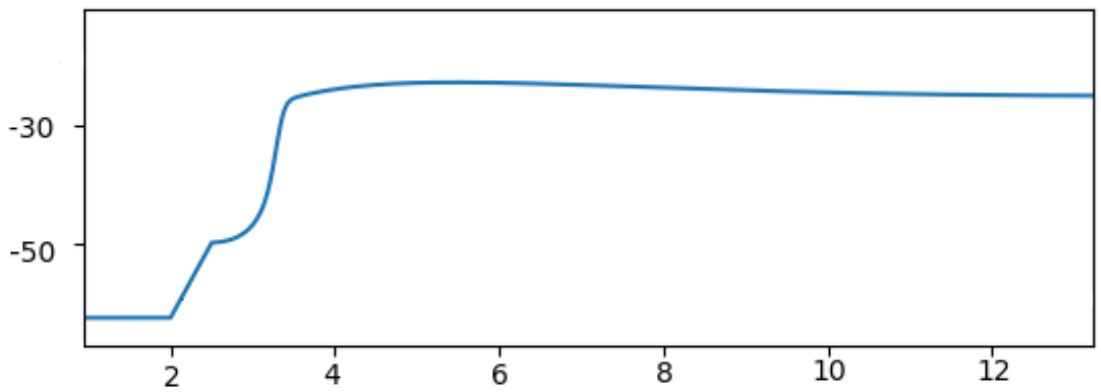

Figure 6.15: Close up of the response observed in a cell membrane after receiving the square wave signal. X-axis represented in ms, Y-axis represented in mV.

6.4.2 Sub-threshold results in individual cells

In these figures we can see the response that the cell will deliver when stimulated with this digital signal, without letting it reach an action potential, the shape of the input signal is what will give this characteristical response.

In this response it can be seen that the duration is 11.09528 ms and 11.39506 ms for the first and second cells respectively, we cannot see a delay to be considered from the response in the first cell to the response in the second cell.

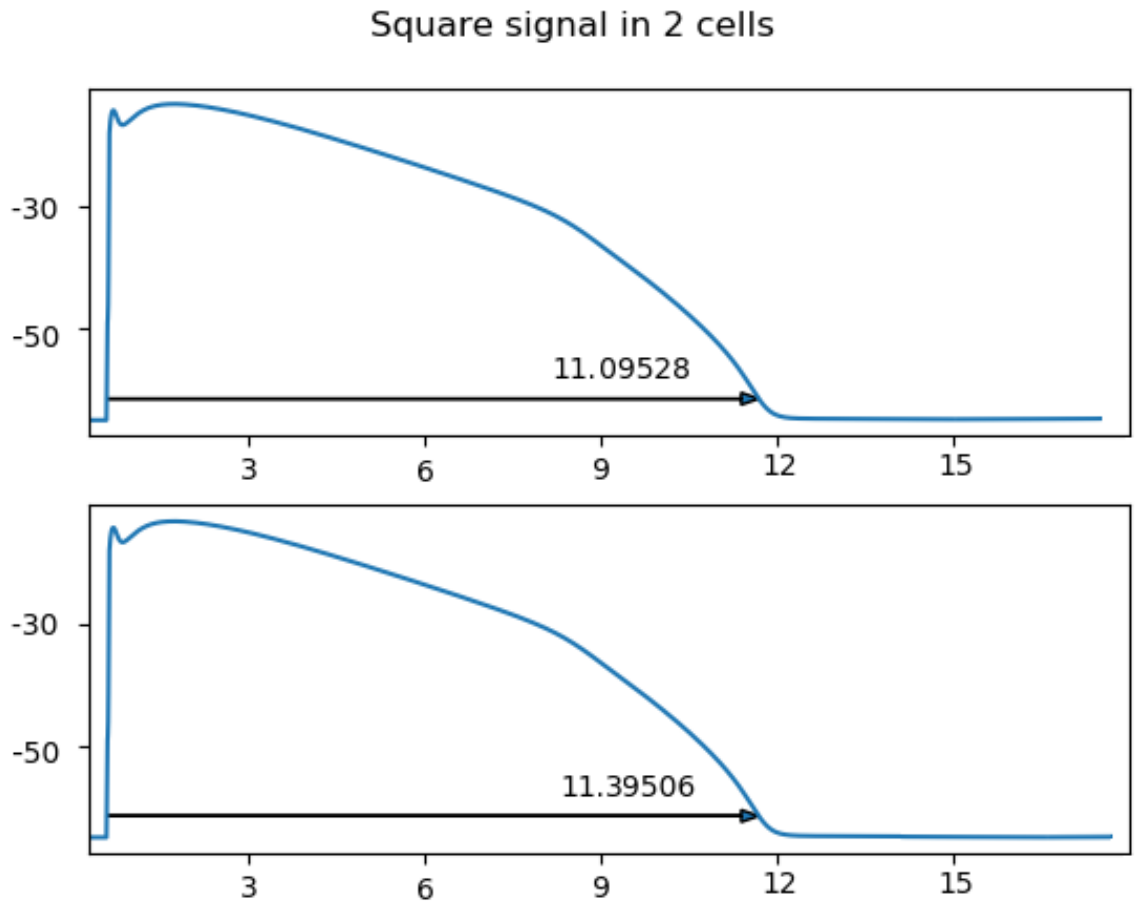

Figure 6.16: Subthreshold response observed in 1 and 2 cells after receiving the Square wave signal. X-axis represented in ms, Y-axis represented in mV.

6.4.3 1D Results

Following the simulations made with the Dirac delta function, we proceeded to make the cable model in which a cell is connected one after the other; two graphs are used to observe the attenuation of the signal after a certain distance traveled and the delay that is going to have after the signal is introduced, until a response is observed in the last cell of the array.

In the first figure we can see the attenuation that our cell will have as it spreads through the array. unlike the Dirac delta function simulations, this signal still has a considerable amplitude even after having traveled 100 cells. We can observe an attenuation of just over 10 mV.

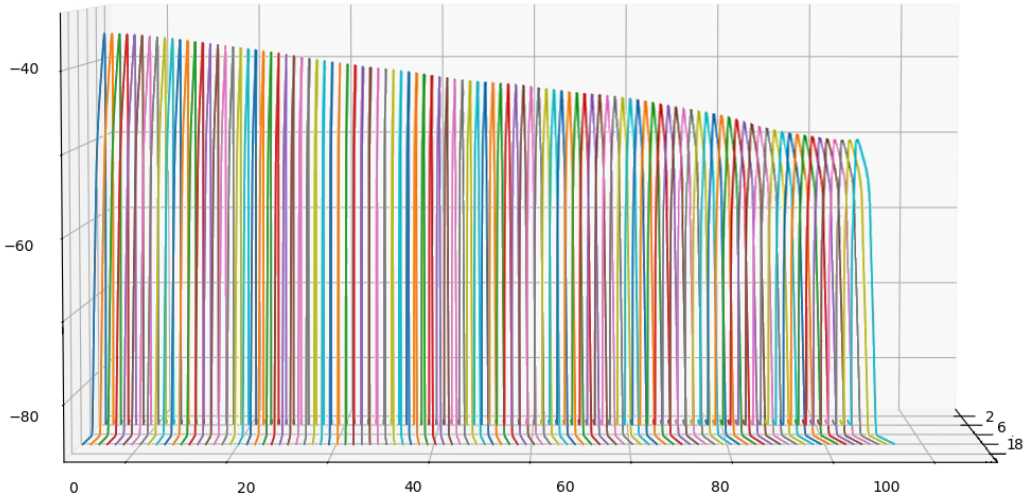

Figure 6.17: This graph represents the cells connected in a cable, we can see 100 cells, and the attenuation the signal presents over this distance. X-axis represented in ms, Y-axis represented in mV.

In the following figure 6.18, the graphs are placed in a way that we can appreciate the moment of time in which the signal arrives at the first cell comparable with the moment of time in which the signal reaches the last cell of the array, the system takes approximately 1 ms to travel through the 100 cells.

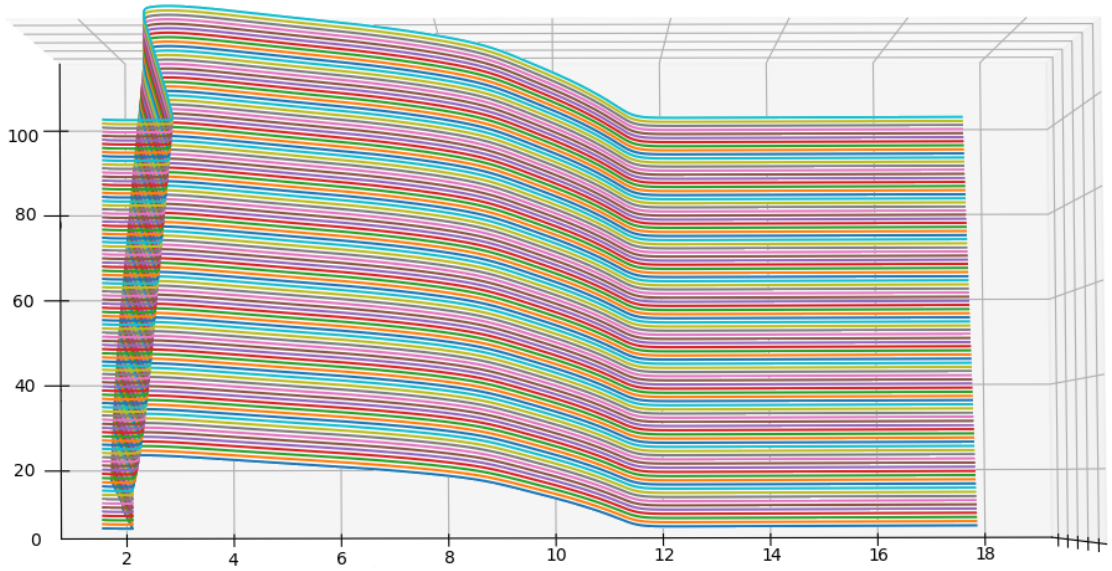

Figure 6.18: Same cable simulation as last figure, but in other perspective, here we can appreciate the delay the signal is presenting, from the point of reaching the first cell to the point of reaching the cell 100. X-axis represents cell index, Y-axis is represented in mV, and Z-axis represents time in ms.

6.4.4 2D Results

Following the simulations made with the Dirac delta function, experiments were performed with the square signal in a 2D tissue arrangement, same conditions, at the beginning the limits of the model were not considered. And in subsequent experiments the limitation of the non-conductive material was introduced.

In all the 2D simulations, an array was considered using an index of 1000 cells, due to the fact that the results obtained in the 1D section showed that the signal did not decay after the first 100 cells, so we were allowed to perform experiments on a larger tissue.

The first two figures correspond to the tissue without limits, as can be seen in the figure 6.19 and in figure 6.20, the propagation is taking place in one axis, without the potential being attenuated as observed in the same conditions for the Dirac delta function.

Our signal travels through all the tissue without attenuating, but when traveling to the other end, the signal is lost due to variations in tissue resistance.

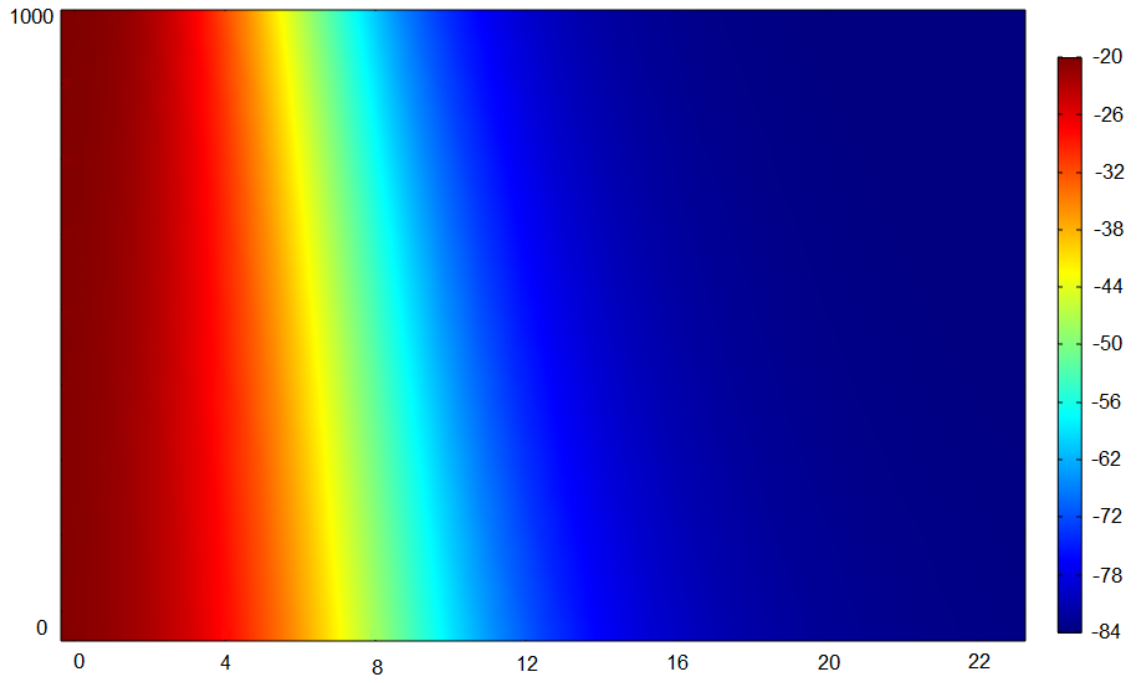

Figure 6.19: 2D graph representing the cardiac tissue, different color represent different levels of potential. This simulation does not consider limits on tissue. X-axis represents time in ms, Y-axis represents cell index.

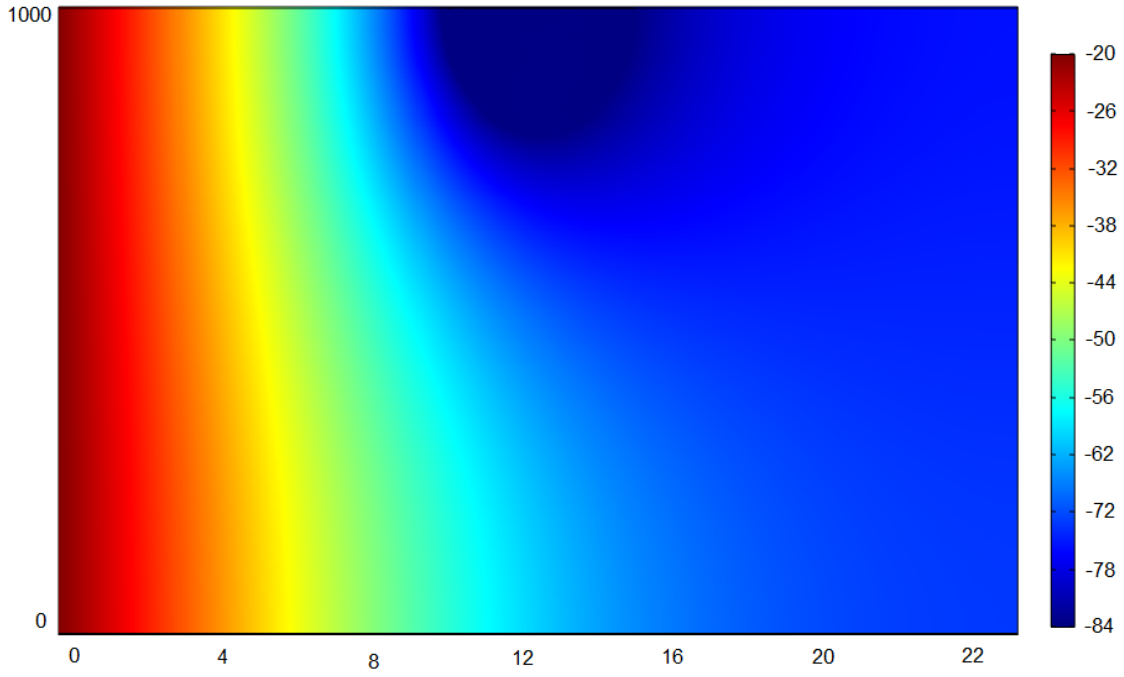

Figure 6.20: 2D graph representing the cardiac tissue, different color represent different levels of potential. This simulation odes not consider limits in tissue. X-axis represents time in ms, Y-axis represents cell index.

From figure 6.21 we are considering the limits of the tissue, so that the model does not try to propagate the signal beyond the end thinking that there are excitable cells in these sections. It can be observed that most of the tissue is being depolarized, only a small section on the opposite end to where the signal is being initialized remains without alteration of its resting state. This means the signal is not reaching that point of the tissue. Despite being a very large tissue compared to past simulations, satisfactory responses are obtained by seeing how most of this is being polarized with the digital signal.

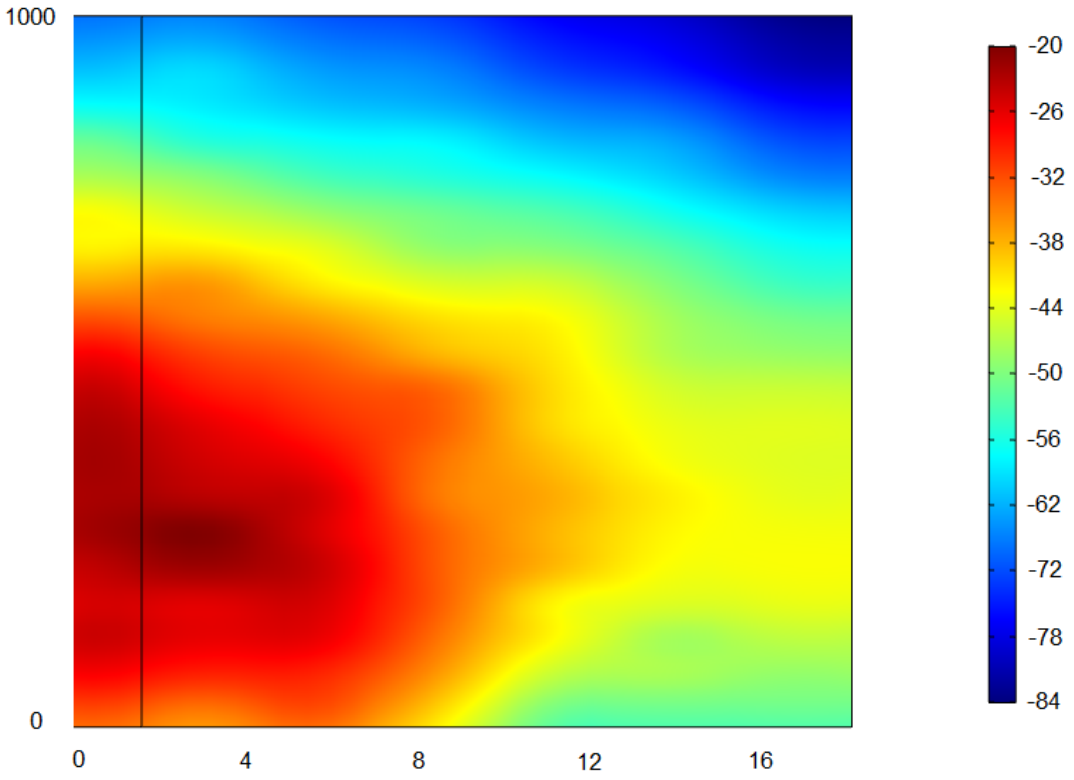

Figure 6.21: 2D graph representing the cardiac tissue, different color represent different levels of potential. X-axis represents time in ms, Y-axis represents cell index.

In the next two simulations, figure 6.22 and figure 6.23 the starting point of our digital signal was changed, and the resistances of the tissue cells were also randomly changed. The results of the past simulation were replicated, in which the signal manages to propagate to most of the modeled cardiac tissue.

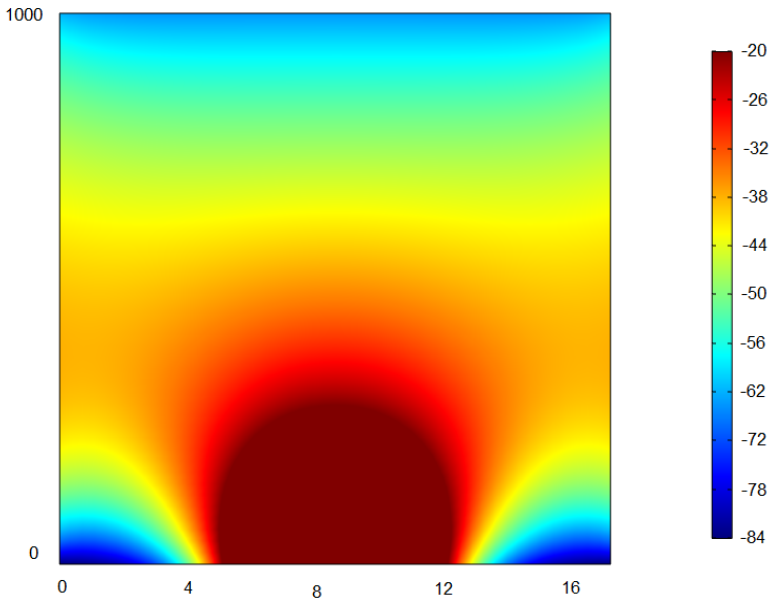

Figure 6.22: 2D graph representing the cardiac tissue, different color represent different levels of potential. The initial signal is shifted to the below of the tissue. X-axis represents time in ms, Y-axis represents cell index.

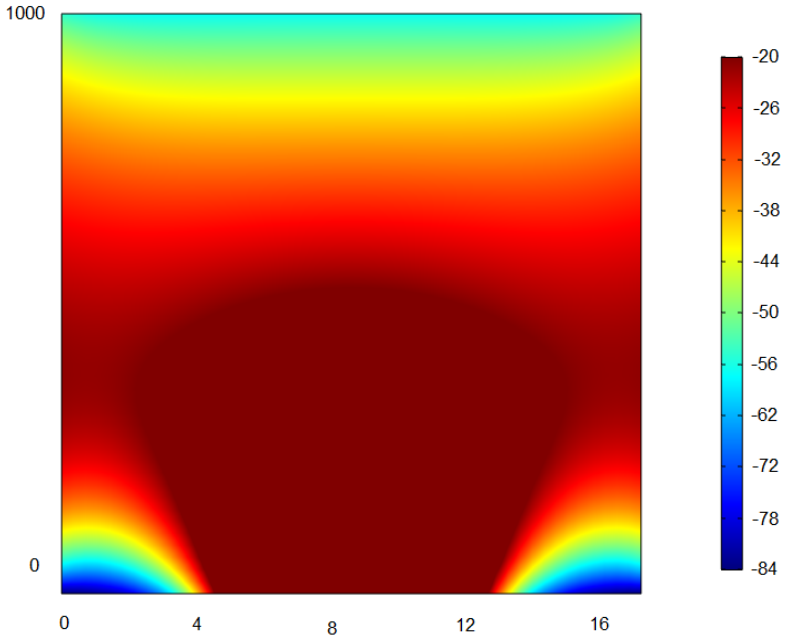

Figure 6.23: 2D graph representing the cardiac tissue, different color represent different levels of potential. The initial signal is shifted to the below of the tissue. X-axis represents time in ms, Y-axis represents cell index.

In the last two figures 6.24 and 6.25 communications are starting from the center of the cellular tissue, there are two variations, in which the only factor that is changing is the resistance of the cellular tissue, it is not possible to maintain the maximum power of the signal for all the cellular tissue, because the signal will always be degraded by the characteristics of the transmission channel. However, despite having a tissue of a large number of cells, it can be observed that the propagation of the digital signal reaches almost all the tissue.

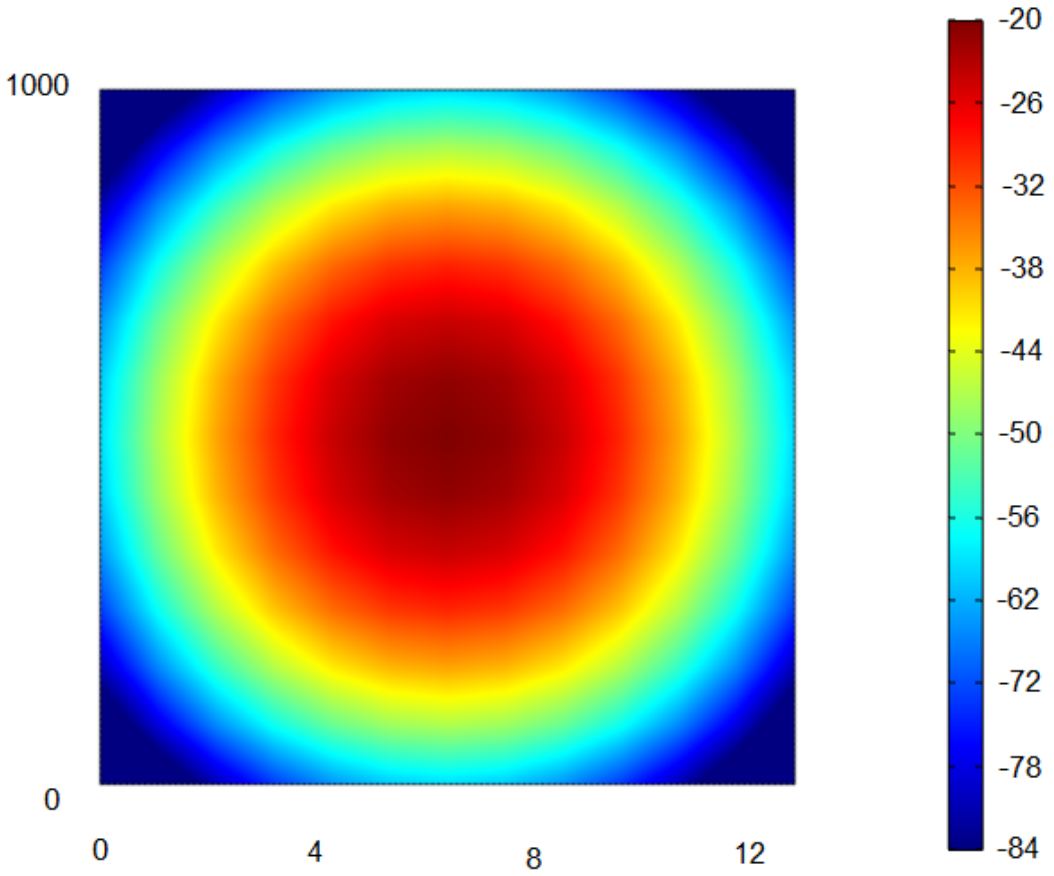

Figure 6.24: 2D graph representing the cardiac tissue, different color represent different levels of potential. The initial signal is shifted to the center of the tissue. X-axis represents time in ms, Y-axis represents cell index.

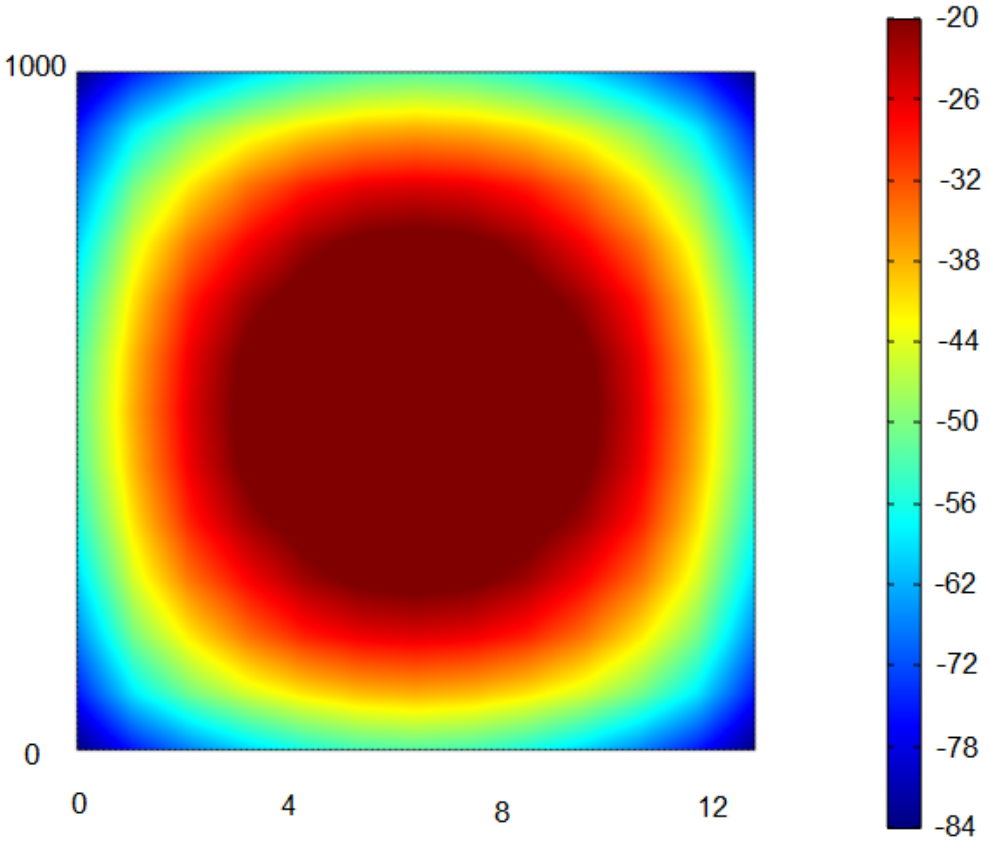

Figure 6.25: 2D graph representing the cardiac tissue, different color represent different levels of potential. The initial signal is shifted to the center of the tissue, only variation with the last simulation are resistances of the tissue. X-axis represents time in ms, Y-axis represents cell index.

Chapter 7

Conclusions

A more accurate model about the operation of action potentials has been provided; its generation, propagation and duration, this in order to obtain a framework that is more suitable for the study of the subthreshold region of operation of these electrical signals. This has allowed us to obtain a set of formulas that describe and model the electrical functioning of cardiac cells, adding a new feature to previous models, the consideration of hyperpolarization currents which can be found under extraordinary conditions when in the bloodstream exists an abnormal amount of potassium. With this we were able to describe the channels and their behaviors in these circumstances.

With this new framework it was possible to obtain a visual demonstration about the electrical behavior of the cells in the scenario in which they do not follow their original purpose of generation of action potential. When carrying out a study of the behavior under the threshold level, we were able to detect that the signals studied have their utility depending on the operating conditions.

The Dirac delta function will be considered more useful when it is required to transmit a greater amount of information in a shorter time, with the disadvantage that since this signal is a delta pulse, it does not have a long duration, which within the transmission channel, will mean that this signal does not have a wide propagation margin, it will be more useful in transmissions of short distances.

The usefulness of the square waveform was identified, as it was considered of a longer duration, it was observed that it had a greater propagation in a tissue of much higher index compared to the previous signal, positive results were observed in the propagation when considering tissues in 1D and 2D, so it can be concluded that this signal will be more useful when it is required to transmit in a larger tissue area, with the attenuating that each bit of data will require a longer time to be transmitted.

Thanks to this model we have been able to study the characteristics of the tissue and its effect on the signals and the feasibility of implementing communication channels between sensors and medical devices without using invasive means or wireless signaling with their respective disadvantages.

The propagation of signals, were studied considering the levels of electrical potential of the cells in the tissue, but as explained during this work, the cells are in equilibrium due to their chemical gradient as with the electrical gradient, as the electrical characteristics vary, the chemical quantities will vary in the same way, which leaves open the possibility that in future work in this area we are not only trying to detect the information that is intended to propagate with sensors that measure the electrical potential, it may also be possible to detect the change in the chemical gradient with chemical sensors, putting in play more concepts of molecular communications.

Due to the limited environment that is available to perform these types of studies, since it is not possible to perform physical experiments with a heart, the work and simulations were carried out with the available tools and scenario.

Appendix A

Model Parameters and Formulas

A.1 Formulas used to implement the model

Fast $Na+$ Current

$$I_{Na} = G_{Na} m^3 h j (V - E_{Na}) \tag{A.1}$$

$$m_\infty = \frac{1}{[1 + e^{(-56.86-V)/9.03}]^2} \tag{A.2}$$

$$\alpha_m = \frac{1}{1 + e^{(-60-V)/5}} \tag{A.3}$$

$$\beta_m = \frac{0.1}{1 + e^{(V+35)/5}} + \frac{0.1}{1 + e^{(V-50)/200}} \tag{A.4}$$

$$\tau_m = \alpha_m \beta_m \tag{A.5}$$

$$h_\infty = \frac{1}{[1 + e^{(V+71.55)/7.43}]^2} \tag{A.6}$$

$$\begin{aligned} &\alpha_h = 0 \quad if \quad V \geq -40 \\ &\alpha_h = 0.057 e^{-(V+80)/6.8} \quad otherwise \end{aligned} \tag{A.7}$$

$$\begin{aligned} \beta_h &= \frac{0.77}{0.13[1+e^{-(V+10.66)/11.1}]} \\ \beta_h &= 2.7e^{0.079V} + 3.1*10^5 e^{0.3485V} \quad otherwise \end{aligned} \tag{A.8}$$

$$\tau_h = \frac{1}{\alpha_h \beta_h} \tag{A.9}$$

$$j_\infty = \frac{1}{[1+e^{(V+71.55)/7.43}]^2} \tag{A.10}$$

$$\begin{aligned} &\alpha_h = 0 \quad if \quad V \geq -40 \\ &\alpha_j = \frac{(-2.5428*10^4 e^{.02444V} - 6.948*10^{-6} e^{-0.04391V})(V+37.78)}{1+e^{0.311(V+79.23)}} \quad otherwise \end{aligned} \tag{A.11}$$

$$\begin{aligned} \beta_j &= \frac{0.6e^{0.057V}}{1+e^{-0.1(V+32)}} \quad if \quad V \geq -40 \\ \beta_j &= \frac{0.02424e^{-0.01052V}}{1+e^{-0.1378(V+40.14)}} \quad otherwise \end{aligned} \tag{A.12}$$

$$\tau_j = \frac{1}{\alpha_j + \beta_j} \tag{A.13}$$

L-type Ca^2+ Current

$$I_{CaL} = G_{CaL} df f_{CaL} 4 \frac{VF^2}{RT} \frac{Ca_i e^{2VF/RT} - 0.341 Ca_o}{e^{2VF/RT} - 1} \tag{A.14}$$

$$d_\infty = \frac{1}{1+e^{(-5-V)/7.5}} \tag{A.15}$$

$$\alpha_d = \frac{1.4}{1+e^{(-35-V)/13}} + 0.25 \tag{A.16}$$

$$\beta_d = \frac{1.4}{1+e^{(V+5)/5}} \tag{A.17}$$

$$\gamma_d = \frac{1}{1+e^{(50+V)/20}} \tag{A.18}$$

$$\tau_d = \alpha_d \beta_d + \gamma_d \tag{A.19}$$

$$f_\infty = \frac{1}{1 + e^{(V+20)/7}} \tag{A.20}$$

$$\tau_f = 1125 e^{-(V+27)2/240} + \frac{165}{1 + e^{(25-V)/10}} + 80 \tag{A.21}$$

$$\alpha_{fca} = \frac{1}{1 + (Ca_i/0.000325)^8} \tag{A.22}$$

$$\beta_{fca} = \frac{0.1}{1 + e^{(Ca_i - 0.0005)/0.0001}} \tag{A.23}$$

$$\gamma_{fca} = \frac{0.2}{1 + e^{(Ca_i - 0.00075)/0.0008}} \tag{A.24}$$

$$f_{ca\infty} = \frac{\alpha_{fca} + \beta_{fca} + \gamma_{fca} + 0.23}{1.46} \tag{A.25}$$

$$\tau_{fca} = 2ms \tag{A.26}$$

$$\frac{\mathrm{df_{ca}}}{\mathrm{dt}} = k \frac{f_{ca\infty} - f_{ca}}{\tau_{fca}} \tag{A.27}$$

$$\begin{aligned} &k = 0 \;\; if \;\; f_{ca\infty} > f_{ca} \;\; and \;\; V > -60mV \\ &k = 1 \;\; otherwise \end{aligned} \tag{A.28}$$

Transient Outward Current

$$I_{to} = G_{to} r s (V - E_k) \tag{A.29}$$

For all cell types

$$r_\infty = \frac{1}{1 + e^{(20-V)/6}} \tag{A.30}$$

$$\tau_r = 9.5e^{-(V+40)^2/1800} + 0.8 \tag{A.31}$$

For epicardial and M cells

$$s_\infty = \frac{1}{1 + e^{(V+20)/5}} \tag{A.32}$$

$$\tau_s = 85e^{-(V+45)^2/320} + \frac{5}{1 + e^{(V-20)/5}} + 3 \tag{A.33}$$

For endocardial cells

$$s_\infty = \frac{1}{1 + e^{(V+28)/5}} \tag{A.34}$$

$$\tau_s = 1,000e^{-(V+67)^2/1,000} + 8 \tag{A.35}$$

Slow Delayed Rectifier Current

$$I_{Ks} = G_{Ks}x_s^2(V - E_{Ks}) \tag{A.36}$$

$$x_{s\infty} = \frac{1}{1 + e^{(-5-V)/14}} \tag{A.37}$$

$$\alpha_{xs} = \frac{1,100}{\sqrt{1 + e^{(-10-V)/6}}} \tag{A.38}$$

$$\beta_{xs} = \frac{1}{1 + e^{(V-60)/20}} \tag{A.39}$$

$$\tau_{xs} = \alpha_{xs}\beta_{xs} \tag{A.40}$$

Rapid Delayed Rectifier Current

$$I_{Kr} = G_{Kr}\sqrt{\frac{K_o}{5.4}}x_{r1}x_{r2}(V - E_K) \tag{A.41}$$

$$x_{r1\infty} = \frac{1}{1 + e^{(-26-V)/7}} \tag{A.42}$$

$$\alpha_{xr1} = \frac{450}{1 + e^{(-45-V)/10}} \tag{A.43}$$

$$\beta_{xr1} = \frac{6}{1 + e^{(V+30)/11.5}} \tag{A.44}$$

$$\tau_{xr1} = \alpha_{xr1}\beta_{xr1} \tag{A.45}$$

$$x_{r2\infty} = \frac{1}{1 + e^{(V+88)/24}} \tag{A.46}$$

$$\alpha_{xr2} = \frac{3}{1 + e^{(-60-V)/20}} \tag{A.47}$$

$$\beta_{xr2} = \frac{1.12}{1 + e^{(V-60)/20}} \tag{A.48}$$

$$\tau_{xr2} = \alpha_{xr2}\beta_{xr2} \tag{A.49}$$

Inward Rectifier $K+$ Current

$$I_{K1} = G_{K1}\sqrt{\frac{K_o}{5.4}}x_{k1\infty}(V - E_K) \tag{A.50}$$

$$\alpha_{k1} = \frac{0.1}{1 + e^{0.06(V-E_K-200)}} \tag{A.51}$$

$$\beta_{k1} = \frac{3e^{0.0002(V-E_K+100)} + e^{0.1(V-E_K+10)}}{1+e^{-0.5(V-E_K)}} \tag{A.52}$$

$$x_{k1\infty} = \frac{\alpha_{k1}}{\alpha_{k1}+\beta_{k1}} \tag{A.53}$$

$Na+/Ca^2+$ Exchanger Current

$$I_{NaCa} = k_{NaCa}\frac{e^{\gamma\ VF/RT}Na_i^3Ca_o - e^{(\gamma\ -1)VF/RT}Na_o^3Ca_i\alpha}{(K_{MNai}^3+Na_o^3)(K_{mCa}+Ca_o)(1+k_{sat}e^{(\gamma\ -1)VF/RT})} \tag{A.54}$$

$Na+/K+$ Pump Current

$$I_{NaK} = P_{NaK}\frac{K_oNa_i}{(K_o+K_{mK})(Na_i+K_{mNa})(1+0.1245e^{-0.1VF/RT}+0.0353e^{-VF/RT})} \tag{A.55}$$

I_{pCa}

$$I_{pCa} = G_{pCa}\frac{Ca_i}{K_{pCa}+Ca_i} \tag{A.56}$$

I_{pK}

$$I_{pK} = G_{pK}\frac{V-E_K}{1+e^{(25-V)/5.98}} \tag{A.57}$$

Background Currents

$$I_{bNa} = G_{bNa}(V-E_{Na}) \tag{A.58}$$

$$I_{bCa} = G_{bCa}(V-E_{Ca}) \tag{A.59}$$

Calcium Dynamics

$$I_{leak} = V_{leak}(Ca_{sr}-Ca_i) \tag{A.60}$$

$$I_{up} = \frac{V_{maxup}}{1+K_{up}^2/Ca_i^2} \tag{A.61}$$

$$I_{rel} = \left(a_{rel} \frac{Ca_{sr}^2}{b_{rel}^2 + Ca_{sr}^2} + c_{rel} \right) dg \tag{A.62}$$

$$\begin{aligned} g_\infty &= \frac{1}{1 + Ca_i^6 / 0.00035^6} \quad if \quad Ca_i \leq 0.00035 \\ g_\infty &= \frac{1}{1 + Ca_i^{16} / 0.00035^{16}} \quad otherwise \end{aligned} \tag{A.63}$$

$$\tau_g = 2ms \tag{A.64}$$

$$\frac{\mathrm{dg}}{\mathrm{d}t} = k \frac{g_\infty - g}{\tau_g} \tag{A.65}$$

$$\begin{aligned} &k = 0 \quad if \quad g_\infty > g \quad and \quad V > -60mV \\ &k = 1 \quad otherwise \end{aligned} \tag{A.66}$$

$$Ca_{ibufc} = \frac{Ca_i * Buf_c}{Ca_i + K_{bufc}} \tag{A.67}$$

$$\frac{\mathrm{dCa_{itotal}}}{\mathrm{d}t} = -\frac{I_{CaL} + I_{bCa} + I_{pCa} - 2I_{NaCa}}{2V_C F} + I_{leak} - I_{up} + I_{rel} \tag{A.68}$$

$$Ca_{srbufsr} = \frac{Ca_{sr} * Buf_{sr}}{Ca_{sr} + K_{bufsr}} \tag{A.69}$$

$$\frac{\mathrm{dCa_{srtotal}}}{\mathrm{d}t} = -\frac{V_C}{V_{SR}}(-I_{leak} + I_{up} - I_{rel}) \tag{A.70}$$

Sodium and Potassium Dynamics

$$\frac{\mathrm{dNa_i}}{\mathrm{d}t} = -\frac{I_{Na} + I_{bNa} + 3I_{NaK} + 3I_{NaCa}}{V_C F} \tag{A.71}$$

$$\frac{\mathrm{dK_i}}{\mathrm{d}t} = -\frac{I_{K1} + I_{to} + I_{Kr} + I_{Ks} - 2I_{NaK} + I_{pk} + I_{stim} - I_{ax}}{V_C F} \tag{A.72}$$

Hiperpolarization - activated current

$$I_f = i_{f,k} + i_{f,Na} \tag{A.73}$$

$$i_{f,k} = G_{f,K} y (V - E_k) \tag{A.74}$$

$$i_{f,Na} = G_{f,Na} y (V - E_N a) \tag{A.75}$$

$$y_\infty = \frac{1}{1 + e^{(V+80.6)/6.8}} \tag{A.76}$$

$$\alpha_y = e^{-2.9-(0.04V)} \tag{A.77}$$

$$\beta_y = e^{3.6+(0.11V)} \tag{A.78}$$

$$\tau_y = \frac{4000}{\alpha_y + \beta_y} \tag{A.79}$$

Potassium Sustained Current

$$I_{sus} = G_{sus} a (V - E_K) \tag{A.80}$$

$$a_\infty = \frac{1}{1 + e^{(5-V)}/17} \tag{A.81}$$

A.2 Initial Conditions

Table A.1: Initial conditions used in the simulation, derived from different experiments and Ten Tusscher model [92].

Parameter	Definition	Value
R	Gas Constant	8.3143 $JK^{-1}mol^{-1}$
T	Temperature	310 K
F	Faraday Constant	96.4867 $C/mmol$
C_m	Cell capacitance per unit surface area	2 $\mu F/cm^2$
S	Surface-to-volume ratio	0.2 μm^{-1}
ρ	Cellular resistivity	162 Ωcm/Variable in 2D
V_c	Cytoplasmic volume	$16,404$ μm^3
V_sr	Sarcoplasmic reticulum volume	$1,094$ μm^3
K_O	Extracellular $K+$ concentration	5.4 mM
Na_O	Extracellular $Na+$ concentration	140 mM
Ca_O	Extracellular Ca^2+ concentration	2 mM
G_Na	Maximal I_{Na} conductance	14.838 nS/pF
G_K1	Maximal I_{K1} conductance	5.405 nS/pF
G_to,epi,M	Maximal epicardial I_{to} conductance	0.294 nS/pF
G_to,endo	Maximal endocardial I_{to} conductance	0.073 nS/pF
G_Kr	Maximal I_{Kr} conductance	0.096 nS/pF
G_Ks, epi, endo	Maximal epi- and endocardial I_{Ks} conductance	0.245 nS/pF
G_Ks, M	Maximal M cell I_{Ks} conductance	0.062 nS/pF
ρ_{KNa}	Relative I_{Ks} permeability to $Na+$	0.03
G_{CaL}	Maximal I_{CaL} conductance	1.75^{-4} $cm^3\mu F^{-1}s^{-1}$
K_{NaCa}	Maximal I_{NaCa}	$1,000$ pA/pF
γ	Voltage dependence parameter of I_{NaCa}	0.35
K_{mCa}	Ca_i half-saturation constant for I_{NaCa}	1.38 mM
K_{mNai}	Na_i half-saturation constant for I_{NaCa}	87.5 mM
K_{sat}	Saturation factor for I_{NaCa}	0.1
α	Factor enhancing outward nature of I_{NaCa}	2.5
P_{NaK}	Maximal I_{NaK}	1.362 pA/pF
K_{mK}	K_O half-saturation constant of I_{NaK}	1 mM
K_{mNa}	Na_i half-saturation constant of I_{NaK}	40 mM
G_{pk}	Maximal I_pK conductance	0.0146 nS/pF
G_{pCa}	Maximal I_pCa conductance	0.025 nS/pF
K_{pCa}	Ca_i half-saturation constant of I_pCa	0.0005 mM
G_{bNa}	Maximal I_{bNa} conductance	0.00029 nS/pF
G_{bCa}	Maximal I_{bCa} conductance	0.000592 nS/pF
V_{maxup}	Maximal I_{up}	0.000425 mM/ms
K_{up}	Half-saturation constant of I_{up}	0.00025 mM
a_{rel}	Maximal Ca_SR-dependent I_{rel}	16.464mM/s
b_{rel}	Ca_SR half-saturation constant of I_{rel}	0.25 mM
c_{rel}	Maximal Ca_SR-independent I_{rel}	8.232 mM/s
V_{leak}	Maximal I_{leak}	0.00008 ms^{-1}
Buf_c	Total cytoplasmic buffer concentration	0.15 mM
K_{bufc}	Ca_i half-saturation constant for cytoplasmic buffer	0.001 mM
Buf_{sr}	Total sarcoplasmic buffer concentration	10 mM
K_{bufsr}	Ca_SR half-saturation constant for sarcoplasmic buffer	0.3 mM

Appendix B

Coding

B.1 Coding for the modified model

```
[[model]]
name: Modified_Model

membrane.V = -84.1370441636
calcium.Ca_i = 0.000101878186157
calcium.Ca_SR = 3.10836886659
calcium.Ca_ss = 0.000446818714055
calcium.R_prime = 0.991580051908
sodium.Na_i = 8.80420286532
potassium.K_i = 136.78189416
if.y = 0.0457562667987
ikr.Xr1 = 0.00550281999719
ikr.Xr2 = 0.313213286438
iks.Xs = 0.00953708522975
ina.m = 0.417391656295
ina.h = 0.0190678733735
```

```
ina.j = 0.238219836154

ical.d = 0.000287906256206

ical.f = 0.989328560288

ical.f2 = 0.995474890442

ical.fCass = 0.999955429598

ito.s = 0.963861017995

ito.r = 0.00103618091197


# Engine


[engine]

time = 0 bind time

pace = 0 bind pace


# Membrane potential


[membrane]

dot(V) = - (i_ion + i_stim + i_diff)

    in [mV]

    label membrane_potential

i_ion = sodium.INa_tot + potassium.IK_tot + calcium.ICa_tot

    desc: Ionic current out of the cell

i_stim = engine.pace * amplitude

    desc: """ Stimulus current."""

    amplitude = -30

i_diff = 0 bind diffusion_current

    desc: Current to neighbouring cells.


# Physical constants
```

```
[phys]
R = 8314.472 [J/mol/K]
T = 310 [K]
F = 96485.3415 [C/mmol]
RTF = R * T / F
FRT = F / R / T
FFRT = F * FRT
Cm = 0.185 [uF]
V_c = 0.016404 [um^3]

#Inwared rectifier current

[ik]
use membrane.V
i_K1 = g_K1 * xK1_inf * (V - 8 - nernst.E_K)
    in [uA/uF]
g_K1 = 0.065 [1/ms]
xK1_inf = 1 / (1 + exp(0.1 * (V + 75.44)))

#Transient outward current

[ito]
use membrane.V
i_to = g_to * r * s * (V - nernst.E_K)
    in [uA/uF]
g_to = 0.08184 [1/ms]
dot(s) = (s_inf - s) / tau_s
    s_inf = 1 / (1 + exp((V + 27) / 13))
```

```
    tau_s = 85 * exp(-(V + 25) ^ 2 / 320) + 5 / (1 + exp((V - 40) / 5)) + 42
dot(r) = (r_inf - r) / tau_r
    r_inf = 1 / (1 + exp((20 - V) / 13))
    tau_r = 10.45 * exp(-(V + 40) ^ 2 / 1800) + 7.3

#Sustained current

[isus]
use membrane.V
i_sus = g_sus * a * (V - nernst.E_K)
    in [uA/uF]
g_sus = 0.0227 [1/ms]
a = 1 / (1 + exp((5 - V) / 17))

#Hyperpolarization-activated current

[if]
use membrane.V
i_f_Na = y * g_f_Na * (V - nernst.E_Na)
    in [uA/uF]
    g_f_Na = 0.0145654 [1/ms]
i_f_K = y * g_f_K * (V - nernst.E_K)
    in [uA/uF]
    g_f_K = 0.0234346 [1/ms]
dot(y) = (y_inf - y) / tau_y
    y_inf = 1 / (1 + exp((V + 80.6) / 6.8))
    tau_y = 4000 / (alpha_y + beta_y)
        in [ms]
    alpha_y = 1 * exp(-2.9 - 0.04 * V)
```

```
        in [1/ms]
    beta_y = 1 * exp(3.6 + 0.11 * V)
        in [1/ms]


#Fast sodium current


[ina]
use membrane.V
g_Na = 130.5744 [1/ms]
i_Na = g_Na * m ^ 3 * h * j * (V - nernst.E_Na)
    in [uA/uF]
dot(m) = (inf - m) / tau
    inf = 1 / (1 + exp((-56.86 - V) / 9.03)) ^ 2
    alpha = 1 / (1 + exp((-60 - V) / 5))
    beta = 0.1 / (1 + exp((V + 35) / 5)) + 0.1 / (1 + exp((V - 50) / 200))
    tau = alpha * beta
dot(h) = (inf - h) / tau
    inf = 1 / (1 + exp((V + 71.55) / 7.43)) ^ 2
    tau = 1 / (alpha + beta)
    alpha = if(V < -40, 0.057 * exp(-(V + 80) / 6.8), 0)
    beta = if(V < -40,
        2.7 * exp(0.079 * V) + 310000 * exp(0.3485 * V),
        0.77 / (0.13 * (1 + exp((V + 10.66) / -11.1))))
dot(j) = (inf - j) / tau
    inf = 1 / (1 + exp((V + 71.55) / 7.43)) ^ 2
    tau = 1 / (alpha + beta)
    alpha = if(V < -40,
        (-25428 * exp(0.2444 * V) - 6.948e-6 * exp(-0.04391 * V)) * (V +
            37.78) / (1 + exp(0.311 * (V + 79.23))),
```

```
        0)
    beta = if(
        V < -40, 0.02424 * exp(-0.01052 * V) / (1 + exp(-0.1378 * (V +
            40.14))),
        0.6 * exp(0.057 * V) / (1 + exp(-0.1 * (V + 32))))

#L-type calcium current

[ical]
use membrane.V
use phys.FFRT, phys.FRT
use nernst.Ca_o
i_CaL = if(abs(V - 15) < 1e-6, a * (b - Ca_o) / (2 * FRT), numer / denom)
    numer = a * (V - 15) * (b * exp((V - 15) * 2 * FRT) - Ca_o)
    denom = (exp(2 * (V - 15) * FRT) - 1)
    a = g_CaL * d * f * f2 * fCass * 4 * FFRT
    b = 0.25 * calcium.Ca_ss
    in [uA/uF]
g_CaL = 3.98e-5 [cm/ms/uF]
dot(d) = (d_inf - d) / tau_d
    d_inf = 1 / (1 + exp((-8 - V) / 7.5))
    tau_d = 1 * alpha_d * beta_d + gamma_d
    alpha_d = 1.4 / (1 + exp((-35 - V) / 13)) + 0.25
    beta_d = 1.4 / (1 + exp((V + 5) / 5))
    gamma_d = 1 / (1 + exp((50 - V) / 20))
dot(f) = (f_inf - f) / tau_f
    f_inf = 1 / (1 + exp((V + 20) / 7))
    tau_f = 1102.5 * exp(-(V + 27) ^ 2 / 225) + 200 / (1 + exp((13 - V) /
        10)) + 180 / (1 + exp((V + 30) / 10)) + 20
```

```
dot(f2) = (f2_inf - f2) / tau_f2
    f2_inf = 0.67 / (1 + exp((V + 35) / 7)) + 0.33
    tau_f2 = 562 * exp(-(V + 27) ^ 2 / 240) + 31 / (1 + exp((25 - V) / 10)) +
       80 / (1 + exp((V + 30) / 10))
dot(fCass) = (fCass_inf - fCass) / tau_fCass
    fCass_inf = 0.6 / (1 + (calcium.Ca_ss / 0.05) ^ 2) + 0.4
    tau_fCass = 80 / (1 + (calcium.Ca_ss / 0.05) ^ 2) + 2
    in [ms]

#Slow delayed rectifier current

[iks]
use membrane.V
i_Ks = g_Ks * Xs ^ 2 * (V - nernst.E_Ks)
    in [uA/uF]
g_Ks = 0.2352 [1/ms]
dot(Xs) = (xs_inf - Xs) / tau_xs
    xs_inf = 1 / (1 + exp((-5 - V) / 14))
    tau_xs = 1 * alpha_xs * beta_xs + 80
    alpha_xs = 1400 / sqrt(1 + exp((5 - V) / 6))
    beta_xs = 1 / (1 + exp((V - 35) / 15))

#Rapid delayed rectifier current

[ikr]
use membrane.V
i_Kr = g_Kr * sqrt(nernst.K_o / 5.4) * Xr1 * Xr2 * (V - nernst.E_K)
    in [uA/uF]
    g_Kr = 0.0918 [1/ms]
```

```
dot(Xr1) = (xr1_inf - Xr1) / tau_xr1
    xr1_inf = 1 / (1 + exp((-26 - V) / 7))
    tau_xr1 = 1 * alpha_xr1 * beta_xr1
    alpha_xr1 = 450 / (1 + exp((-45 - V) / 10))
    beta_xr1 = 6 / (1 + exp((V + 30) / 11.5))
dot(Xr2) = (xr2_inf - Xr2) / tau_xr2
    xr2_inf = 1 / (1 + exp((V + 88) / 24))
    tau_xr2 = 1 * alpha_xr2 * beta_xr2
    alpha_xr2 = 3 / (1 + exp((-60 - V) / 20))
    beta_xr2 = 1.12 / (1 + exp((V - 60) / 20))


#Na/Ca exchange current


[inaca]
use membrane.V
use sodium.Na_i, nernst.Na_o, calcium.Ca_i, nernst.Ca_o
i_NaCa = K_NaCa * (exp(g * vfrt) * Na_i^3 * Ca_o - exp((g - 1) * vfrt) * nao3
   * Ca_i * alpha) / (
        km * (1 + K_sat * exp((g - 1) * V * phys.FRT)))
    in [uA/uF]
    vfrt = V * phys.FRT
    g = 0.35
    nao3 = Na_o^3
    km = (Na_o^3 + Km_Nai^3) * (Km_Ca + Ca_o)
    K_NaCa = 1000 [uA/uF]
    K_sat = 0.1
    alpha = 2.5
    Km_Ca = 1.38 [mmol/L]
    Km_Nai = 87.5 [mmol/L]
```

```
#Na/K pump current

[inak]
use membrane.V
use nernst.K_o, sodium.Na_i
i_NaK = P_NaK * K_o / (K_o + K_mk) * Na_i / (Na_i + K_mNa) / (1 + 0.1245 *
    exp(-0.1 * vfrt) + 0.0353 * exp(-vfrt))
    in [uA/uF]
    vfrt = V * phys.FRT
P_NaK = 2.724 [uA/uF]
K_mk = 1 [mmol/L]
K_mNa = 40 [mmol/L]

#Calcium pump current

[ipca]
i_p_Ca = g_pCa * calcium.Ca_i / (calcium.Ca_i + K_pCa)
    in [uA/uF]
g_pCa = 0.1238 [uA/uF]
K_pCa = 0.0005 [mmol/L]

#Potassium pump current

[ipk]
use membrane.V
i_p_K = g_pK * (V - nernst.E_K) / (1 + exp((25 - V) / 5.98))
    in [uA/uF]
g_pK = 0.0146 [1/ms]
```

```
#Sodium background current

[ibna]
use membrane.V
i_b_Na = g_bna * (V - nernst.E_Na)
    in [uA/uF]
g_bna = 0.00029 [1/ms]

#Calcium background current

[ibca]
use membrane.V
i_b_Ca = g_bca * (V - nernst.E_Ca)
    in [uA/uF]
g_bca = 0.000592 [1/ms]

#Calcium dynamics

[calcium]
use membrane.V
ICa_cyt = ibca.i_b_Ca + ipca.i_p_Ca - 2 * inaca.i_NaCa
ICa_tot = ICa_cyt + ical.i_CaL
dot(Ca_i) = Ca_i_bufc * ((i_leak - i_up) * V_sr / phys.V_c + i_xfer - ICa_cyt
    * phys.Cm / (2 * phys.V_c * phys.F))
    in [mmol/L]
dot(Ca_SR) = Ca_sr_bufsr * (i_up - (i_rel + i_leak))
    in [mmol/L]
dot(Ca_ss) = Ca_ss_bufss * (-1 * ical.i_CaL * phys.Cm / (2 * 1 * V_ss *
```

```
   phys.F) + i_rel * V_sr / V_ss - i_xfer * phys.V_c / V_ss)
    in [mmol/L]
i_rel = V_rel * O * (Ca_SR - Ca_ss)
    in [mmol/L/ms]
i_up = Vmax_up / (1 + K_up ^ 2 / Ca_i ^ 2)
    in [mmol/L/ms]
i_leak = V_leak * (Ca_SR - Ca_i)
    in [mmol/L/ms]
i_xfer = V_xfer * (Ca_ss - Ca_i)
    in [mmol/L/ms]
O = k1 * Ca_ss ^ 2 * R_prime / (k3 + k1 * Ca_ss ^ 2)
dot(R_prime) = -k2 * Ca_ss * R_prime + k4 * (1 - R_prime)
k1 = k1_prime / kcasr
    in [m^6/s/mol^2 (1000.0)]
k2 = k2_prime * kcasr
    in [m^3/s/mol (1000.0)]
k1_prime = 0.15
    in [m^6/s/mol^2 (1000.0)]
k2_prime = 0.045
    in [m^3/s/mol (1000.0)]
k3 = 0.06 [1/ms]
k4 = 0.005 [1/ms]
EC = 1.5 [mmol/L]
max_sr = 2.5
min_sr = 1
kcasr = max_sr - (max_sr - min_sr) / (1 + (EC / Ca_SR) ^ 2)
V_rel = 0.102 [1/ms]
V_xfer = 0.0038 [1/ms]
K_up = 0.00025 [mmol/L]
```

```
V_leak = 0.00036 [1/ms]
Vmax_up = 0.006375 [mmol/L/ms]
Ca_i_bufc = 1 / (1 + Buf_c * K_buf_c / (Ca_i + K_buf_c) ^ 2)
Ca_sr_bufsr = 1 / (1 + Buf_sr * K_buf_sr / (Ca_SR + K_buf_sr) ^ 2)
Ca_ss_bufss = 1 / (1 + Buf_ss * K_buf_ss / (Ca_ss + K_buf_ss) ^ 2)
Buf_c = 0.2 [mmol/L]
K_buf_c = 0.001 [mmol/L]
Buf_sr = 10 [mmol/L]
K_buf_sr = 0.3 [mmol/L]
Buf_ss = 0.4 [mmol/L]
K_buf_ss = 0.00025 [mmol/L]
V_sr = 0.001094 [um^3]
V_ss = 5.468e-5 [um^3]

#Sodium dynamics

[sodium]
INa_tot = ina.i_Na + ibna.i_b_Na + if.i_f_Na + 3 * inak.i_NaK + 3 *
   inaca.i_NaCa
dot(Na_i) = -INa_tot / (phys.V_c * phys.F) * phys.Cm
    in [mmol/L]

#Potassium dynamics

[potassium]
IK_tot = ik.i_K1 + ito.i_to + if.i_f_K + isus.i_sus + ikr.i_Kr + iks.i_Ks +
   ipk.i_p_K - 2 * inak.i_NaK
dot(K_i) = -IK_tot / (phys.V_c * phys.F) * phys.Cm # phys.Cm is not in the
   appendix!
```

```
    in [mmol/L]


# Nernst potentials


[nernst]
use potassium.K_i
use sodium.Na_i
use calcium.Ca_i
K_o = 5.4 [mmol/L]
E_K = phys.RTF * log(K_o / K_i)
    in [mV]
E_Ks = phys.RTF * log((K_o + P_kna * Na_o) / (K_i + P_kna * Na_i))
    in [mV]
P_kna = 0.03
Na_o = 140 [mmol/L]
E_Na = phys.RTF * log(Na_o / Na_i)
    in [mV]
Ca_o = 2 [mmol/L]
E_Ca = 0.5 * phys.RTF * log(Ca_o / Ca_i)
    in [mV]
```

B.2 Script to run cable simulation

```
[[scriptcable]]
import myokit
import numpy as np
import matplotlib.pyplot as plt
from mpl_toolkits.mplot3d import axes3d

n = 1000
m = get_model()
p = get_protocol()
s = myokit.Simulation1d(m, p, n)
s.set_conductance(5)
s.set_step_size(0.01)
d = s.run(6000, log=['engine.time', 'membrane.V'])

f = plt.figure()
x = f.gca(projection='3d')
z = np.ones(len(d['engine.time']))
for i in range(0, n):
    x.plot(d['engine.time'], z*i, d['membrane.V', i])
f = plt.figure()

plt.show()
```

B.3 Script for 2D simulation

```
[[script2D]]
import myokit
import matplotlib.pyplot as plt


n = 1000
m = get_model()
p = get_protocol()
s = myokit.SimulationOpenCL(m, p, ncells=n)
s.set_conductance(9)
s.set_step_size(0.01)


try:


    t = 300
    d = s.run(t, log_interval=1, log=['engine.time', 'membrane.V'])


    b = d.block2d()


    cv = b.cv('membrane.V')
    print('Conduction velocity: ' + str(cv) + ' [cm/s]')


    x,y,z = b.grid('membrane.V')
    plt.figure()
    plt.pcolormesh(x,y,z)
    plt.grid(False)
    plt.xlim(0, t)
    plt.ylim(0, n)
    plt.colorbar()
```

```
    plt.show()


except myokit.SimulationError as e:
    print(str(e))
```

References

[1] D.R. Adam. Propagation of depolarization and repolarization processes in the myocardium-an anisotropic model. *IEEE Transactions on Biomedical Engineering*, 38(2):133–141, Feb. 1991.

[2] I. F. Akyildiz and J. M. Jornet. The internet of nano-things. *IEEE Wireless Communications*, 17(6):58–63, December 2010.

[3] Ian F. Akyildiz, Fernando Brunetti, and Cristina Blzquez. Nanonetworks: A new communication paradigm. *Computer Networks*, 52(12):2260 – 2279, 2008.

[4] Ian F. Akyildiz, Fernando Brunetti, and Cristina Blzquez. Nanonetworks: A new communication paradigm. *Computer Networks*, 52(12):2260 – 2279, 2008.

[5] Ahmad S. Amin, Hanno L. Tan, and Arthur A.M. Wilde. Cardiac ion channels in health and disease. *Heart Rhythm*, 7(1):117 – 126, 2010.

[6] Inc. Anaconda. Miniconda. `https://docs.conda.io/en/latest/miniconda.html`. Last Accessed: 2019-03-15.

[7] Alex M. Andrew. Nanomedicine, volume 1: Basic capabilities, by robert a. freitas jr., landes bioscience, austin, texas, 1999, xxi + 509 pp., isbn 1-57059-645-x index (hardback, $89.000). *Robotica*, 18(6):687–689, November 2000.

[8] D. M. Barakah and M. Ammad-uddin. A survey of challenges and applications of wireless body area network (wban) and role of a virtual doctor server in existing architecture. In *2012 Third International Conference on Intelligent Systems Modelling and Simulation*, pages 214–219, Feb 2012.

[9] Philippe Beauchamp, Kathryn A. Yamada, Alex J. Baertschi, Karen Green, Evelyn M. Kanter, Jeffrey E. Saffitz, and Andr G. Klber. Relative contributions of connexins 40 and 43 to atrial impulse propagation in synthetic strands of neonatal and fetal murine cardiomyocytes. *Circulation Research*, 99(11):1216–1224, 2006.

[10] Jonathan Guy Bensley, Robert De Matteo, Richard Harding, and Mary Jane Black. Three-dimensional direct measurement of cardiomyocyte volume, nuclearity, and ploidy in thick histological sections. *Scientific Reports*, 06, 2016.

[11] O. Bernus, R. Wilders, C. W. Zemlin, H. Verschelde, and A. V. Panfilov. A computationally efficient electrophysiological model of human ventricular cells. *American Journal of Physiology-Heart and Circulatory Physiology*, 282(6):H2296–H2308, 2002. PMID: 12003840.

[12] Robert E. BoSmith, Ian Briggs, and Nicholas C. Sturgess. Inhibitory actions of zeneca zd7288 on whole-cell hyperpolarization activated inward current (if) in guinea-pig dissociated sinoatrial node cells. *British Journal of Pharmacology*, 110(1):343–349, 1993.

[13] Hugh Bostock, Katia Cikurel, and David Burke. Threshold tracking techniques in the study of human peripheral nerve. *Muscle & Nerve*, 21(2):137–158, 1998.

[14] Andrew Bruening-Wright and H. Peter Larsson. Slow conformational changes of the voltage sensor during the mode shift in hyperpolarization-activated cyclic-nucleotide-gated channels. *Journal of Neuroscience*, 27(2):270–278, 2007.

[15] David Burke, James Howells, Louise Trevillion, Penelope A. McNulty, Stacey K. Jankelowitz, and Matthew C. Kiernan. Threshold behaviour of human axons explored using subthreshold perturbations to membrane potential. *The Journal of Physiology*, 587(2):491–504, 2009.

[16] George D Byrne and Alan C Hindmarsh. Stiff ode solvers: A review of current and coming attractions. *Journal of Computational Physics*, 70(1):1 – 62, 1987.

[17] Fernando Sancho Caparrini. Sobre el modelado matemtico. `http://www.cs.us.es/~fsancho/?e=49`. Last Accessed: 2019-05-17.

[18] William A. Catterall. Structure and regulation of voltage-gated ca2+ channels. *Annual Review of Cell and Developmental Biology*, 16(1):521–555, 2000. PMID: 11031246.

[19] William A. Catterall. Voltage-gated calcium channels. *Cold Spring Harbor Perspectives in Biology*, 3(8), 2011.

[20] Michael Clerx. Myokit. `http://myokit.org/`. Last Accessed: 2019-06-15.

[21] Kenneth S. Cole. Permeability and impermeability of cell membranes for ions. *Cold Spring Harbor Symposia on Quantitative Biology*, 8:110–122, 1940.

[22] NVIDIA High Performance Computing. OpenCLnvidia. `https://developer.nvidia.com/opencl`. Last Accessed: 2019-06-09.

[23] M.B. Conover. *Understanding Electrocardiography*. Mosby, 2002.

[24] Simon J Conway and Srinagesh V Koushik. Cardiac sodiumcalcium exchanger: a double-edged sword. *Cardiovascular Research*, 51(2):194–197, 08 2001.

[25] M. Cooklin, W. R. J. Wallis, D. J. Sheridan, and C. H. Fry. Conduction velocity and gap junction resistance in hypertrophied, hypoxic guinea-pig left ventricular myocardium. *Experimental Physiology*, 83(6):763770, 1998.

[26] Lavan A. David, McGuire Terry, and Langer Robert. Small-scale systems for in vivo drug delivery. *Nanotechnology*, 21:1184–1191, sep 2003.

[27] Silvia de Miguel-Bilbao, Erik Aguirre, Peio Lopez Iturri, Leire Azpilicueta, Jose Roldan, Francisco Falcone, and Victoria Ramos. Evaluation of electromagnetic interference and exposure assessment from s-health solutions based on wi-fi devices. *BioMed Research International*, 2015:9, 2015.

[28] S. Dokos, B. Celler, and N. Lovell. Ion currents underlying sinoatrial node pacemaker activity: A new single cell mathematical model. *Journal of Theoretical Biology*, 181(3):245 – 272, 1996.

[29] Joachim R. Ehrlich, Tae-Joon Cha, Liming Zhang, Denis Chartier, Louis Villeneuve, Terence E. Hbert, and Stanley Nattel. Characterization of a hyperpolarization-activated time-dependent potassium current in canine cardiomyocytes from pulmonary vein myocardial sleeves and left atrium. *The Journal of Physiology*, 557(2):583–597, 2004.

[30] W. Howard Evans and Patricia E. M. Martin. Gap junctions: structure and function (review). *Molecular Membrane Biology*, 19(2):121–136, 2002.

[31] F.M. Filipoiu. *Atlas of Heart Anatomy and Development*. Springer London, 2013.

[32] The Database Center for Life Science. Body Parts 3D anatomography. `http://lifesciencedb.jp/bp3d/`. Last Accessed: 2019-06-10.

[33] Python Software Foundation. Python. `https://www.python.org/about/`. Last Accessed: 2019-05-20.

[34] H. A. Fozzard. Membrane capacity of the cardiac purkinje fibre. *The Journal of Physiology*, 182(2):255–267, 1966.

[35] Silvana Franceschetti, Tatiana Lavazza, Giulia Curia, Patrizia Aracri, Ferruccio Panzica, Giulio Sancini, Giuliano Avanzini, and Jacopo Magistretti. Na+-activated k+ current contributes to postexcitatory hyperpolarization in neocortical intrinsically bursting neurons. *Journal of Neurophysiology*, 89(4):2101–2111, 2003. PMID: 12686580.

[36] Barry A. Franklin and Mary Cushman. Recent advances in preventive cardiology and lifestyle medicine. *Circulation*, 123(20):2274–2283, 2011.

[37] C. Gear and L. Petzold. Ode methods for the solution of differential/algebraic systems. *SIAM Journal on Numerical Analysis*, 21(4):716–728, 1984.

[38] George A. Gutman, K. George Chandy, John P. Adelman, Jayashree Aiyar, Douglas A. Bayliss, David E. Clapham, Manuel Covarriubias, Gary V. Desir, Kiyoshi Furuichi, Barry Ganetzky, Maria L. Garcia, Stephan Grissmer, Lily Y. Jan, Andreas Karschin, Donghee Kim, Sabina Kuperschmidt, Yoshihisa Kurachi, Michel Lazdunski, Florian Lesage, Henry A.

Lester, David McKinnon, Colin G. Nichols, Ita O'Kelly, Jonathan Robbins, Gail A. Robertson, Bernardo Rudy, Michael Sanguinetti, Susumu Seino, Walter Stuehmer, Michael M. Tamkun, Carol A. Vandenberg, Aguan Wei, Heike Wulff, and Randy S. Wymore. International union of pharmacology. xli. compendium of voltage-gated ion channels: Potassium channels. *Pharmacological Reviews*, 55(4):583–586, 2003.

[39] David E. Gutstein, Fang-yu Liu, Marian B. Meyers, Andrew Choo, and Glenn I. Fishman. The organization of adherens junctions and desmosomes at the cardiac intercalated disc is independent of gap junctions. *Journal of Cell Science*, 116(5):875–885, 2003.

[40] Craig S. Henriquez, Adam L. Muzikant, and Charles K. Smoak. Anisotropy, fiber curvature, and bath loading effects on activation in thin and thick cardiac tissue preparations:. *Journal of Cardiovascular Electrophysiology*, 7(5):424–444, 1996.

[41] CS Henriquez. Simulating the electrical behavior of cardiac tissue using the bidomain model. *Critical reviews in biomedical engineering*, 21(1):177, 1993.

[42] A. L. Hodgkin and A. F. Huxley. A quantitative description of membrane current and its application to conduction and excitation in nerve. *The Journal of physiology*, 117(4):500–544, 1952.

[43] Huan-Bang Li, Kenichi Takizawa, and Ryuji Kohno. Trends and standardization of body area network (ban) for medical healthcare. In *2008 European Conference on Wireless Technology*, pages 1–4, Oct 2008.

[44] N.B. Ingels, G.T. Daughters, and J. Baan. *Systolic and Diastolic Function of the Heart*. Studies in Health Technology a. IOS Press, 1996.

[45] S. Ito, E. Sato, and W. R. Loewenstein. Studies on the formation of a permeable cell membrane junction. *The Journal of Membrane Biology*, 19(1):305–337, Dec 1974.

[46] R.F. Jaffet. Fisiologa cardiaca ciencias bsicas. `https://www.medigraphic.com/pdfs/revmed/md-2009/md093d.pdf`. Last Accessed: 2019-06-12.

[47] A. Jameson, Wolfgang Schdmit, and Eli Turkel. *Numerical solution of the Euler equations by finite volume methods using Runge Kutta time stepping schemes.*

[48] Emil Jovanov, Aleksandar Milenkovic, Chris Otto, and Piet C. de Groen. A wireless body area network of intelligent motion sensors for computer assisted physical rehabilitation. *Journal of NeuroEngineering and Rehabilitation*, 2(1):6, Mar 2005.

[49] Hyacinthe Tchewonpi Kankeu, Priyanka Saksena, Ke Xu, and David B Evans. The financial burden from non-communicable diseases in low- and middle-income countries: a literature review. *Health Research Policy and Systems*, 11:31, 2013.

[50] Elissavet Kardami, Xitong Dang, Dumitru A. Iacobas, Barbara E. Nickel, Madhumathy Jeyaraman, Wattamon Srisakuldee, Janna Makazan, Stephane Tanguy, and David C. Spray. The role of connexins in controlling cell growth and gene expression. *Progress in Biophysics and Molecular Biology*, 94(1):245 – 264, 2007. Gap junction channels: from protein genes to diseases.

[51] A.M. Katz. *Physiology of the Heart.* Wolters Kluwer Health/Lippincott Williams & Wilkins Health, 2010.

[52] Evgeny Katz and Vladimir Privman. Enzyme-based logic systems for information processing. *Chem. Soc. Rev.*, 39:1835–1857, 2010.

[53] O. Kiehn and R. M. Harris-Warrick. 5-ht modulation of hyperpolarization-activated inward current and calcium-dependent outward current in a crustacean motor neuron. *Journal of Neurophysiology*, 68(2):496–508, 1992. PMID: 1382120.

[54] R.E. Klabunde. *Cardiovascular Physiology Concepts.* Lippincott Williams & Wilkins, 2005.

[55] A G Klber. Resting membrane potential, extracellular potassium activity, and intracellular sodium activity during acute global ischemia in isolated perfused guinea pig hearts. *Circulation Research*, 52(4):442–450, 1983.

[56] Christof Koch, Ojvind Bernander, and Rodney J. Douglas. Do neurons have a voltage or a current threshold for action potential initiation? *Journal of Computational Neuroscience*, 2(1):63–82, Mar 1995.

[57] B. Koeppen and Stanton B. *Physiology*. Mosby, 6 edition, 2010.

[58] Christosa Koutras, Marinab Bitsaki, Georgiosb Koutras, Christosc Nikolaou, and Hansjoerga Heep. Socioeconomic impact of e-health services in major joint replacement: A scoping review. *Technology and Health Care*, 23(6):809–817, 2015.

[59] Yasutaka Kurata, Ichiro Hisatome, Sunao Imanishi, and Toshishige Shibamoto. Dynamical description of sinoatrial node pacemaking: improved mathematical model for primary pacemaker cell. *American Journal of Physiology-Heart and Circulatory Physiology*, 283(5):H2074–H2101, 2002. PMID: 12384487.

[60] Brenda R. Kwak and Habo J. Jongsma. Regulation of cardiac gap junction channel permeability and conductance by several phosphorylating conditions. *Molecular and Cellular Biochemistry*, 157(1):93–99, Apr 1996.

[61] Paul D. Lampe and Alan F. Lau. The effects of connexin phosphorylation on gap junctional communication. *The International Journal of Biochemistry & Cell Biology*, 36(7):1171 – 1186, 2004.

[62] C O Lee and H A Fozzard. Activities of potassium and sodium ions in rabbit heart muscle. *The Journal of General Physiology*, 65(6):695–708, 1975.

[63] Jane H.-C. Lin, Jay Yang, Shujun Liu, Takahiro Takano, Xiaohai Wang, Qun Gao, Klaus Willecke, and Maiken Nedergaard. Connexin mediates gap junction-independent resistance to cellular injury. *Journal of Neuroscience*, 23(2):430–441, 2003.

[64] Catherine M. Lloyd, Matt D.B. Halstead, and Poul F. Nielsen. Cellml: its future, present and past. *Progress in Biophysics and Molecular Biology*, 85(2):433 – 450, 2004. Modelling Cellular and Tissue Function.

[65] C. H. Luo and Y. Rudy. A dynamic model of the cardiac ventricular action potential. i. simulations of ionic currents and concentration changes. *Circulation Research*, 74(6):1071–1096, 1994.

[66] H. C. Luttgau and Rolf Niedergerke. The antagonism between ca and na ions on the frog's heart. *The Journal of physiology*, 143 3:486–505, 1958.

[67] Amal Mattu, William J. Brady, and David A. Robinson. Electrocardiographic manifestations of hyperkalemia. *The American Journal of Emergency Medicine*, 18(6):721 – 729, 2000.

[68] R. E. McAllister and D. Noble. The effect of subthreshold potentials on the membrane current in cardiac purkinje fibres. *The Journal of Physiology*, 190(2):381–387, 1967.

[69] R.E. Mehler. *How the Circulatory System Works*. How It Works. Wiley, 2014.

[70] Microsoft. Microsoft Visual C++ Compiler for Python 2.7. `https://www.microsoft.com/en-us/download/details.aspx?id=44266`. Last Accessed: 2019-03-15.

[71] Sven Moosmang, Juliane Stieber, Xiangang Zong, Martin Biel, Franz Hofmann, and Andreas Ludwig. Cellular expression and functional characterization of four hyperpolarization-activated pacemaker channels in cardiac and neuronal tissues. *European Journal of Biochemistry*, 268(6):1646–1652, 2001.

[72] Anna Moroni, Luisa Gorza, Monica Beltrame, Biagio Gravante, Thomas Vaccari, Marco E. Bianchi, Claudia Altomare, Renato Longhi, Catherine Heurteaux, Maurizio Vitadello, Antonio Malgaroli, and Dario DiFrancesco. Hyperpolarization-activated cyclic nucleotide-gated channel 1 is a molecular determinant of the cardiac pacemaker current if. *Journal of Biological Chemistry*, 276(31):29233–29241, 2001.

[73] T. Nakano, A.W. Eckford, and T. Haraguchi. *Molecular Communication*. Cambridge University Press, 2013.

[74] T. Nakano, T. Suda, M. Moore, R. Egashira, A. Enomoto, and K. Arima. Molecular communication for nanomachines using intercellular calcium signaling. In *5th IEEE Conference on Nanotechnology, 2005.*, pages 478–481 vol. 2, July 2005.

[75] Tadashi Nakano, Tatsuya Suda, Takako Koujin, Tokuko Haraguchi, and Yasushi Hiraoka. *Molecular Communication through Gap Junction Channels*, pages 81–99. Springer Berlin Heidelberg, Berlin, Heidelberg, 2008.

[76] M. P. Nash and P. J. Hunter. Computational mechanics of the heart - from tissue structure to ventricular function. *Journal of Elasticity*, 61:113, 2000.

[77] D. Noble and R. B. Stein. The threshold conditions for initiation of action potentials by excitable cells. *The Journal of Physiology*, 187(1):129–162, 1966.

[78] H-C Pape. Queer current and pacemaker: The hyperpolarization-activated cation current in neurons. *Annual Review of Physiology*, 58(1):299–327, 1996. PMID: 8815797.

[79] A. Pullan, M. Buist, and Leo K Cheng. *Mathematically Modelling the Electrical Activity of the Heart*. World Scientific, 2005.

[80] Stphanie Ratt, Milad Lankarany, Young-Ah Rho, Adam Patterson, and Steven A. Prescott. Subthreshold membrane currents confer distinct tuning properties that enable neurons to encode the integral or derivative of their input. *Frontiers in Cellular Neuroscience*, 8:452, 2015.

[81] J. Russell and R. Cohn. *Nernst Equation*. Book on Demand, 2012.

[82] Nadrian C Seeman, Hui Wang, Xiaoping Yang, Furong Liu, Chengde Mao, Weiqiong Sun, Lisa Wenzler, Zhiyong Shen, Ruojie Sha, Hao Yan, Man Hoi Wong, Phiset Sa-Ardyen, Bing Liu, Hangxia Qiu, Xiaojun Li, Jing Qi, Shou Ming Du, Yuwen Zhang, John E Mueller, Tsu-Ju Fu, Yinli Wang, and Junghuei Chen. New motifs in DNA nanotechnology. *Nanotechnology*, 9(3):257–273, sep 1998.

[83] N.J. Severs. The cardiac gap junction and intercalated disc. *International Journal of Cardiology*, 26(2):137 – 173, 1990.

[84] C. E. Stafstrom, P. C. Schwindt, J. A. Flatman, and W. E. Crill. Properties of subthreshold response and action potential recorded in layer v neurons from cat sensorimotor cortex in vitro. *Journal of Neurophysiology*, 52(2):244–263, 1984. PMID: 6090604.

[85] Philip Stewart, Oleg V. Aslanidi, Denis Noble, Penelope J. Noble, Mark R. Boyett, and Henggui Zhang. Mathematical models of the electrical action potential of purkinje fibre cells. *Philosophical Transactions of the Royal Society A: Mathematical, Physical and Engineering Sciences*, 367(1896):2225–2255, 2009.

[86] J F Storm. Action potential repolarization and a fast after-hyperpolarization in rat hippocampal pyramidal cells. *The Journal of Physiology*, 385(1):733–759, 1987.

[87] Jorge E. Suarez and Alicia I. Bravo. Conexinas y sistema cardiovascular. *Revista Argentina de Cardiologia*, 74:149–156, 2006.

[88] SUNDIALS. CVODE computation. `https://computation.llnl.gov/projects/sundials/cvode`. Last Accessed: 2019-06-06.

[89] SUNDIALS. CVODE download sundials software. `https://computation.llnl.gov/projects/sundials/sundials-software`. Last Accessed: 2019-03-06.

[90] Goran Shl and Klaus Willecke. Gap junctions and the connexin protein family. *Cardiovascular Research*, 62(2):228–232, 05 2004.

[91] Peter Taggart, Peter MI Sutton, Tobias Opthof, Ruben Coronel, Richard Trimlett, Wilfred Pugsley, and Panny Kallis. Inhomogeneous transmural conduction during early ischaemia in patients with coronary artery disease. *Journal of Molecular and Cellular Cardiology*, 32(4):621 – 630, 2000.

[92] K. H. W. J. ten Tusscher, D. Noble, P. J. Noble, and A. V. Panfilov. A model for human ventricular tissue. *American Journal of Physiology-Heart and Circulatory Physiology*, 286(4):H1573–H1589, 2004. PMID: 14656705.

[93] X. Teng, Y. Zhang, C. C. Y. Poon, and P. Bonato. Wearable medical systems for p-health. *IEEE Reviews in Biomedical Engineering*, 1:62–74, 2008.

[94] Rice University. OpenStax cnx. `https://cnx.org/`. Last Accessed: 2019-06-10.

[95] James N. Weiss, Zhilin Qu, and Kalyanam Shivkumar. Electrophysiology of hypokalemia and hyperkalemia. *Circulation: Arrhythmia and Electrophysiology*, 10(3):e004667, 2017.

[96] Tsutomu Yamazaki, Issei Komuro, Sumiyo Kudoh, Yunzeng Zou, Ryozo Nagai, Ryuichi Aikawa, Hiroki Uozumi, and Yoshio Yazaki. Role of ion channels and exchangers in mechanical stretch induced cardiomyocyte hypertrophy. *Circulation Research*, 82(4):430–437, 1998.

[97] Xiao-Jian Yuan. Voltage-gated k+ currents regulate resting membrane potential and ca2+ in pulmonary arterial myocytes. *Circulation Research*, 77(2):370–378, 1995.

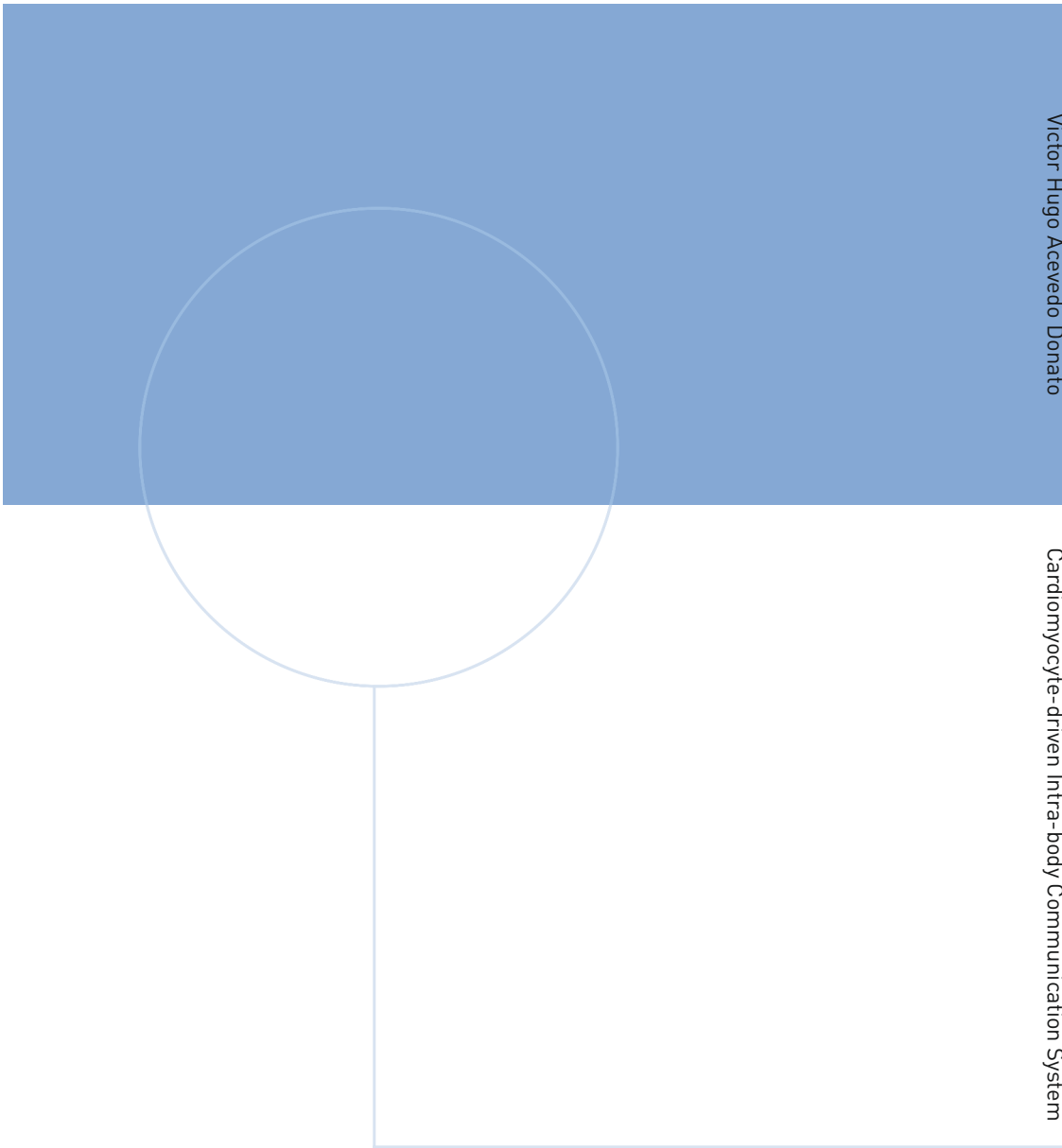

Victor Hugo Acevedo Donato

Cardiomyocyte-driven Intra-body Communication System

NTNU
Norwegian University of
Science and Technology